Order Number 9202084

Parameter estimation in reconstructing temperature fields during hyperthermia

Liauh, Chihng-Tsung, Ph.D.

The University of Arizona, 1991

U·M·I
300 N. Zeeb Rd.
Ann Arbor, MI 48106

PARAMETER ESTIMATION IN RECONSTRUCTING TEMPERATURE FIELDS DURING HYPERTHERMIA

by

Chihng-Tsung Liauh

A Dissertation Submitted to the Faculty of

DEPARTMENT OF AEROSPACE AND MECHANICAL ENGINEERING

In Partial Fulfillment of the Requirements
For the Degree of

DOCTOR OF PHILOSOPHY
WITH A MAJOR IN MECHANICAL ENGINEERING

In the Graduate College

THE UNIVERSITY OF ARIZONA

1 9 9 1

THE UNIVERSITY OF ARIZONA
GRADUATE COLLEGE

As members of the Final Examination Committee, we certify that we have read the dissertation prepared by Chihng-Tsung Liauh

entitled PARAMETER ESTIMATION IN RECONSTRUCTING TEMPERATURE FIELDS DURING HYPERTHERMIA

and recommend that it be accepted as fulfilling the dissertation requirement for the Degree of Doctor of Philosophy.

Robert B Roemer	8/28/91
Robert B. Roemer	Date
C C Chan	8/20/91
Cholik Chan	Date
Hal Tharp	8/20/91
Hal Tharp	Date
	Date
	Date

Final approval and acceptance of this dissertation is contingent upon the candidate's submission of the final copy of the dissertation to the Graduate College.

I hereby certify that I have read this dissertation prepared under my direction and recommend that it be accepted as fulfilling the dissertation requirement.

Robert B Roemer	8/28/91
Dissertation Director Robert B. Roemer	Date

STATEMENT BY AUTHOR

This dissertation has been submitted in partial fulfillment of requirements for an advanced degree at The University of Arizona and is deposited in the University Library to be made available to borrowers under rules of the Library.

Brief quotations from this dissertation are allowable without special permission, provided that accurate acknowledgement of source is made. Requests for permission for extended quotation from or reproduction of this manuscript in whole or in part may be granted by the head of the major department or the Dean of the Graduate College when in his or her judgment the proposed use of the material is in the interests of scholarship. In all other instances, however, permission must be obtained from the author.

SIGNED: 

ACKNOWLEDGEMENTS

The author would like to express his sincere thanks to Dr. R. Roemer for his constant advice, guidance and support during the research process. Special thanks go to Drs. H. Tharp, C. Chan, K. Hynynen, and S. Clegg who provided technical support and advice. The author would also like to thank W-L. Lin, Z-P. Chen, J-S. Chen, H-W. Huang, J. Yeh, A. Dutton, and J. K. Potocki who provided friendship and advice. Special thanks go to D. Webber for her many contributions.

The author would like to express the greatest thanks to his family, especially to his parents, Min-Lun Liauh and Yu-Li Chen Liauh for their moral support and encouragement.

TABLE OF CONTENTS

LIST OF ILLUSTRATIONS

LIST OF ILLUSTRATIONS--Continued

LIST OF ILLUSTRATIONS--Continued

LIST OF ILLUSTRATIONS--Continued

LIST OF ILLUSTRATIONS--Continued

LIST OF ILLUSTRATIONS--Continued

LIST OF TABLES

LIST OF TABLES--Continued

LIST OF TABLES--Continued

ABSTRACT

In this dissertation, a state and parameter estimation algorithm is implemented and modified to predict the blood perfusions and thus the complete steady-state temperature fields based on input from a limited number of temperature measurements taken during simulated hyperthermia treatments. Several fundamental phenomena related to this inverse problem are investigated from simple direct models. Using one-, two-, and three-dimensional numerical simulation models it is shown that multiple minima solutions exist for some inverse hyperthermia temperature estimation problems. The general conditions under which these multiple minima occur are shown to be solely due to the existence of symmetries in the inverse problem formulation.

Both an adjoint formulation and a sensitivity equation method are derived and used to determine the elements in the Jacobian matrix associated with the inverse problem of estimating the blood perfusion and temperature fields during hyperthermia cancer treatments. These methods and a previously developed influence coefficient method for obtaining that matrix are comparatively evaluated by solving a set of numerically simulated inverse hyperthermia problems. Comparisons of the performance of the adjoint formulation and the influence coefficient method show that the total CPU time for the adjoint formulation is larger than that for the influence coefficient method for all of the cases which are solved successfully. The performance of

the sensitivity equation and the influence coefficient methods were also compared. Results showed that these two methods had the same performance.

An improved state and parameter estimation algorithm has been developed to reduce the total computational time required. If the change of the unknown perfusion parameters is small a linear approximation scheme is implemented in which the old Jacobian matrix (or sensitivity matrix) is used, instead of recalculating the new Jacobian matrix for the next iteration. Results show that if the temperature is approximated as a linear (or quasi-linear) function of the blood perfusion, the linearizing approach considerably reduces the CPU time required to accurately reconstruct the temperature field.

One of the model mismatch problems between the actual tumor and the simulated models is selected and investigated for the one-dimensional case. The model mismatch present in this dissertation is caused by the discretization of a perfusion field into several discrete zones. It is our attempt to understand the effects of the model mismatch problems from a simple model, and then generalize to more complicated three-dimensional cases which could occur during hyperthermia treatments.

To simulate the ultrasound hyperthermia treatments, a scanned focussed ultrasound power field is generated and then used to create the transient power-on data and the steady-state temperature field. The feasibility of using the transient power-on data to estimate the attenuation coefficient and the blood perfusion and thus reconstruct the steady-state temperature field is presented.

CHAPTER 1

INTRODUCTION

1.1 HYPERTHERMIA

Hyperthermia, from the Greek hyper meaning beyond and therme meaning heat, has been one of the more promising cancer therapies of recent decades. The use of heat in the treatment of various ailments, including cancer, dates back to Egyptian and Greek physicians. In late 1800s and early 1900s, many investigators (Coley 1893; Rohdenburg 1918) described that after infection with pyrogenic bacteria the regression of both primary and secondary tumors occurs. Although these early works showed the potential of hyperthermia, they provided little quantitative data on dose response to heat. The modern era of hyperthermia did not start until the works of Crile (1961, 1962, 1963). Crile (1963) showed that some transplantable tumors in mice are cured using hyperthermia with no permanent damage to normal tissue. Since that study, many oncologists interested in hyperthermia have focused on the cellular factors. Dewey et al. (1971) reported that hyperthermia is cytotoxic to cells even after elevating their temperature mildly. Ben Hur et al. (1972) reported that hyperthermia increases the cells' rate of inactivation to X-irradiation and the

cells, S-phase and hypoxic cells, that are radioresistant tend to be heat sensitive. Several reports in recent years have shown that normal and malignant tissues can become heat-resistant by subsequent heat exposures (Hahn et al. 1977, Law et al. 1979, Law 1979, Hume and Margold 1980, Kamura et al. 1981).

One important factor of evaluating the success/failure of a hyperthermia cancer treatment requires knowledge of the temperature distribution throughout the entire treatment region. In 1986, Hand and James proposed a general definition of hyperthermia which is a therapy in which tissue temperature is elevated to 41 °C or higher by external means in opposition to the thermoregulatory processes which control body temperature around the normal set-point. Dewhirst et al. 1984, Van der Zee et al. 1986, and Oleson et al. 1984 have shown that the effectiveness of hyperthermia is correlated to the minimum measured tumor temperature. Similarly, Barlogie et al. 1979, Larkin et al. 1977, and Pettigrew et al. 1974 have also shown that there are temperatures above which damage to normal tissue can be expected. The goal of hyperthermia treatments is to elevate the temperature of the tissue target region containing malignant cells to a therapeutic value (e.g. 43 °C) while maintaining the temperature in the normal tissue below unacceptable, damaging values over a duration of at least 30 to 60 minutes. To achieve this goal, clinical personnel should have knowledge of the entire temperature field in the treatment region. This knowledge is used to control the heating sources to deliver energy to the treatment target volume to raise its minimum temperature

above 43 °C, while limiting the temperatures in the normal tissue to prevent pain and/or damage.

External heating modalities for hyperthermia involve sources of electromagnetic (EM) or ultrasound (US) energy that transmit the energy into tissues via waves. The EM devices are roughly classified into two groups: microwave (MW) and radio-frequency (RF). The frequencies above 100 MHz being generally considered MW, although the line between MW and RF is not well defined. For interstitial or intracavitary hyperthermia, the EM devices use either MW antennas or RF electrodes, respectively, implanted directly into tumors or placed into body cavities. Field and Franconi 1987, and Hand and James 1986 have shown that these two techniques can localize the power deposition to deep tumors, but have the disadvantage of being invasive. On the other hand, US is a noninvasive heating method and can focus power into desired regions. Lele and Parker 1982, Lele 1983, 1986, Lele and Goddard 1987, and Hynynen et al. 1985, 1987a, 1987b have utilized several ultrasound systems in in vitro and in vivo experiments and in human patients, and they have shown that US can induce well-controlled localized power depositions in tumors at different depths.

1.2 BIOHEAT TRANSFER EQUATION

In 1948, Pennes proposed a governing equation to describe the temperature distribution in the resting human forearm. This equation, the so-called bioheat transfer equation (BHTE), was derived from the general conservation of energy equation with some additional assumptions. One of the assumptions is that the thermal equilibrium

between capillary blood and surrounding tissue is reached and maintained. That is, the blood flow, with a perfusion rate of W kg/m^3-s, enters the control volume at the arterial temperature (T_a) and leaves the control volume at the local tissue temperature (T). Therefore, the net rate of convection of thermal energy by blood flow in the control volume is approximated by $Wc_b(T_a-T)$, which acts like an energy sink/source. The general expression of the Pennes' bioheat transfer equation can be written as

$$\rho c\frac{\partial T}{\partial t} = \nabla\bullet(k\nabla T) - Wc_b(T-T_a) + Q, \qquad (1.1)$$

where ρ denotes the tissue density; c denotes the tissue specific heat; c_b denotes the blood specific heat; k denotes the thermal conductivity; W denotes the blood perfusion which is the unknown parameter; T_a denotes the arterial blood temperature; and Q denotes the power deposition.

This equation was derived basically from an engineering approximation. Thus, several detailed physical effects, such as the following, are not taken into account: the existence of large blood vessels; the arterial temperature as a function of position; the directionality of blood perfusion rates; and the countercurrent heat exchange between thermally significant vessels. Several investigators (e.g., Weinbaum et al. 1984, Weinbaum and Jiji 1985, Chen and Holmes 1980, Lagendijk, et al. 1984, Baish, et al. 1986) have recently developed different mathematical formulations to describe the temperature distribution. For example, the new bioheat transfer

equation of Weinbaum and Jiji (1985) uses an enhanced thermal conductivity which is related to parameters describing the local vascular anatomy and blood flow instead of the linear sink/source term of the BHTE which is proportional to the local blood-tissue temperature difference.

Still, the BHTE has been used in almost all of the models employed for predicting temperature fields in all modalities of hyperthermia. This fact can be primarily attributed to the following: 1) despite the complexity of both blood flow patterns and of the anatomy of living tissues, the simple energy sink/source term introduced by Pennes (as an approximation) has made the BHTE a good predictor and a very useful tool (e.g., Chen and Holmes 1980, Chato 1980, Emery and Sekins 1982, Hand et al. 1982, Hynynen et al. 1989, Pennes 1948, Sekins et al. 1982, 1984, Valvano et al. 1984, Roemer et al. 1989, Charny and Levin 1989); and 2) the new (since 1980) mathematical formulations of tissue heat transfer are less tractable and require knowledge of certain parameters that are always difficult (if not impossible) to obtain, such as details involving the vascular anatomy and/or the blood flow velocity field (e.g., Chen and Holmes 1980a, Jiji et al. 1984, Lagendijk et al. 1984, Weinbaum and Jiji 1985, Weinbaum et al. 1984, Wulff 1974). Moreover, although the newer derivations (since 1984) of tissue heat transfer represent improvements over the derivation of the BHTE of Pennes and have stimulated needed research efforts in this field, they still seem to be in the developmental and refining stages (Weinbaum and Jiji 1987, Wissler 1987a, 1987b, Sekins 1989) and have not been experimentally

verified. Also, the application of these newer equations to hyperthermia has been questioned in terms of their simplifying assumptions and their validity in vascularized cancerous tumors (Charny and Levin 1989, Roemer et al. 1989). Although, as the new models are refined and their use become practical, one must rely on existing relatively "simple" formulations (like the BHTE) or on "simplified" equations from more complex formulations.

For hyperthermia treatments, the power deposition term (Q) includes the rate of energy generated by the metabolic process and the rate of applied energy from the external heating devices. In most localized hyperthermia situations, the metabolic effect is generally small and can be neglected when compared to the applied power deposition. For example, the basal metabolism for an average person is on the order of 10^3 W/m^3, whereas the applied power depositions are on the order of $10^5 \sim 10^6$ W/m^3. In this dissertation, Q represents only the applied power deposition.

Recently, Roemer et al. 1989 showed that Pennes' bioheat transfer equation can be used under some hyperthermia conditions to describe the temperature field in perfused biological tissue reasonably well. Thus, the thermal model used in this study is the Pennes' bioheat transfer equation. Due to the unknown blood perfusion term in the Pennes' bioheat transfer equation for specific clinical cases, the entire temperature field for a certain applied power distribution cannot be obtained directly by solving the bioheat transfer equation. Thus, the problem studied here is one of inverse problems. In this dissertation, inverse techniques will be presented

in an attempt to accurately reconstruct the temperature fields from limited, noisy temperature measurements.

1.3 INVERSE PROBLEM

Generally, many engineering problems can be classified into two major fields: one is the direct problem; and the other is the inverse problems. For a direct problem, the response of the system is governed by an ordinary or partial differential equation with all parameters imbedded in the equation known and known boundary and initial conditions. Many theories and skills have been developed to solve these direct problems exactly or numerically. Unfortunately, not all problems can have all parameters or boundary conditions known. Consequently, the problems with unknown parameters or unknown boundary conditions cannot be solved directly, and therefore they are in the realm of the inverse (or indirect) problems. Most of the inverse problems concern the optimal determination of the unknown parameters (which could be spatially dependent) or the unknown boundary conditions by observing the dependent variable collected in the spatial and time domain.

Inverse problems arise in many branches of the physical and mathematical sciences, such as:

(1) inverse heat conduction problem (IHCP),

(2) hydrology field,

(3) medical tomography,

(4) image enhancement,

(5) temperature reconstruction,

(6) curve fitting,

(7) earthquake location,

(8) satellite navigation,

(9) factor analysis, etc.

In the IHCP problem, a classical example is the estimation of transient surface heat flux as estimated from interior temperature measurements made in a heat conducting body. This application is important when heat flux sensors cannot be attached directly to the surface due to the presence of an extremely hostile environment. An example of such an environment is on the nose cone of a space re-entry vehicle. In hydrology, many problems require the estimation of hydrological parameters associated with the movement of ground water, pollutants, and oil during extraction from in-situ measurements.

During hyperthermia cancer therapies, the complete temperature field throughout and surrounding the treated tissue must be carefully controlled to maximize the effectiveness of the treatment while minimizing the risk of damage to the surrounding tissue. However, the temperature can be monitored at only a few discrete locations throughout the treatment region due to practical limitations associated with thermal instrumentation and patient comfort. Because of these difficulties, inverse techniques are being developed to estimate the spatial distribution of blood perfusion which, in turn, can be used in the bioheat transfer equation to estimate the temperature distributions that exist during various hyperthermia treatment scenarios.

The inverse problem is often ill-posed. The ill-posedness is generally characterized by the nonuniqueness and instability of the identified parameters and the associated instabilities that occur during their estimation. Chavent (1974) studied the uniqueness problem in partial differential equations for two situations: (1) the case of constant parameters; and (2) the case of distributed parameters in space. In case 1, there are generally more measurements than unknowns, so that, in general, the inverse problem is unique. In case 2, if only point measurements are available, the inverse problem is always nonunique. The notion of identifiability addresses the question of whether it is at all possible to obtain unique solutions of the inverse problem for unknown parameters of interest in a mathematical model from data collected in the spatial and time domains. Kitamura and Nakagiri (1977) formulated the parameter identification problem as the one-to-one property of the inverse problem. They obtained some results for parameter identifiability (or nonidentifiability) for a system characterized by a linear, one-dimensional parabolic partial differential equation. Identification is usually not achievable in the case of point measurements where data is only available at a limited number of locations in the spatial domain.

Theoretically, when the unknown parameters are spatially dependent, there will be an infinite number of parameters associated with the contiguous points to exactly represent these spatial parameters. In practice, spatial unknown parameters are approximated when the system is subdivided into several subregions (or zones) in which the parameter is constant by using a finite difference or finite

element scheme. This results in reducing the number of parameters from an infinite number to a finite number. Reduction of the number of parameters can make the inverse solution numerically stable and solvable. It has been generally understood that as the number of zones is increased, the modeling error decreases while the error in parameter uncertainty increases. The error in parameter uncertainty can be represented by a norm of the covariance matrix of the estimated parameters (Yeh and Yoon, 1976; Shah et al., 1978). The covariance matrix of the estimated parameters also provides information regarding the reliability of each of the estimated parameters. The more sensitive the parameter, the closer and quicker the parameter will converge. Bayesian estimation methods that incorporate prior information have also been applied to parameter identification (Gavalas et al., 1976). Bayesian estimation reduces to a quadratic minimization problem, provided the parameters and the measurement errors are normally distributed and the model is linear in the parameters. When these conditions are not satisfied, a rigorous application of Bayesian estimation is impractical. The primary purpose for incorporating the prior information into the inverse problem is to reduce the parameter uncertainty, not to improve the model fit (Yeh 1986).

1.4 STATE AND PARAMETER ESTIMATION

In recent years, simulation and mathematical models have been developed to analyze many scientific and engineering problems solved numerically by the finite difference, finite element, or boundary element methods. Many of these models are distributed parameter

models. That is, the response of the system is governed by a partial differential equation, and parameters imbedded either in the governing equation or in the boundary or initial conditions are spatially dependent. In general, some of these parameters are not directly measurable from the physical point of view and have to be determined from historical observations. Once all unknown parameters (Parameter) are estimated, the solutions of the system (State) can be then also be estimated.

Many investigators have used state and parameter estimation techniques in diverse inverse problems. For example, Beck (1968, 1970), Reynaud and Beck (1985), Hills and Hensel (1986), and Hensel and Hills (1989) have proposed several methods for estimating the surface heat flux history for linear and nonlinear inverse heat conduction problems. Lauster, Ray, and Martens (1980) used an iterative filter equation to estimate the transient temperature responses for the two-dimensional heated ingot without having any knowledge of the initial temperature field. Divrik et al. (1984), Clegg and Roemer (1985a, 1985b), Winget et al. (1986), Plancot et al. (1986), Liauh et al. (1991), Liauh (1988) used state and parameter estimation techniques to simultaneously estimate both the temperature fields and the parameters which appears in Pennes' bioheat transfer equation. Yeh and Sun (1984), Yeh and Yoon (1976), Neuman (1973) have shown the success of the technique in hydrology problems. Kravaris and Seinfeld (1985 and 1986), and Kitamura and Nakagiri (1977) have used this technique to determine the spatially varying parameters in distributed systems.

In solving the inverse problem, an efficient method must be used in the calculation of the sensitivity coefficients, which are the partial derivatives of the measurements with respect to each of the parameters. Literature reviews indicate that three methods have been used in the past to calculate these sensitivity coefficients. First, the influence coefficient method presented by Becker and Yeh in 1972 uses the concept of parameter perturbation. Each element in the matrix represents the ratio of change in the measurement to the change in a particular parameter. Second, in the sensitivity equation method by Beck and Arnold (1977), a set of sensitivity equations are obtained by taking the partial derivatives with respect to each parameter in the governing equation and initial and boundary conditions. Finally, the variational method (or adjoint formulation) utilizes integral equations with kernels which are derived from solutions to the governing equation. It was first used for solving the inverse problem of parameter identification by Jacquard and Jain (1965) and then by Carter et al. (1974 and 1982) in problems associated with finite difference schemes. Sun and Yeh in 1985 extended the method to the case of a finite element scheme.

Comparing the above mentioned three methods in the calculation of sensitivity coefficients, it is clear that the variational method could be advantageous if the number of unknown parameters (N_p) is greater than the number of measurement sensors (N_s). On the other hand, if $N_p < N_s$, the influence coefficient and sensitivity equation methods are preferred. Dogru and Seinfeld (1981), McElwee (1982), and Sykes et al. (1985) showed that in order to reduce the computational

times in solving inverse problems, an efficient method was needed to calculate the sensitivity coefficients.

1.5 GOAL

The goal of this study is to predict the maximum normal tissue and minimum tumor temperatures in the treatment region during hyperthermia treatments from a limited number of temperature measurements. In most of simulated hyperthermia treatments studied here it is assumed that the perfusion model (pattern) is given but not the magnitude of the perfusion for each zone. A (semi-linear) state and parameter estimation algorithm has been developed to estimate the perfusion field and thus predict the complete temperature field.

Several tasks are investigated in this dissertation. First, some fundamental characteristics of the multiple solutions (i.e., nonunique solutions) for this inverse problem are first studied. To show the nonuniqueness of this inverse hyperthermia temperature estimation problem, we start from a simple one-dimensional case and then extend to a more complicated three-dimensional case. A general rule for determining the number of global minimum points is obtained. Second, in an attempt to reduce the computational time for the optimal algorithm, several efforts are made to: (1) develop and utilize three methods of forming the Jacobian (or the sensitivity) matrix-- the influence coefficient method, the sensitivity equation method, and the adjoint formulation; and (2) implement a semi-linear scheme to establish a criterion to reduce the need for repeated evaluations of the elements in the Jacobian matrix. Third, the effect of model

mismatch on the performance of the estimation algorithm is studied for a simple one-dimensional case. It is our goal to use this simple model to understand the characteristics of the effects of model mismatch and then to apply them to more complicated problems which may occur in clinical situations. Finally, a modified state and parameter estimation algorithm is developed to utilize the transient power-on temperatures to estimate either the uniform power or the blood perfusion, or both. To simulate the ultrasound hyperthermia treatments, the power field is a function of space, which is generated from a scanned and focussed ultrasound transducer system, rather than a uniform power.

CHAPTER 2

METHODOLOGY

During hyperthermia treatments, the complete temperature field throughout and surrounding the treated tissue should be carefully controlled to maximize the effectiveness of the treatment, while minimizing the risk of damage to the surrounding tissue. However, the temperature can be monitored at only a few discrete locations throughout the treatment region due to practical limitations. In addition, due to the complexity and diversity of the vascular system in vivo, its corresponding heat transfer in the treatment region is hard to quantitively measure. Therefore, it is difficult to solve any governing equation directly with these uncertain factors. (Note that the thermal model used in this dissertation was Pennes' bioheat transfer equation (1948).) Because of these difficulties, inverse techniques are being developed to estimate the spatial distribution of blood perfusion which, in turn, can be used in the bioheat transfer equation to estimate the complete temperature distributions that exist during particular hyperthermia treatments. In this dissertation, the first step in estimating the spatial distribution of blood perfusion is to use the zonal approach by approximating the perfusion field in

terms of a spatially dependent parameterized model with N_p parameters. The resulting model was then used in a bioheat transfer equation simulation of a treatment which was solved using finite difference schemes for the temperatures at the locations for which internal temperature measurements were available. The parameters in the perfusion model are adjusted such that the resulting predicted temperatures agree with the measured temperatures in a least-squares sense. This requires a nonlinear minimization procedure. A common approach is to use Gaussian minimization which utilizes an estimate for the Jacobian matrix to refine the latest guess for the unknown parameters as used by many investigators (Clegg, et al. 1986, Liauh 1988, Liauh, et al., 1991). Figure 2.1 shows the flow chart of the estimation algorithm utilizing an iterative Gauss method.

2.1 GAUSS METHOD

In this inverse hyperthermia application, the major goal is to estimate the complete steady-state temperature field during a treatment in which the perfusion field is unknown. Thus, to reach this goal one attempts to estimate the magnitudes of a piecewise continuous spatially dependent perfusion W using a limited number of temperature measurements (T_m),

$$T^j_{m,i} = T_m(x_i, y_i, z_i, t_j), \qquad (2.1)$$

where $i=1,2,\ldots,N_s$ and $j=1,2,\ldots,N_t$. N_s denotes the number of temperature sensors and N_t denotes the number of sampling time steps.

STATE AND PARAMETER ESTIMATION ALGORITHM

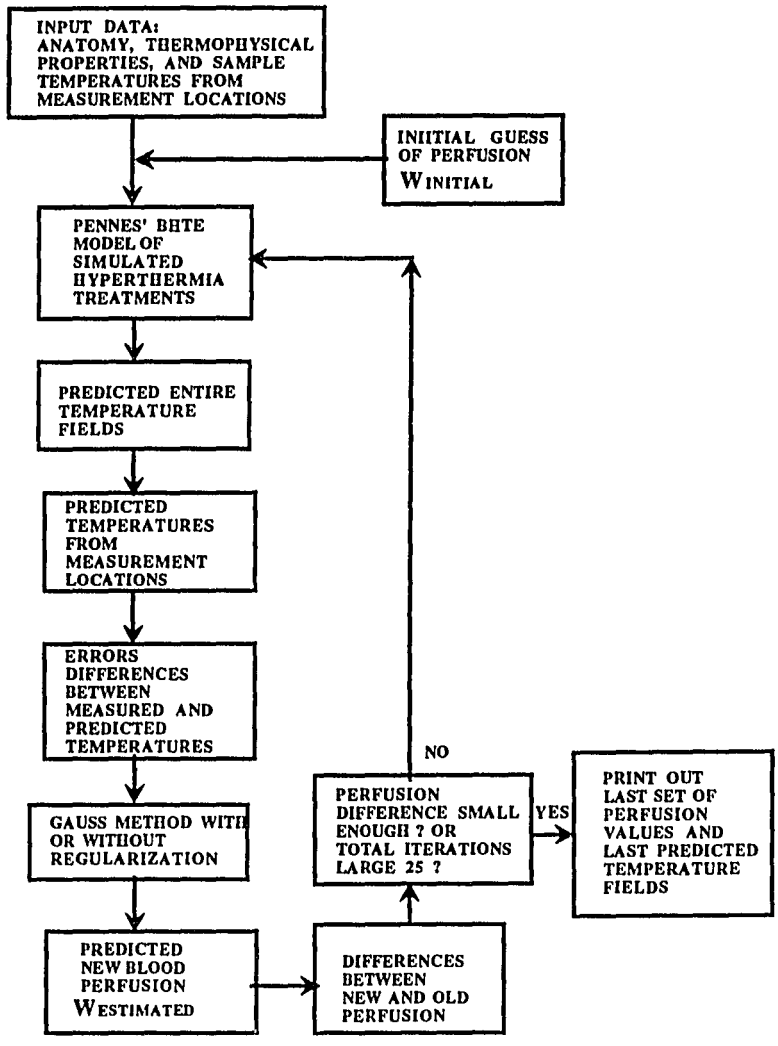

Figure 2.1 Flow chart showing the process of predicting the complete temperature field using state and parameter estimation algorithms by optimizing the unknown perfusion parameters in the bioheat transfer equation.

These transient temperatures are introduced in order to obtain additional data for use in the inverse calculations. An iterative Gauss method is used to optimize the unknown perfusion parameters by minimizing the least-squares difference between the predicted and measured temperature fields. When an estimated perfusion vector is used during a search for the true solution they are denoted as the predicted temperatures, T_{pr}. The least squares objective function (S) to be minimized in these inverse problem solutions (for which the true perfusion vector is assumed to be unknown) is defined as

$$S = E^T E. \qquad (2.2)$$

Here the error vector E has dimension $(N_s \times N_t) \times 1$, and is defined as the sum of the differences between the true and the predicted temperatures,

$$E_\xi = (T^j_{m,i} - T^j_{pr,i})$$

with $\xi = (i-1) \times N_t + j$

where $i = 1,\ldots,N_s$ and $j = 1,\ldots,N_t$.

This iterative method requires the calculation of a Jacobian matrix (J), whose elements are the first derivatives of the predicted temperatures at the measurement locations and times with respect to the unknown perfusion parameters. Once the Jacobian is obtained, the latest estimates for the unknown perfusion parameters can be expressed in terms of

$$W^{new} = W^{old} + (J^T J)^{-1} J^T [T_m - T_{pr}], \qquad (2.3)$$

where T_{pr} is the vector of predicted temperature at the measurement locations. A detailed derivation of equation (2.3) was given by Liauh (1988).

2.1.1 INPUT TEMPERATURE MEASUREMENTS

Using Gauss' method the unknown perfusion parameters are optimized by minimizing the least-squares difference between the predicted and measured temperatures at a limited number of locations and times. For the simulated clinical hyperthermia cancer treatments, the measurement temperatures are recorded from the beginning to the end. That is, the measurement temperatures include the transient power-on, steady-state, and transient power-off temperatures. Clegg, et al. 1985 proposed algorithms to solve this inverse problem by using the steady-state temperatures for simulated hyperthermia treatments. That is, N_t is equal to 1 in equation (2.1). Clegg concluded that using the steady-state temperatures only for this problem, the number of unknown parameters and the number of the measurement sensors should be identical to obtain accurate reconstruction of the temperature field. To improve the performance of Gauss' method, Clegg et al. (1988), Liauh 1988, and Liauh et al. (1991) have used both the steady-state and transient power-off temperatures instead of the steady-state temperatures only. That is, N_t is greater than 1 in equation (2.1). The steady-state data (as j=1) is a result of the introduction of an

experimental power (Q), and the transient data (j≥2) is a result of the subsequent transient decay following a power-off (Q=0). With more information obtained from the transient power-off temperatures the temperature field can be accurately reconstructed from a limited number of temperature sensors in which the number of unknown perfusion parameters are greater than the number of temperature sensors. One of the disadvantages of using the steady-state and/or the transient power-off data is that we have to calculate the steady-state temperature field for the simulated treatment, or wait until the steady-state temperature field has been reached during the clinical treatment.

To overcome this problem the transient power-on temperatures for the first few minutes of treatment were used as input data for the optimization algorithm to accurately estimate the blood perfusion, and then to evaluate the corresponding steady-state temperature field. These transient power-on data (including the initial temperatures j=1) is a result of the introduction of an experimental power (Q), which is either a uniform power or the scanned focussed ultrasound power. From several dog's thigh experiments, it is seen experimentally that there exits a certain time during which the temperature rises linearly with the applied power. In this period, the effect of the blood perfusion term on the temperature field is small and can be neglected. Using this fact, we also try to use the transient power-on data to estimate the magnitude of the uniform power or the attenuation coefficient of a scanned, focussed ultrasound power field. During the heating-up procedures in the clinical treatments, the perfusion could change

because of vessel dilation, especially when the tissue temperature rise is too high. As can be expected, the resulting perfusion estimate based on the initial transient power-on data will not be good enough to describe the final steady-state temperature field for a fixed applied power field. Nevertheless, these initial transient power-on data can still provide information to estimate the attenuation coefficient of the ultrasound power and the initial perfusion. When the attenuation coefficient is accurately estimated from the transient power-on data the ultrasound power field used to calculate the final steady-state temperature field can be easily evaluated. Although the initial perfusion is not good enough, this perfusion can be used as a priori information for estimating the final perfusion field for the final steady-state temperature field. When the scheme using the transient power-off temperature data is introduced to estimate the final steady-state temperature field, the applied power field is always known and a good initial guess of the blood perfusions can also be obtained from the transient power-on solutions.

2.1.2 REDUCING OF THE COMPUTATIONAL TIME

In an attempt to reduce the computational time for the estimation algorithm, two efforts were investigated in this dissertation. First, a fast way to evaluate the sensitivity coefficients of the Jacobian matrix is investigated. Second, a semi-linear scheme to establish a criterion to reduce the need for repeated evaluations of the elements in the Jacobian matrix is investigated.

2.1.2.1 FORMING THE JACOBIAN MATRIX

The Jacobian matrix (J) relates small changes in the unknown parameters to small changes in the predicted temperatures at the measurement locations and times. The elements of the Jacobian matrix, sometimes called the sensitivity coefficients, are the partial derivatives of the temperature with respect to each of the parameters. These elements depend on the latest guess for the parameters and are usually recalculated during each iteration. The resulting set of linear equations are used iteratively until satisfactory convergence in the parameter values is obtained. Unfortunately, the evaluation of the Jacobian matrix is numerically very CPU intensive and its evaluation dominates the CPU effort in the nonlinear estimation procedure.

Literature reviews indicate that three methods have been proposed to estimate the elements in the Jacobian matrix in the past. They are the influence coefficient method (Becker and Yeh 1972), the sensitivity equation method (Beck and Arnold 1977), and the variational, or adjoint method (Hills and Hensel 1986, Jacquard and Jain 1965, and Carter et al. 1974).

INFLUENCE COEFFICIENT METHOD

The influence coefficient method uses small perturbations from the latest estimate for the parameters to approximate the sensitivity coefficients (Liauh 1988). To obtain these coefficients the bioheat transfer equation is first solved once using the latest estimate for the parameters without perturbation. Then a parameter in the unknown

perfusion field model is perturbed and the resulting perfusion field is used in the numerical approximation to the bioheat transfer equation to find the perturbed temperatures at all of the measurement locations and times. The derivatives in the Jacobian matrix are then approximated using finite differences, i.e., J can be expressed as

$$J = \begin{bmatrix} \frac{\partial T^1_{pr,1}}{\partial W_1} & \frac{\partial T^1_{pr,1}}{\partial W_2} & \cdots & \frac{\partial T^1_{pr,1}}{\partial W_{N_p}} \\ \frac{\partial T^2_{pr,1}}{\partial W_1} & \frac{\partial T^2_{pr,1}}{\partial W_2} & \cdots & \frac{\partial T^2_{pr,1}}{\partial W_{N_p}} \\ & \vdots & & \\ \frac{\partial T^{N_t}_{pr,1}}{\partial W_1} & \frac{\partial T^{N_t}_{pr,1}}{\partial W_2} & \cdots & \frac{\partial T^{N_t}_{pr,1}}{\partial W_{N_p}} \\ \frac{\partial T^1_{pr,2}}{\partial W_1} & \frac{\partial T^1_{pr,2}}{\partial W_2} & \cdots & \frac{\partial T^1_{pr,2}}{\partial W_{N_p}} \\ & \vdots & & \\ \frac{\partial T^{N_t}_{pr,N_s}}{\partial W_1} & \frac{\partial T^{N_t}_{pr,N_s}}{\partial W_2} & \cdots & \frac{\partial T^{N_t}_{pr,N_s}}{\partial W_{N_p}} \end{bmatrix}$$

where the element $\partial T^j_{pr,i}/\partial W_n$ of the Jacobian represents the rate of change of the predicted temperature at position (x_i, y_i, z_i), and at the discrete sampling time t_j, with respect to the perfusion in zone n. This procedure is repeated once for each of the N_p perfusion parameters. In addition, the bioheat transfer equation is solved once

using the latest estimate for the parameters without perturbation. A total of N_p+1 solutions to the bioheat transfer equation are thus required to estimate the sensitivity coefficients for each evaluation of the Jacobian matrix. This means that the number of bioheat transfer solutions required for the evaluation of the Jacobian is linearly related to the number of unknown perfusion parameters, and is not related to the number of measurement sensors. In this method the elements of the Jacobian is computed numerically using a forward difference method where the step size is 10% of the current perfusion estimate except when the perfusion is less that 1.0 kg/m^3-s; then the step size is fixed at 0.1 kg/m^3-s.

SENSITIVITY EQUATION METHOD

In this approach, a set of equations are derived for the sensitivity of the temperature distribution to the N_p unknown parameters, by taking the partial derivatives with respect to each parameter in the governing equation and initial and boundary conditions. After taking the partial derivatives, the following set of sensitivity equations for the bioheat transfer equation result:

$$\rho c \frac{\partial\left(\frac{\partial T}{\partial W_i}\right)}{\partial t} = k\nabla^2\left(\frac{\partial T}{\partial W_i}\right) - Wc_b\left(\frac{\partial T}{\partial W_i}\right) - \left(\frac{\partial W}{\partial W_i}\right)c_b(T - T_a) \qquad (2.4a)$$

with the initial and boundary conditions

$$\frac{\partial T(x,y,z,0)}{\partial W_i} = 0, \qquad (2.4b)$$

$$\frac{\partial T(x,y,x,t)}{\partial W_i} = 0 \quad \text{on the boundary surfaces } \Gamma \qquad (2.4c)$$

for $i = 1,2,\ldots,N_p$.

Letting $X_i = \partial T/\partial W_i$, and assuming that $W=W(x,y,z)$ is a piecewise constant distribution, that is, when the zonal approach is used, the entire domain (Ω) is divided into N_p zones (Ω_i, $i=1,2,\ldots,N_p$),

$$W(x,y,z) = \sum_{n=1}^{N_p} W_n h_n,$$

where $h_n=1$ inside subregion Ω_n and $h_n=0$ outside Ω_n, the resulting sensitivity equations yield

$$\rho c \frac{\partial X_i}{\partial t} = k\nabla^2 X_i - Wc_b X_i - h_i c_b(T - T_a) \qquad (2.5a)$$

with the initial and boundary conditions

$$X_i(x,y,z,0) = 0, \qquad (2.5b)$$

$$X_i(x,y,z,t) = 0 \quad \text{on the boundary surfaces } \Gamma \qquad (2.5c)$$

for $i = 1,2,\ldots,N_p$.

The values of $T=T(x,y,z,t)$ are obtained from the solution of the bioheat transfer equation. If we replace the term $h_l c_b(T-T_a)$ as Q, the set of sensitivity equations would be of the same form as that of the bioheat transfer equation. Hence, the numerical schemes used for solving the bioheat transfer equation can be used to solve the set of sensitivity equations. Again, as in the influence coefficient method one partial differential equation must be solved for each unknown parameter and one must be solved for the bioheat transfer equation for a total of N_p+1 solutions to form the Jacobian matrix. As is the case for the influence coefficient method, the number of measurement locations does not affect the number of partial differential equations requiring solution per iteration.

ADJOINT FORMULATION

In contrast, the variational or adjoint method (Hills and Hensel 1986, Jacquard and Jain 1965, and Carter et al. 1974) utilizes integral equations with kernels which are derived from solutions to the governing partial differential equation. To evaluate these integrals, the governing partial differential equation has to be solved once and the partial differential equation for the adjoint variable has to be solved for N_s adjoint variables, where N_s is the number of measurement sensors. These solutions are obtained numerically, and the results used to evaluate the multidimensional integrals which then provide estimates for the sensitivity coefficients. Since the adjoint method requires N_s+1 rather than N_p+1 partial differential equation solutions to estimate the Jacobian

matrix, the adjoint method has the potential of being more efficient than the influence coefficient method when the number of unknowns (N_p) exceeds the number of measurement sensors (N_s). While the adjoint method appears to have promise when the number of sensors is less than the number of unknown perfusion parameters, the realization of that potential will rely on the particular problems. We know of no application of this method to the bioheat transfer equation for which a faster inversion process would be beneficial for generally reducing computational time, but it is particularly useful when inverse solutions are used in adaptive control schemes. Since it is clinically preferable to minimize the number of sensors present during a treatment, it is thus of interest to investigate inverse methods that have advantages when N_s is small, such as the adjoint approach.

An adjoint formulation is derived, as below, to evaluate the Jacobian matrix. To obtain the adjoint formulation let

$$\tilde{T} = T(x,y,z,t) - T_a(x,y,z,t) \tag{2.6}$$

with $T_a(x,y,z,t)$ satisfying

$$\rho c \frac{\partial T_a}{\partial t} = \nabla \cdot (k \nabla T_a).$$

Equation (1.1) can be rewritten as

$$\rho c \frac{\partial \tilde{T}}{\partial t} = \nabla \cdot (k \nabla \tilde{T}) - W c_b \tilde{T} + Q \tag{2.7a}$$

$$\text{I.C.: } \tilde{T}(x,y,z,0) = f(x,y,z) - T_a(x,y,z,0) \tag{2.7b}$$

$$\text{B.C.: } \alpha \tilde{T} + \beta (\partial \tilde{T}/\partial n) = g(x,y,z,t) - (\alpha T_a + \beta (\partial T_a/\partial n)) \text{ on } \Gamma \tag{2.7c}$$

A system of integral equations are now developed which relates the variation in $\tilde{T}$ to perturbations in the perfusion parameters. Let δW represent the perturbation in W and $\bar{T} = \tilde{T}+\delta T$ be the solution of equation (2.7) corresponding to $W+\delta W$; that is,

$$\rho c \frac{\partial \bar{T}}{\partial t} = \nabla\cdot(k\nabla\bar{T}) - (W+\delta W)c_b\bar{T} + Q \qquad (2.8a)$$

$$\text{I.C.: } \bar{T}(x,y,z,0)=f(x,y,z)-T_a(x,y,z,0) \qquad (2.8b)$$

$$\text{B.C.: } \alpha\bar{T}+\beta(\partial\bar{T}/\partial n)=g(x,y,z,t)-(\alpha T_a+\beta(\partial T_a/\partial n)) \text{ on } \Gamma \qquad (2.8c)$$

Subtracting equations (2.7) from equations (2.8) and assuming $\delta W\delta Tc_b$ is negligible yields

$$\rho c \frac{\partial(\delta T)}{\partial t} = \nabla\cdot[k\nabla(\delta T)] - \delta W c_b\tilde{T} - Wc_b\delta T \qquad (2.9a)$$

$$\text{I.C.: } \delta T(x,y,z,0) = 0 \qquad (2.9b)$$

$$\text{B.C.: } \alpha(\delta T)+\beta[\partial(\delta T)/\partial n] = 0 \text{ on } \Gamma \qquad (2.9c)$$

Multiplying equation (2.9) by an adjoint variable $\psi(x,y,z,t)$ and integrating over the total domain Ω and over time from zero to t_j gives

$$\int_0^{t_j}\int_\Omega \psi\left\{\frac{\partial(\delta T)}{\partial t} - \frac{1}{\rho c}\nabla\cdot[k\nabla(\delta T)] + \frac{Wc_b}{\rho c}\delta T\right\}dVdt = -\frac{c_b}{\rho c}\int_0^{t_j}\int_\Omega \psi\tilde{T}\delta W\, dVdt$$

Applying integration by parts over time, Green's first identity over space, and the initial condition (see the details in Appendix D) yields

$$\int_\Omega (\psi\delta T)\big|_{t=t_j}\, dV - \int_0^{t_j}\int_\Omega \delta T\left\{\frac{\partial\psi}{\partial t} + \frac{1}{\rho c}\nabla\cdot k\nabla\psi - \frac{Wc_b}{\rho c}\psi\right\} dVdt -$$

$$\int_0^{t_j}\int_S \frac{k}{\rho c}\left\{\psi\frac{\partial(\delta T)}{\partial n} - \delta T\frac{\partial\psi}{\partial n}\right\} dAdt = -\frac{c_b}{\rho c}\int_0^{t_j}\int_\Omega \psi\tilde{T}\delta W\, dVdt \quad (2.10)$$

Now $\psi = \psi_{ij}(x,y,z,t)$ is chosen such that

$$\rho c\frac{\partial\psi_{ij}}{\partial t} = -\nabla\cdot(k\nabla\psi_{ij}) + Wc_b\psi_{ij} \quad (2.11a)$$

and with

$$\psi_{ij}(x,y,z,t) = \delta(x-x_i)\delta(y-y_i)\delta(z-z_i) \text{ at } t=t_j \quad (2.11b)$$

$$\alpha\psi_{ij}+\beta\left(\frac{\partial\psi_{ij}}{\partial n}\right) = 0 \text{ on the boundary } \Gamma \quad (2.11c)$$

where (x_i,y_i,z_i) represents the i^{th} measured location. Letting $t=t_j-\tau$, $\phi_i(x,y,z,\tau)=\psi_{ij}(x,y,z,t_j-\tau)$ equation (2.11) can be written as

$$\rho c\frac{\partial\phi_i}{\partial\tau} = \nabla\cdot(k\nabla\phi_i) - Wc_b\phi_i \quad (2.12a)$$

and

$$\phi_i(x,y,z,\tau) = \delta(x-x_i)\delta(y-y_i)\delta(z-z_i) \text{ at } \tau=0 \quad (2.12b)$$

$$\alpha\phi_i+\beta\left(\frac{\partial\phi_i}{\partial n}\right) = 0 \text{ on the boundary } \Gamma \quad (2.12c)$$

Using equations (2.9c), (2.11), and (2.12) in equation (2.10), and the symmetry property of the convolution gives

$$\delta T(\bar{r}_i,t_j)=-\frac{c_h}{\rho c}\int_0^{t_j}\int_\Omega \phi_i(\bar{r},t_j-t)\tilde{T}(\bar{r},t)\delta W(\bar{r},t)dVdt \qquad (2.13)$$

where $\bar{r} = (x,y,z)$.

Equation (2.13) is the general adjoint solution which approximates the perturbation in $\tilde{T}$ at a measurement point (x_i,y_i,z_i) and the time (t_j) due to the variation in the perfusion distribution δW over the entire domain Ω. To develop a more specific solution to account for a given type of perfusion field, assume that $W(\bar{r})$ is a piecewise constant distribution

$$W(\bar{r}) = \sum_{n=1}^{N_p} W_n h_n, \qquad (2.14)$$

Thus, δW can be expressed as

$$\delta W(\bar{r}) \simeq \sum_{n=1}^{N_p} \delta W_n h_n. \qquad (2.15)$$

Using equation (2.15) in (2.13) yields

$$\delta T(\bar{r}_i,t_j) = \sum_{n=1}^{N_p} a_{ij}^n \, \delta W_n, \qquad (2.16)$$

where (see equations (2.6) and (2.13))

$$a_{ij}^n=-\frac{c_h}{\rho c}\int_0^{t_j}\int_{\Omega_n}\phi_i(\bar{r},t_j-t)\left\{T(\bar{r},t)-T_a(\bar{r},t)\right\}h_n \, dVdt. \qquad (2.17)$$

Ω_n is the subregion of Ω (i.e., $\sum_{n=1}^{N_p} \Omega_n=\Omega$), δW_n is a known parameter, and $h_n=1$ inside Ω_n and $h_n=0$ outside Ω_n for $n=1,2,\ldots,N_p$.

After the values of a_{ij}^n in equation (2.17) are estimated, the Jacobian matrix is formed as

$$J = \begin{bmatrix} a_{11}^1 & a_{11}^2 & a_{11}^3 & \cdots & a_{11}^{N_p} \\ \vdots & & & & \\ a_{ij}^1 & a_{ij}^2 & a_{ij}^3 & \cdots & a_{ij}^{N_p} \\ \vdots & & & & \\ a_{N_sN_t}^1 & a_{N_sN_t}^2 & a_{N_sN_t}^3 & \cdots & a_{N_sN_t}^{N_p} \end{bmatrix}. \qquad (2.18)$$

As in the influence coefficient method, a set of linear equations is obtained by rewriting equation (2.16) as

$$\delta T = J\delta W, \qquad (2.19)$$

where $\delta\bar{T}$ is a vector of size $(N_s x N_t)x1$ composed of the elements $\delta T(r_i,t_j)$; $i=1,\ldots,N_s$; $j=1,\ldots,N_t$; J is the Jacobian and δW is a vector of size $N_p x1$.

COMPARISON OF JACOBIAN MATRIX FORMULATION CPU TIME

Using the influence coefficient method to form the Jacobian matrix requires the solution of $N_p + 1$ finite difference bioheat transfer equations. No integrals need to be evaluated. Therefore, the computational time required to form a Jacobian matrix for the

influence coefficient method (see Appendix C) can be simply approximated as

$$(CPU_{JAC})_{Inf} \sim (N_p + 1) \times \tau_{FDT}. \tag{2.20}$$

Here τ_{FDT} denotes the computational time needed to solve the bioheat transfer equation for both the steady-state and transient power-off temperatures.

As is illustrated by the above procedure for the adjoint formulation, evaluating the elements in the Jacobian J requires that: a bioheat transfer equation (equation (1.1)) be solved once each iteration for the temperature field; an adjoint variable equation (equation (2.12)) be solved N_s times for each iteration; and, using these numerical results, the integrals given by equation (2.17) must then be evaluated numerically for each iteration, for each measurement location and discretized time. Theoretically, the computational time required to form a Jacobian matrix for the adjoint formulation (see Appendix C) can be approximated as

$$(CPU_{JAC})_{Adj} \sim \tau_{FDT} + N_s \times \tau_{FDA} + N_s \times \tau_{INT}. \tag{2.21}$$

Here τ_{FDA} denotes the computational time needed to obtain the solution of an adjoint variable by solving equation (2.12), and τ_{INT} denotes the computational time needed to evaluate the convolution integral(equation (2.17)). A simple rectangular rule which requires the minimum number of operations is used for the integrations of equation (2.17) over both time and space.

The ratio of the computational time required to form a Jacobian matrix for the adjoint formulation to the time required for the influence coefficient method is thus

$$\chi = \frac{(CPU_{JAC})_{Adj}}{(CPU_{JAC})_{Inf}} \tag{2.22}$$

Using equations (2.20) and (2.21) in equation (2.22) yields

$$\chi = \frac{1+\left[\frac{\tau_{INT}+\tau_{FDA}}{\tau_{FDT}}\right]N_s}{1+N_p} \tag{2.23}$$

Equation (2.23) provides a rough guideline to determine which method can form the Jacobian matrix faster for each iteration based on the values of N_p, N_s, τ_{FDT}, τ_{FDA}, and τ_{INT}. Three possible situations exist:

- $\chi > 1$, which occurs when $N_s/N_p > \tau_{FDT}/(\tau_{INT}+\tau_{FDA})$; the adjoint formulation is slower.
- $\chi = 1$, which occurs when $N_s/N_p = \tau_{FDT}/(\tau_{INT}+\tau_{FDA})$; both methods have the same speed.
- $\chi < 1$, which occurs when $N_s/N_p < \tau_{FDT}/(\tau_{INT}+\tau_{FDA})$; the adjoint formulation is faster.

It should be noted that the values of τ_{FDT}, τ_{FDA}, and τ_{INT} depend upon the numerical schemes for solving the partial differential equations of the temperature and the adjoint variables, and for the convolution integral. They can thus be expressed in terms of the basic computational operations for the algorithms; i.e., the number of nodes in space, the number of time steps, and the computational time

required for addition, subtraction, multiplication, and division (see Appendix C). Equation (2.24) can thus be written in terms of basic computer operations as

$$\chi = \frac{1}{1+N_p}\left\{1+N_s\frac{\left\{\left[1+\frac{1}{N_z}+\frac{1}{N_yN_z}+2(1+u)\right](N_t+1)/2+2^{\kappa}(9+7u+v+w)\right\}}{\left\{2^{\kappa}(9+7u+v+w)+\frac{N_{Iter}}{N_t}(9+5u+v+w)\right\}}\right\}. \quad (2.25)$$

For the VAX 8600 computer, the average values of the computational time for addition, subtraction, multiplication, and division have been tested and found to be close to one another, i.e., $u = v = w \simeq 1$. For further simplification, letting $u = v = w = 1$ and neglecting the small terms $1/N_z$ and $1/(N_yN_z)$ (in this study $N_x = N_y = N_z = 21$), equation (2.25) yields a simplified version of the basic computer operation equation

$$\chi \simeq \frac{1}{1+N_p}\left\{1+N_s\frac{1+0.14\,\frac{N_t}{2^{\kappa}}}{1+0.89\,\frac{N_{Iter}}{2^{\kappa}N_t}}\right\}. \quad (2.26)$$

Here N_{Iter} is the total number of iterations required to obtain a steady-state temperature field using an SOR (successive overrelaxation) scheme. In calculating the N_t transient power-off temperatures, if the input time interval is larger than the maximum time interval obtained from the stability analysis (Liauh 1988), there will be a need to divide this time interval into several smaller equal time intervals (2^{κ} intervals, κ a positive integer) such that the algorithm is stable. Equation (2.26) shows that the value of χ is

independent of the number of nodes in space, and the adjoint formulation becomes faster as 1) κ becomes larger; 2) N_t becomes smaller; and 3) N_{Iter} becomes larger.

There are two ways to evaluate the value of χ for a simulated hyperthermia treatment. One is to use the basic computer operation equation (equation (2.26)) (the BCOE values) as a function of N_s and N_p. The other is to measure the computational time needed by the subroutines which form the Jacobian matrices for the adjoint and influence coefficient methods, and then the values of χ (the subroutine program (SP) values) are calculated from equation (2.22) for different N_s and N_p.

2.1.2.2 SEMI-LINEARITY

An improved state and parameter estimation algorithm has been developed which decreases the total computational time required to accurately reconstruct complete hyperthermia temperature fields. During this improved iterative estimation algorithm, if the change in the unknown perfusion parameters is small a linear approximation scheme is implemented in which the old Jacobian matrix (sensitivity matrix) is used, instead of recalculating the new Jacobian matrix for the next iteration. Using equation (2.2), ΔW can be calculated and thus the perfusion vector is updated.

Since the calculation of the Jacobian is the most time consuming part of these calculations (Liauh, et. al., 1991) it is worthwhile to reduce their number as much as possible. To do this, one can look at some measure of the magnitude of ΔW. If this value is

small, it is known that W has not changed significantly between iterations, and thus it is known that J will not have changed drastically. Thus, for the next iteration the old J values can be possibly reused, thus saving significant computational time. To implement such a strategy, if the maximum absolute value of the elements in the vector ΔW is less than DELTA1, it is assumed that the search direction of the algorithm is correct and the old Jacobian matrix (based on W^k) is used for the next iteration. If the maximum absolute value of the element in the vector ΔW is larger than $DELTA_1$, it is assumed that the search direction should change and a recalculation of the Jacobian matrix (based on W^{k+1}) is needed.

The vector of perfusion values is iteratively calculated until either the root mean square difference between two successive estimates of the vectors of perfusion values is less than some small value , i.e., the norm of ΔW is less than $DELTA_2$ (here we use 0.001 kg/m^3-s, much less than $DELTA_1$) or the number of iterations exceeds some number. Here we use a maximum of 25 iterations to avoid excessive computational time for both nonconvergent and slowly converging cases.

Unfortunately, it is impossible to know a priori whether the relationship between the temperature and the perfusion is approximately linear because the perfusion field is always unknown from the clinical point of view. Theoretically, however, there are two possible situations which might activate this semi-linear algorithm. First, when the perfusion vector is close to the true solution, it is known that the relationship between the temperature and the perfusion

can be approximated to be linear since the perfusion step sizes will be small. Hence, it is not necessary to recalculate the Jacobian matrix when this situation occurs. Second, when the perfusion vector is far from the true solution but conditions are such that the relationship between the temperature and the perfusion is close to linear, it is not necessary to recalculate the Jacobian matrix for each iteration. The value of $DELTA_1$ used in the algorithm is critical. That is, if the value of $DELTA_1$ is equal to zero, the problem is essentially assumed to be totally nonlinear, and thus the Jacobian matrix needs to be recalculated for each iteration. On the other hand, when the value of $DELTA_1$ is very large, the relationship between the temperature and the perfusion is essentially assumed to be linear and the search will never vary from its original direction. Thus, if the problem is not linear, the search algorithm will not be successful. In an attempt to find an optimal value of $DELTA_1$, in which the total computational time required to obtain the final solution is minimum, but the accuracy of the estimation algorithm is not lost, several values of ERR_1 are used in this study. There were selected as 0.0, 0.01, 0.1, 0.5, 1.0, 5.0, and 10.0.

2.2 REGULARIZATION

Most inverse problems are extremely sensitive to measurement noise. By using the standard least-square methods many problems cannot be solved because of the ill-posedness inherent to least squares estimation or because of the problem itself. In these cases we are forced to recast the problem into a nonsigular, so-called regularized

problem whose solution approximates the original problem. The use of regularization parameters or regulizers may be interpreted as minimizing a norm of the unknown parameter estimates. Regularization parameters are one effective means of constraining the singular system of equations. The zero-order regularization tends to minimize the length of the parameter solution vector, the first-order regularization tends to minimize the slope of the parameter solution vector, and the second-order regularization tends to minimize the curvature of the parameter solution vector.

A modification to equation (2.3) is required to implement the Tikhonov regularizer. The zeroth-, first-, and second-oder regularization methods were derived in Appdenix E. The goal is to require that the change in the predicted perfusion (ΔW^k) for a particular iteration has some smoothness in order to prevent oscillations in the perfusion guesses which can readily occur due to the ill-posed nature of this problem and the concomitant near-singular matrices. In Appendix E, a test was given to determine which order of regularizer can have a better performance (i.e. with more successful temperature reconstructions). Results showed that the zeroth-order regularizer is better than the others. Thus, the zeroth-order regularizer will be used when the regularization method is implemented in this study. Tikhonov (1963), and Kravaris and Seinfeld (1985) have shown that for an ill-posed problem such as the present one, the following functional should be minimized to prevent oscillations in the parameter estimates and thus produce more successful, and improved solutions by using a zeroth-order regularizer:

$$g(\Delta W^k) = || J\Delta W^k - E ||^2 + \epsilon || \Delta W^k ||^2. \qquad (2.27)$$

where $||\bullet||$ is the Euclidian norm, and ϵ is the regularization parameter. Minimization of this function with respect to ΔW^k yields the modified version of equation (2.3):

$$W^{k+1} = W^k + (J^TJ + \epsilon I)^{-1}J^TE,$$

or

$$W^{k+1} = W^k + (J^TJ + \epsilon I)^{-1}J^T[T_m - T_{pr}], \qquad (2.28)$$

where I is the identity matrix. It is this regularized equation that is solved to determine the optimal perfusion relative to the measured data. It should be noted that equation (2.28) is equivalent to equation (2.3) if ϵ is equal to zero. It has been shown by Liauh et al. (1991) that there is an optimal value of regularization which is large enough to eliminate the ill-posedness, but is small enough not to significantly distort the original problem for some ill-posed, inverse problems. They concluded that the optimal value of the regularization parameter be a function of the perfusion pattern and magnitude. Therefore, in this dissertation, no attempt was made to find out the optimal value of the regularization parameter for the present perfusion fields. The values of the regularization parameter used in this dissertation were selected from the conclusions of the studies by Liauh (1988).

2.3 SCANNED FOCUSSED ULTRASOUND POWER

It has been shown that ultrasound is one of the most promising and effective heating sources for hyperthermia cancer treatments (Hynynen et al. 1985, 1987a, 1987b, 1989, Lele 1983, 1986, Lele and Goddard 1987). One of the advantages of the ultrasound device is its ability to induce well-controlled localized power depositions in tumors at different depths (Lele and Parker 1982, Lele 1983, 1986, Lele and Goddard 1987, Hynynen et al. 1985, 1987a, 1987b, Shimm et al. 1988, Harari et al. 1991, and Guthkelch et al. 1989).

In this study several assumptions were made for the numerical simulations of ultrasound power distribution. First, the effects of reflections from interfaces between the transducer, local absorption irregularities and the tissue and scattering effects were small and could be neglected. When the ultrasound waves penetrate into the tissue, it will be attenuated because of the absorption and scattering of the energy. In this dissertation, all of the attenuated energy has been assumed to be absorbed locally in the tissue to raise the tissue temperature. Second, the local ultrasound power deposition for homogeneous absorbing tissue is given by the product of the local absorption coefficient and the local acoustic intensity (Hynynen 1990). Third, the transducer radiates uniformly over its surface. The intensity distribution can be calculated by squaring the local acoustic velocity potential which is evaluated from the Rayleigh-Sommerfeld diffraction integral by applying Huygen's principle to the face of the transducer. To evaluate this double integral several investigators (Madsen et al., 1981 and Swindell et al., 1982) proposed

faster techniques to reduce the double integral into a one-dimensional integral. Their techniques reduced the two-dimensional integral into an one-dimensional integral by summing the contributions at a point in the field from all sources on the transducer face that were equidistant from this point.

In the Swindell et al.'s 1982 approach (also similar to Madsen et al. 1981), the model was based on a one-dimensional integration technique of the Rayleigh-Sommerfeld diffraction integral over the surface area (S) of the transducer. The original double integral can be written as follows:

$$\psi(r_0) = \iint_S \frac{e^{-ikr}}{r} \Phi(s)\, ds,$$

where $\psi(r_0)$ is the acoustic velocity potential; r is the distance from a source on the transducer face to the point of interest located at r_0; k is the wave number ($k = 2\pi/\lambda$, where λ is the wavelength of the ultrasound); $\Phi(s)$ is the source normal-velocity weighting function; and $i=(-1)^{1/2}$. Notice that the integration has to be evaluated for each point (r_0) of interest. For simplicity, this double integral was reduced to a single integral by assuming 1) $\Phi(s)$ is constant over the transducer; and 2) since r is now the only variable inside the integral, those elements of area on the transducer surface over which r is essentially constant are considered simultaneously. This approximation required considerably less computing effort. From the

acoustic velocity potential, the relative pressure amplitude squared distribution at r_0 was calculated as follows,

$$[P(r_0)]^2 = (kZ)^2 |\psi(r_0)|^2,$$

where $P(r_0)$ is the acoustic pressure at r_0 and Z is the specific acoustic impedance of the tissue. The absorbed power density (W/m^3) was then computed, including attenuation, from the following equation,

$$Q = \alpha Z^{-1} P(r_0)^2 e^{-2\alpha r'}.$$

Notice that the effect of soft tissue ultrasonic attenuation was accounted for by simply multiplying the right hand side of the above equation by $e^{-2\alpha r'}$ where α is the pressure amplitude linear attenuation coefficient and r' is the path length into the tissue. In order to further reduce the computational effort, r' was assumed constant at tissue planes perpendicular to the axis of symmetry of the propagating wave and equal to the normal distance from the field point r_0 to the soft tissue-water interface (this is true in the case of a planar transducer and a good approximation for many of the transducers used in this study).

CHAPTER 3

NUMERICAL SIMULATIONS

To study the performance of the state and parameter estimation algorithm, well controlled numerical experiments generating one- and three-dimensional temperature fields from limited, noisy temperature measurements were used. It is easier and more accurate to generate the measured temperatures numerically than to clinically obtain them. Numerically generated treatments also have the advantage that the complete temperature field is known and thus the accuracy of the estimated results can be evaluated-- something which is extremely difficult for real clinical conditions. These advantages make the numerically simulated treatments useful in evaluating the capabilities and limitations of the estimation procedure in its early development stages. The treatments were simulated numerically by solving equation (1.1) assuming all parameters (including the perfusion term) were known prior to a treatment. The complete temperature fields (the direct case) were determined from the steady state temperatures with a known applied power. Following a power-off transient, a limited number of the simulated transient temperatures at assigned locations were used as input data to the estimation algorithm to reconstruct the

complete temperature fields (the indirect case). These direct case transient temperatures are introduced in order to obtain additional data for use in the inverse calculations. The steady-state temperature field of the direct case was used to assess the accuracy of the estimated steady-state temperature field of the indirect case by looking at the maximum absolute temperature difference for all finite difference node locations.

In all studies, the thermophysical properties of tissue were assumed constant and known; the tissue thermal conductivity (k) was 0.5 W/m/°C; the tissue specific heat (c) was 4000 J/kg/°C; the tissue density (ρ) was 1000 kg/m^3. The arterial blood temperature (T_a) was fixed at 37 °C and the blood specific heat (c_b) was 4000 J/kg/°C. The boundary surface temperatures were all fixed at 40 °C in all simulations. For the one- and three-dimensional simulations, the sizes of the domain were 10.5 cm and 10.5 x 10.5 x 10.5 cm^3, respectively. For the three-dimensional cases, the cubic model was divided into seven perfusion zones as illustrated in Figure 3.1. The value of blood perfusion of a given zone in space was constant and varied from one zone to another. The perfusion (W) can be thought of as a vector where each element of the vector corresponds to the magnitude of the perfusion of one zone. The numbers in the lower right-hand corner of Figure 3.1 represent the elemental positions of the perfusion vector. In this simulation, the perfusion patterns were classified into two models: a symmetric model in which the perfusion pattern had high symmetry; and an asymmetric model in which the perfusion pattern had at least one direction of asymmetry.

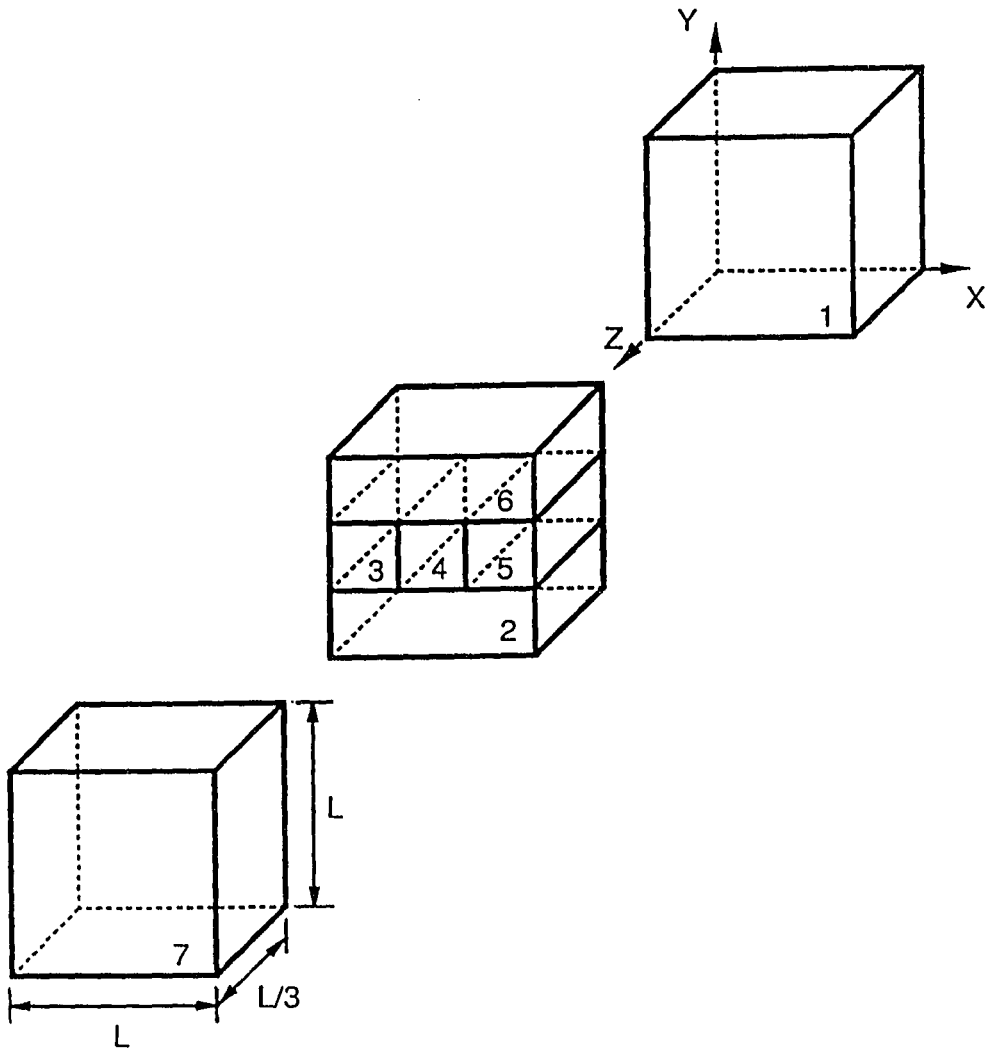

Figure 3.1 Schematic of the three-dimensional treatment model. Each zone represents a volume of different perfusion and the center of each zone is the location of the temperature measurement. The perfusion zone numbers are indicated in the near lower right-hand corner of each zone.

The steady-state temperature fields for the one- and three-dimensional models were calculated numerically in double precision using a tridiagonal temperature solver and a successive overrelaxation (SOR) scheme, respectively. In all one-dimensional cases, the grid spacing used in solving the temperature field numerically was 1 mm and the total number of finite difference nodes was 105. For the three-dimensional cases, the grid system was 21 x 21 x 21 with a uniform spacing of 5 mm. The steady-state temperature iterations were numerically terminated when the root mean square difference of the temperature fields between the last two iterations was less than 10^{-6}°C. The computed power-on, steady-state temperatures were used as the initial temperature distribution for the transient, power-off temperature calculations. The transient power-on and power-off temperature fields were calculated in double precision using an explicit forward difference formula. The finite difference time step used in calculating the transient decay data was chosen such that after one hundred time steps the complete temperature field was within 0.2 °C of the basal temperature field at all finite difference nodes. This time step interval was also used for calculating the transient power-on temperature fields for the cases with the same perfusion field. Hence, it should be noticed that after one hundred time steps the power-on temperature field may not be equal to the steady-state temperature field under the same applied power.

The parameter estimation procedure requires an initial guess for the zonal perfusions. For the zones in which temperature measurements are available, the method used calculates an initial

estimate of the overall tissue cooling coefficient (Roemer 1990). In this method, the first six temperatures at each measurement location following power off are fitted to an exponential function for the corresponding zone. Since the resulting exponent is roughly related to the perfusion immediately surrounding the measurement, perfusion at this location can be estimated. For the zones without temperature measurements, the perfusions are initially set to zero.

Since the temperature measurements in the clinic are noisy, a sequence of noisy data is created for addition to the steady-state and transient temperature measurements. Five noise levels are generated (Liauh 1988) to simulate noisy data for the simulated treatments. The noise is randomly chosen from a normal distribution with zero mean and a constant variance. The variance is chosen such that 95% of the sampled noise lies within a specified value (Liauh 1988). The direct case transient temperatures with additive noise are used as inputs to the estimation algorithm.

3.1 MULTIPLE MINIMA

The general conditions under which these multiple minima occur are shown to be solely due to the existence of symmetries in the inverse problem formulation. General rules for determining the number of global and local minimum points in the unknown parameter space are obtained for several geometrically symmetric one-, two- and three-dimensional multiple perfusion problems. A general strategy for (a) detecting when the inverse algorithm has converged to a local minimum, and (b) for using that knowledge to direct the search algorithm

towards the global minimum is presented. A three-dimensional, random perfusion distribution example is given which illustrates the effects of the multiple minima on the performance of a state and parameter estimation algorithm in reconstructing the entire temperature field during simulated hyperthermia treatments based on a limited number of temperature measurements.

None of those previous studies have addressed the problem of the possible existence of multiple minima solution which could cause the inverse search routines to converge to incorrect solutions. The present study shows that such multiple minima can exist when certain symmetries are present in the inverse problem formulation, and investigates their characteristics.

DIRECT CASE SOLUTIONS

The first studies solve a large number of direct cases to determine if and when multiple minima exist in the objective function (S) values for the one-dimensional, piecewise constant two perfusion zone case shown in Figure 3.2. That is, for a given sensor (thermocouple) location, it is of interest to determine if multiple combinations of $[W_1,W_2]$ give minima solutions, or if the only minimum which occurs is at the true perfusion $[W_1,W_2]_{true}$. Table 3.1 shows the magnitudes of the perfusions and the applied power, and the sampling time interval for three perfusion patterns. This simple geometric case is used first to illustrate the presence of multiple minima for a clearly understandable model whose results can be readily generalized to more complex problems. To illustrate the general temperature

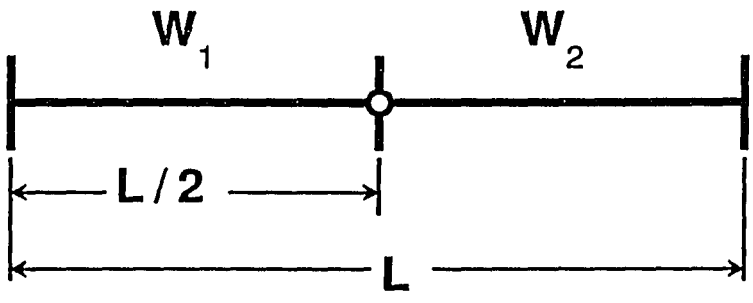

O denotes the sensor location

Figure 3.2 Schematic of the one-dimensional perfusion pattern model with 2 equal-sized zones.

Table 3.1 Perfusion vector, magnitude of applied power, and the sampling time interval for three one-dimensional, two zone models.

PERFUSION (kg/m^3-s) W_1	W_2	POWER (W/m^3) Q	TIME STEP (sec)
0.5	8.0	36,800	60
0.5	0.8	30,900	60
5.0	8.0	261,000	10

patterns present, Figure 3.3 shows the steady-state, power on spatial temperature fields used in this study for three perfusion patterns, [0.5,8.0], [0.5,0.8], and [5.0,8.0]. Figure 3.4 plots the transient power-off data versus time step for the perfusion pattern [0.5,8.0]. Curves A, B, C, D, E, and F denote the cases with the sensor at 50, 45, 40, 55, 35, and 60 mm, respectively. Figures 3.5, 3.6, and 3.7 plot constant values of S versus the perfusions W_1 and W_2 for various sensor locations for the perfusion patterns of [0.5,8.0], [0.5,0.8], and [5.0,8.0], respectively. These results were obtained by solving a large set of direct case problems for the perfusion ranges of $0 < W_1 < 10$ and $0 < W_2 < 10$ in perfusion step sizes of ΔW_1 and $\Delta W_2 = 0.1$ $kg/m^3/s$. For every pair of perfusions the objective function value S was calculated (equation 2.2) for each of the sensor locations used in Figures 3.5, 3.6, and 3.7. Results from this exhaustive search show that multiple perfusion sets minimize S. In particular, if a single sensor is located at the center (node 53) of this one-dimensional model containing two equal-sized perfusion zones, then two perfusion vectors exist that provide identical steady state and transient data at the sensor (see Figures 3.5, 3.6, and 3.7). That is, in the contour plot of S in the (W_1,W_2) space of Figure 3.5 when the sensor is located at 53 mm, for example, the true global minimum point appears at [0.5,8.0], but a second global minimum point [8.0,0.5] also appears since the thermocouple at this center location has no directional information and cannot tell its right hand from its left.

To further investigate the existence of the multiple global minimum point when sensors are located at the symmetric points of

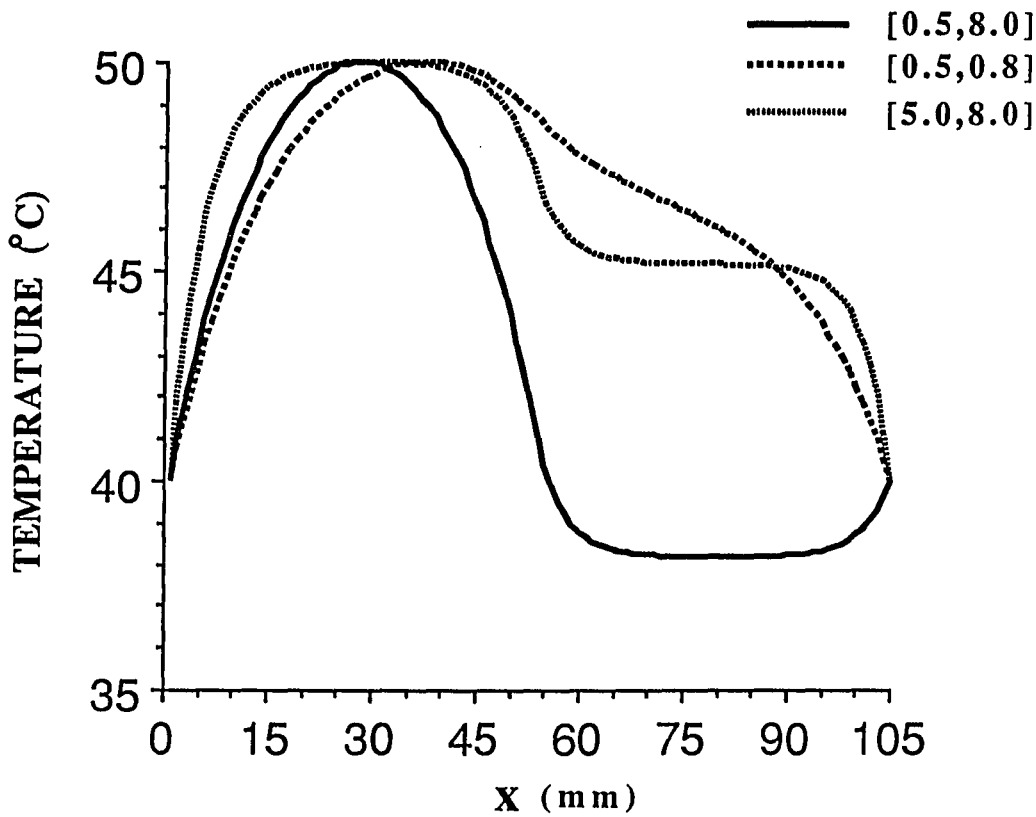

Figure 3.3 Steady-state temperature fields for the one-dimensional, two zone model with perfusion vectors [0.5,8.0], [0.5,0.8], and [5.0,8.0].

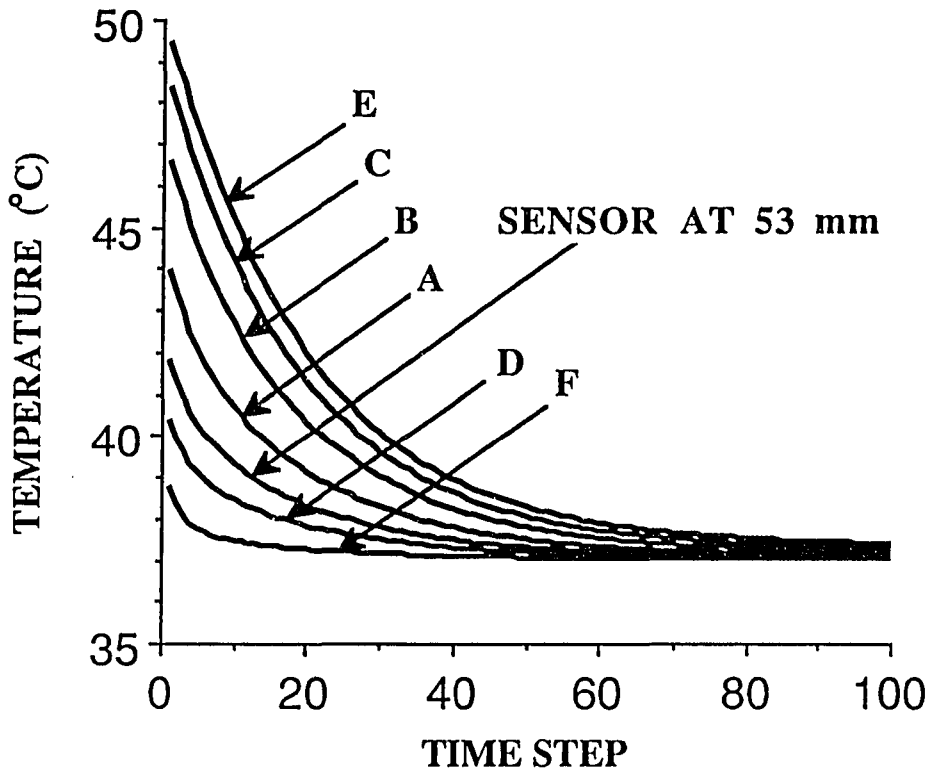

Figure 3.4 Transient decay temperatures at 7 sensor locations of 35, 40, 45, 50, 55, and 60 mm denoted by E, C, B, A, D, and F, respectively, for the perfusion vector [0.5,8.0].

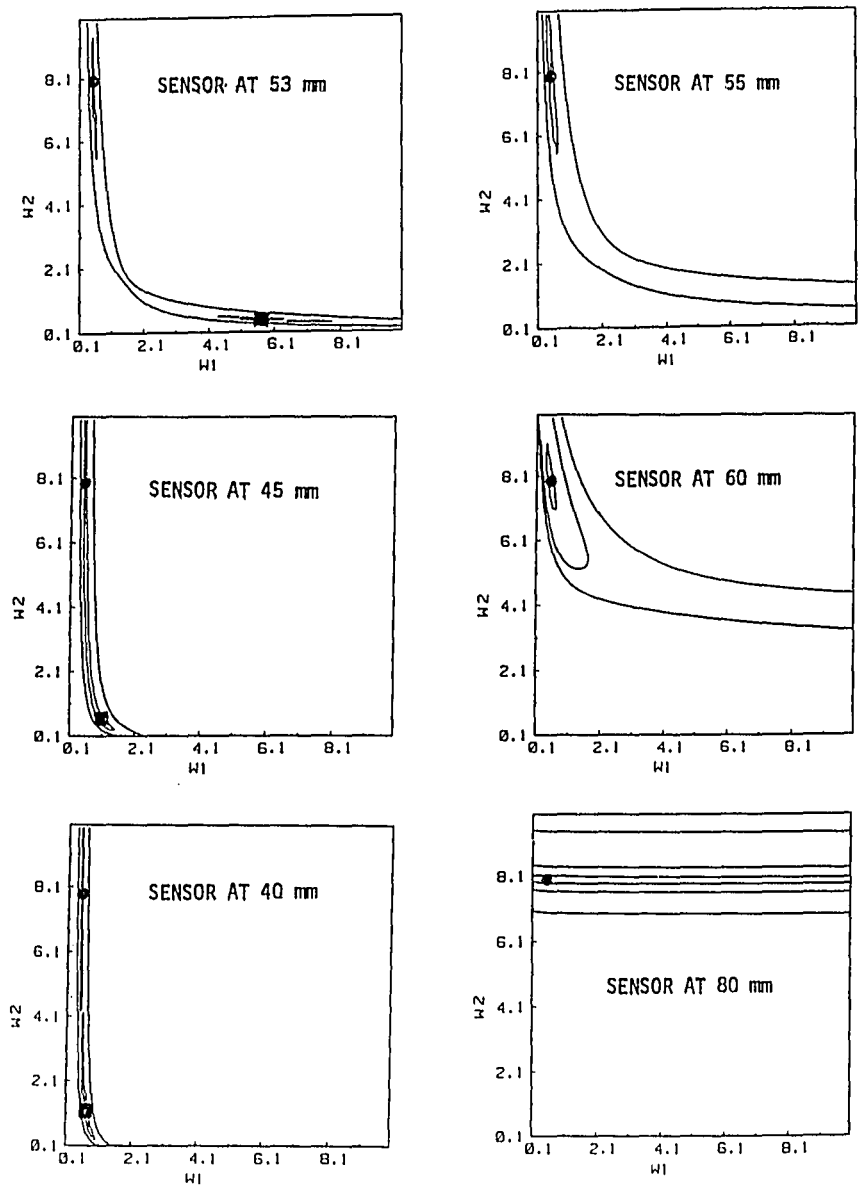

Figure 3.5 Contour plots of S versus W_1 and W_2 for the [0.5,8.0] perfusion case. S is the sum of the squared temperature differences between the transient temperature decay data for the true perfusion vector [0.5,8.0] and any case of $[W_1,W_2]$ where W_1 and W_2 are between 0 and 10 kg/m^3-s. The sensor locations are at 40, 45, 53, 55, 60, and 80 mm.

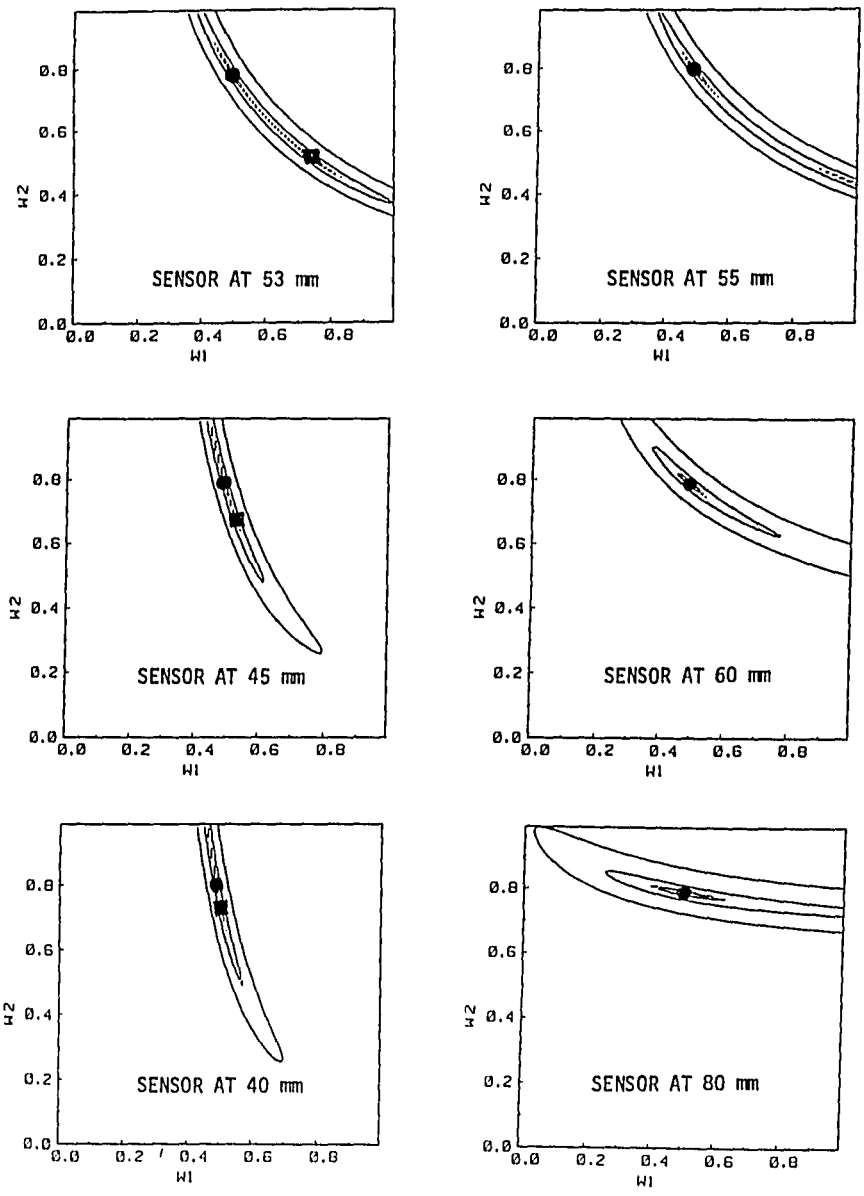

Figure 3.6 Contour plots of S versus W_1 and W_2 for the [0.5,0.8] perfusion case. S is the sum of the squared temperature differences between the transient temperature decay data for the true perfusion vector [0.5,0.8] and any case of $[W_1,W_2]$ where W_1 and W_2 are between 0 and 10 kg/m^3-s. The sensor locations are at 40, 45, 53, 55, 60, and 80 mm.

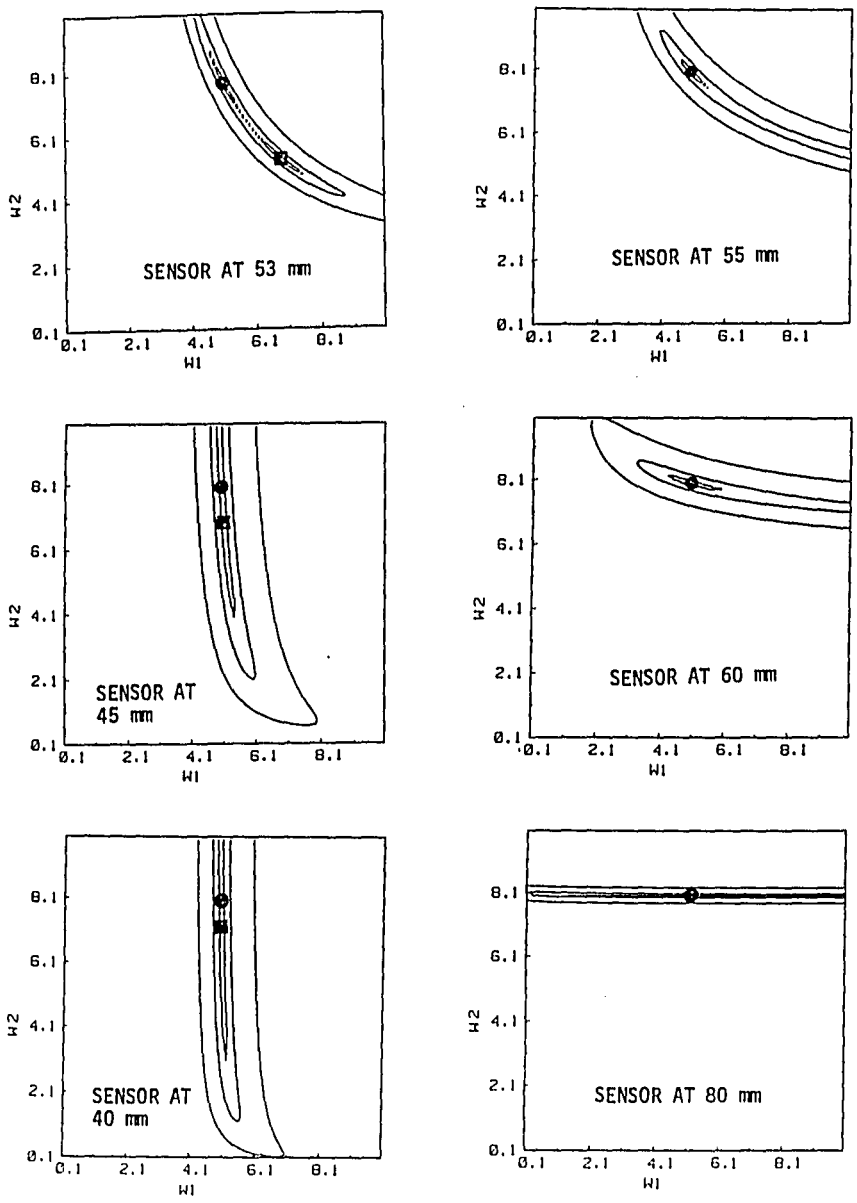

Figure 3.7 Contour plots of S versus W_1 and W_2 for the [5.0,8.0] perfusion case. S is the sum of the squared temperature differences between the transient temperature decay data for the true perfusion vector [5.0,8.0] and any case of $[W_1,W_2]$ where W_1 and W_2 are between 0 and 10 kg/m^3-s. The sensor locations are at 40, 45, 53, 55, 60, and 80 mm.

uniformly heated domains with symmetric perfusion patterns and boundary conditions, several one-, two-, and three-dimensional cases were studied. For the one-dimensional case, the domain was divided into N equal-sized zones (see Figure 3.8) with $N \geq 2$. For the two- and three-dimensional cases, the domain was divided into N^2 and N^3 equal-sized zones (see Figures 3.9 and 3.10), respectively. In choosing the new sensor locations for this study, whose results are shown in Table 3.2, the added positions were chosen to maintain the most possible symmetry, yet to always add independent information when a sensor was added. That is, using the three dimensional case to illustrate this process, when a single sensor is used it is always at the intersection of the three orthogonal axis of symmetry of the large cube defining the system (Figure 3.10). When two sensors are used, they are always located on one of those axes (e.g. the x-axis) and are equally spaced from the center point. When three sensors are used two of them are located the same as for the two sensor case, and the third is located at some point on one of the other orthogonal axis (e.g. the y-axis). When four sensors are used, the above three locations are used, and the fourth sensor is symmetrically located on the same axis as the third sensor (e.g., the y-axis) used in the three sensor case. When five sensors are used, the above four locations are used, and the fifth sensor is at the center point, as in the one sensor case. When six sensors are used, there are two sensor locations on each of the three orthogonal axes. For these geometries, simple geometric considerations show (Table 3.2) the possible number of global minimum points when there are different perfusion values for each zone. These

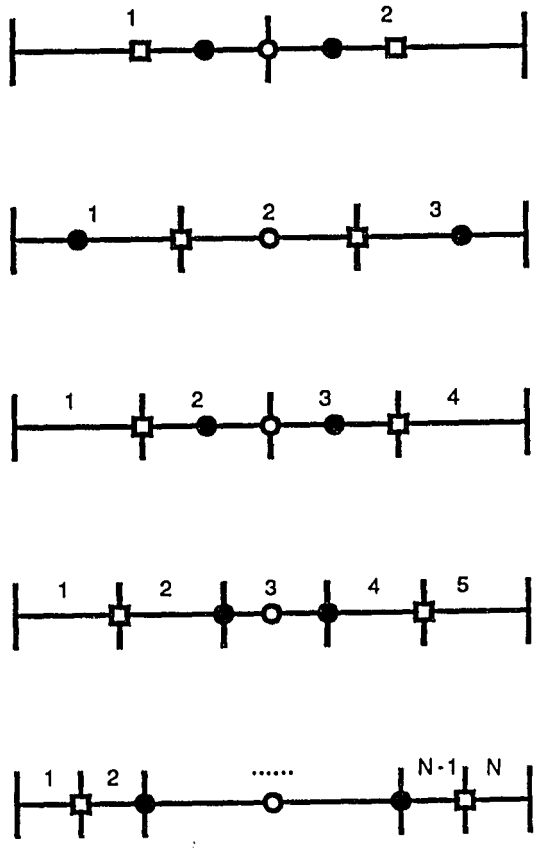

Figure 3.8 Schematic of the one-dimensional model with 2,3,4,5, and N equal-sized zones; The open circle represents the sensor location for the single sensor case; the open squares represent the sensor locations for the two sensor case; for the three sensor cases both the open squares and open circle positions were used; for the four sensor cases these same sensor positions were used (solid circles and open squares); for five sensor cases all the open squares, open circle, and solid circles were used.

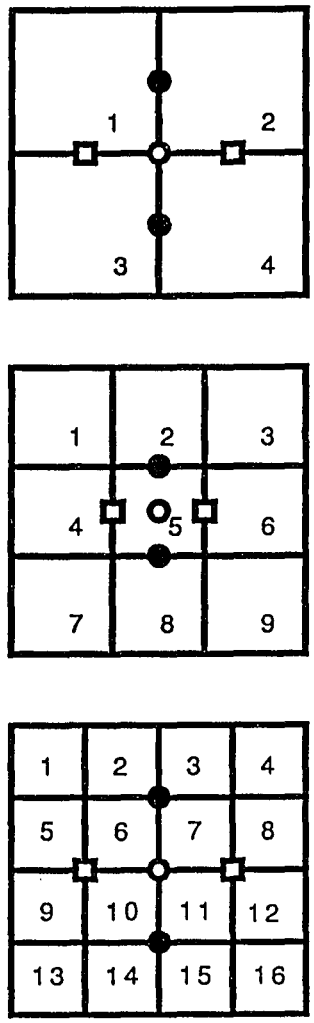

Figure 3.9 Schematic of the two-dimensional model with 2^2,3^2, and 4^2 equal-sized zones. (See Figure 3.8 for explanation of symbols)

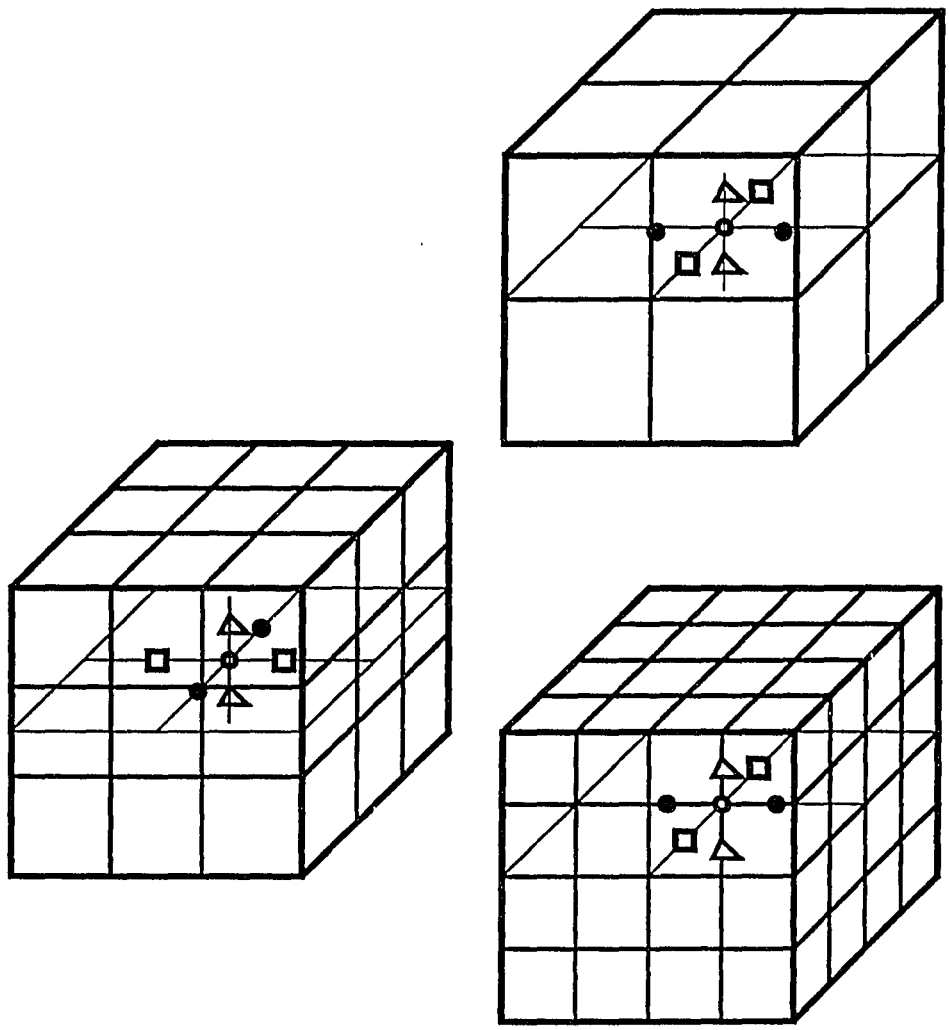

Figure 3.10 Schematic of the three-dimensional model with 2^3,3^3, and 4^3 equal-sized zones. (See Figure 3.8 for explanation of symbols, in addition, the open triangles represent additive two sensor locations for the six sensor case using the same sensor positions for the four sensor case.)

Table 3.2 The number of global minima points for the one-, two-, and three-dimensional cases when increasing numbers of sensors are located along the major axis. The added sensors are always located at positions which maintain the most symmetry with respect to axis, yet add additional directional information when this is possible without violating the symmetry condition (See Figures 3.8, 3.9, and 3.10).

Dimension	Number of Perfusion Zones (N^{ND})	Number of Global Minima Points					
		Number of Symmetrically Located Sensors					
		1	2	3	4	5	6
ND = 1	2^1	2	1	1	1	1	1
	3^1	2	1	1	1	1	1
	4^1	2	1	1	1	1	1
	5^1	2	1	1	1	1	1
	N^1	2	1	1	1	1	1
ND = 2	2^2	8	2	2	1	1	1
	3^2	8	2	2	1	1	1
	4^2	8	2	2	1	1	1
	5^2	8	2	2	1	1	1
	N^{ND}	8	2	2	1	1	1
ND = 3	2^3	48	3	2	2	2	1
	3^3	48	3	2	2	2	1
	4^3	48	3	2	2	2	1
	5^3	48	3	2	2	2	1
	N^{ND}	48	3	2	2	2	1

multiple global minima occur only when multiple symmetric perfusion patterns result in temperature signals at the sensors that are exactly the same. When the number of perfusion zones (N^{ND}) is greater than 1 (the N=1 case has only one minimum) a general rule for determining the total number of global minimum points can be obtained from Table 3.2 for the case of a single sensor. Figures 3.11 and 3.12 illustrate that all possible perfusion patterns provide exactly the same temperature signals when the sensor is located at the center of the two-dimensional domain with 2^2 and 3^2 equal-sized zones. Each number denotes the perfusion in that zone. As seen from Figures 3.11 and 3.12, all solutions are either rotating by 90° without changing the order, or exchanging rows which are symmetric with respect to the sensor location and then rotating 90°. For an ND-dimensional case, the number of such global minimum points is equal to $ND! \times 2^{ND}$.

When the number of sensors increases, the total number of global minimum points decreases rapidly to become equal to or less than the problem dimensionality (ND) regardless of the number of perfusion zones (N^{ND}) because of the additional directional information available to the algorithm. For example with only two symmetric sensors (Figure 1), the total number of global minimum points is equal to ND for all values of N. The number of global minimum points is 1 for all cases when the number of symmetrically placed sensors is greater than or equal to 2xND.

It is also of interest to study these multiple minima when asymmetries are present. First, from Figures 3.5, 3.6, and 3.7, it can be seen that as the sensor location moves away from the center

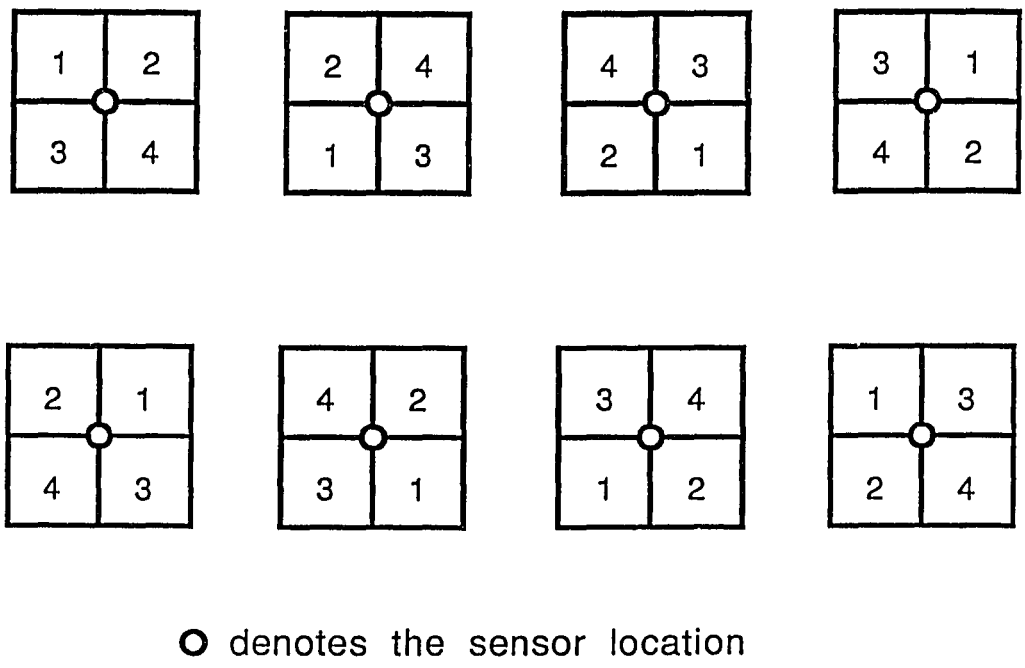

Figure 3.11 All possible perfusion patterns providing identical temperature signals at the sensor for the two-dimensional, 2^2 equal-sized zone model.

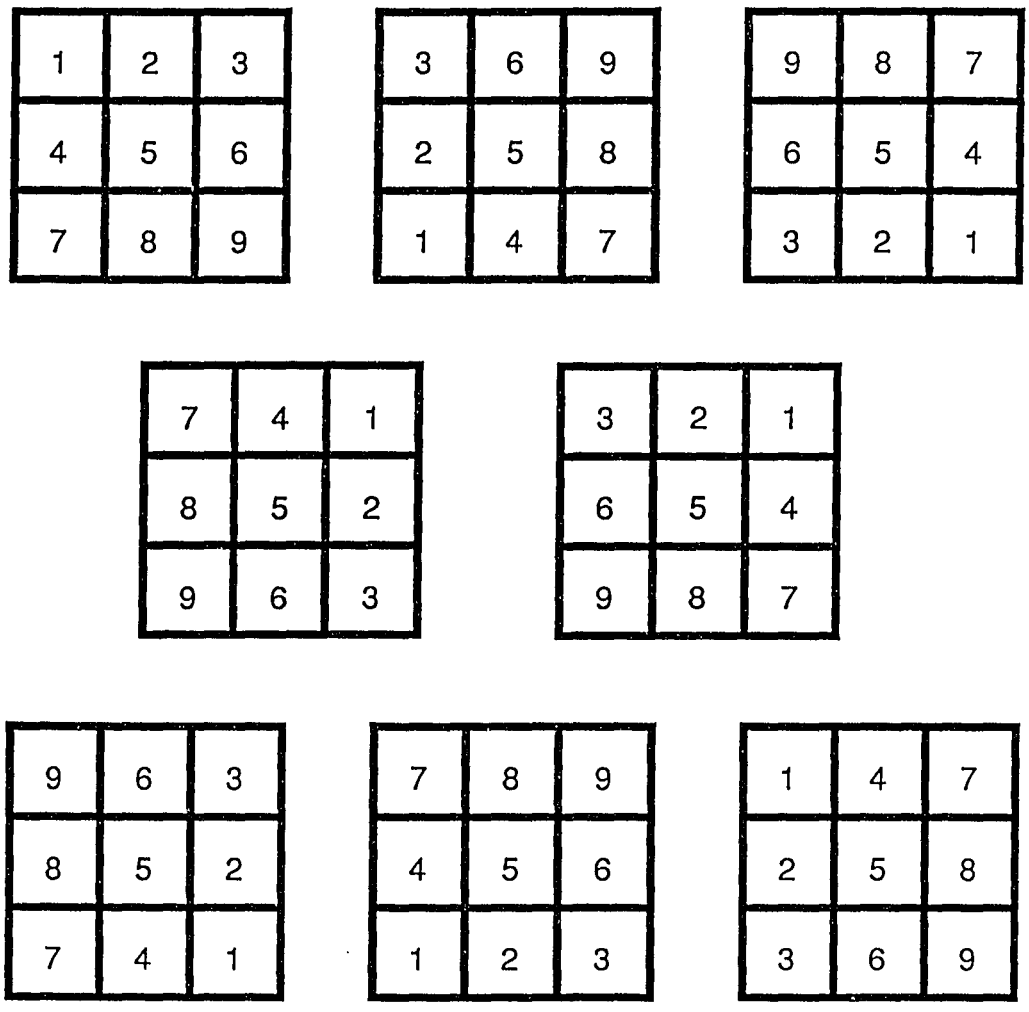

Figure 3.12 All possible perfusion patterns providing identical temperature signals at the sensor for the two-dimensional, 3^2 equal-sized zone model.

(symmetric) position the second (global) minimum point moves in the (W_1,W_2) space and takes on nonzero values of S (i.e., it becomes a local (non-global) minimum (denoted by a solid square)). For example, for the [0.5,8.0] case, when the sensor is moved away from the interface into the low perfusion zone, the true global minimum point [0.5,8.0] (denoted by a solid circle) is unchanged, but the second global minimum point [8.0,0.5] is moved to the left in the (W_1,W_2) space and becomes a local minimum with a nonzero value of S as illustrated in the left part of Figure 3.5. Second, when the sensor is moved away from the interface into the high perfusion zone, the second minimum point again becomes a local minimum and it moves to the right beyond the range of interest (i.e. $0 \leq W_1, W_2 \leq 10$ kg/m^3-s) as illustrated in the right part of Figure 3.5. To illustrate how and why these local minima change as they do, the steady-state and transient decay fields are plotted in Figures 3.13 and 3.14 for the perfusion vectors corresponding to the second minimum points for the sensor locations which were used to obtain the results in Figure 3.5. First, Figure 3.13 illustrates, as expected, that the steady-state temperature for each of the local minimum points is very close to the true steady-state temperature at the global minimum. The true field curve represents the true steady-state temperature field for the case with the perfusion vector [0.5,8.0]. Curve A represents the steady-state temperature field for the case with the perfusion vector [2.27,0.45], which is the local minimum point shown in Figure 3.5 when the sensor is located at 50 mm. Curve B represents the steady-state temperature field for the case with the perfusion vector [1.14,0.53],

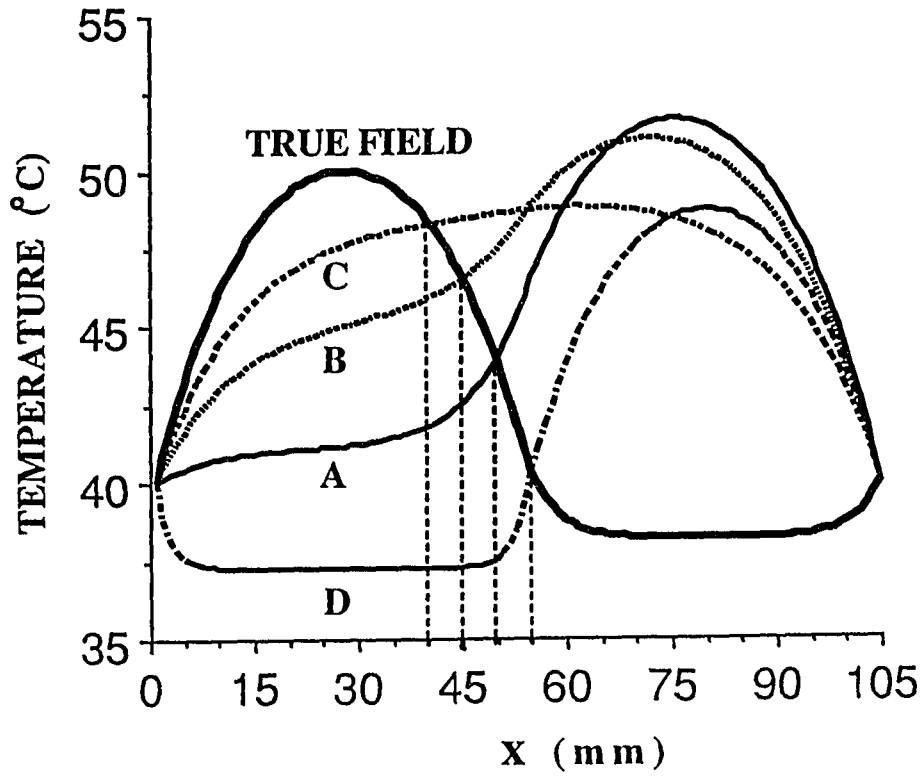

Figure 3.13 Steady-state temperature fields for the true perfusion vector [0.5,8.0] (denoted by TRUE FIELD) and for the second minimum points corresponding to the four different sensor locations are used; 40, 45, 50, and 55 mm.

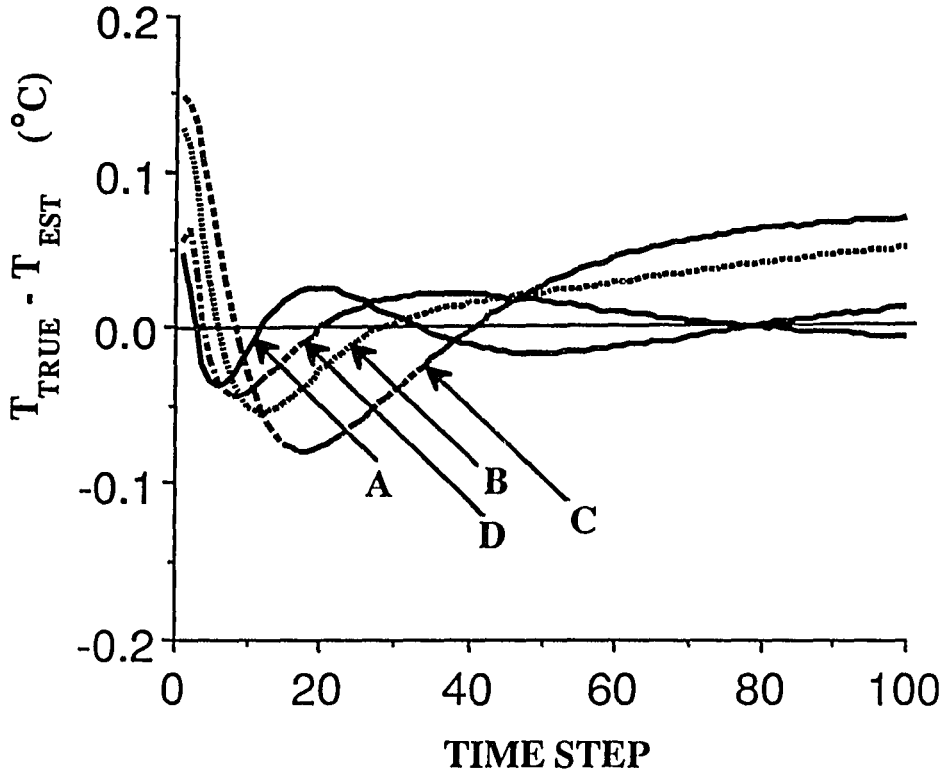

Figure 3.14 Temperature difference between the transient decay response for the true perfusion vector [0.5,8.0] and [W_1,W_2] values corresponding to the second minimum points for the sensor locations of 40, 45, 50, and 55 mm.

which is the local minimum point when the sensor is at 45 mm. Curve C represents the steady-state temperature field for the case with the perfusion vector [0.8,0.74], which is the local minimum point shown in Figure 3.5 when the sensor is located at 40 mm. Curve D represents the steady-state temperature field for the case with the perfusion vector [36.78,0.55], which is the local minimum point when the sensor is located at 55 mm. Second, Figure 3.14 plots the difference between the transient decay solutions for the true perfusion vector and the second minimum point in the (W_1,W_2) space for the same four sensor locations (40, 45, 50, and 55 mm).

To explain why the second local minimum moves as it does in Figures 3.5, 3.6, and 3.7, it is best to consider the information seen by the sensor. That is, as the sensor moves further away from the interface, it obtains more and more of its information from the perfusion zone in which it is located. Thus, the transient decay data at the sensor becomes dominated by the local perfusion value, and the second minimum point approaches a position which contains the true perfusion in that region. So, when the sensor moves to the left into region 1 the location of the second minimum approaches a position on a vertical line corresponding to the true perfusion value for region one (W_1). Similarly, when the sensor moves further into region 2, the location of the second minimum approaches a point on the horizontal line corresponding to the perfusion in region 2 (W_2). That is, when the sensor is located well into region 1, the model needs to have W_1 predicted correctly in order to obtain a good match of the actual transient decay data, but the effect of W_2 on the temperature decay

rate at the sensor location is minimal. The same general argument holds when the sensor is moved into region 2. This argument can be easily generalized to more complex cases. As the sensor is moved away from an interface, its information content becomes dominated by the perfusion of the zone in which is is located. The solution space becomes characterized by long, narrow valleys parallel to the axis of the perfusion zone in which the sensor is located. Determining the perfusion in the zone where the sensor is located becomes easier (it dominates the sensor's temperatures), but determining the perfusion values in the neighboring perfusion zones becomes more difficult. It is important to note that these troughs contain two minima (the global minimum and one local minimum), and thus they also contain a saddle point somewhere between these two minima. These saddle points are important since inverse algorithms can also converge to them since the Jacobian elements are small there, and the inverse algorithms will only call for small perfusion changes; thus the algorithms terminate. The above results have been draw from the cases shown in Figures 3.5, 3.6, and 3.7 with the perfusion vectors of [0.5,8], [0.5,0.8], and [5.0,8.0], respectively.

To illustrate the effect of other asymmetries in the above problem, consider first the [0.5,8.0] perfusion case in which the applied power is made asymmetric and is configured such that the corresponding steady-state temperature field is close to uniform (Figure 3.15). In this model, the applied power is a function of x having two values (one for each perfusion region) rather than a uniform value. Figure 3.16 plots the contour values of S in the

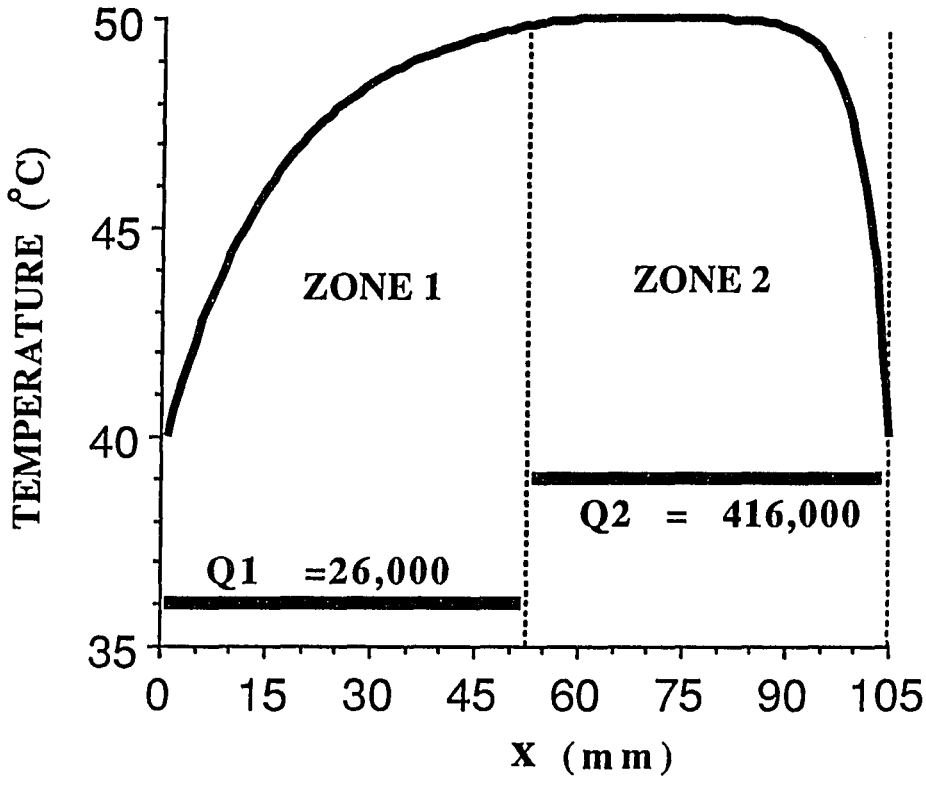

Figure 3.15 Steady-state temperature field for the [0.5,8.0] case, with an asymmetric 2 zone power vector which yields a close to uniform temperature profile.

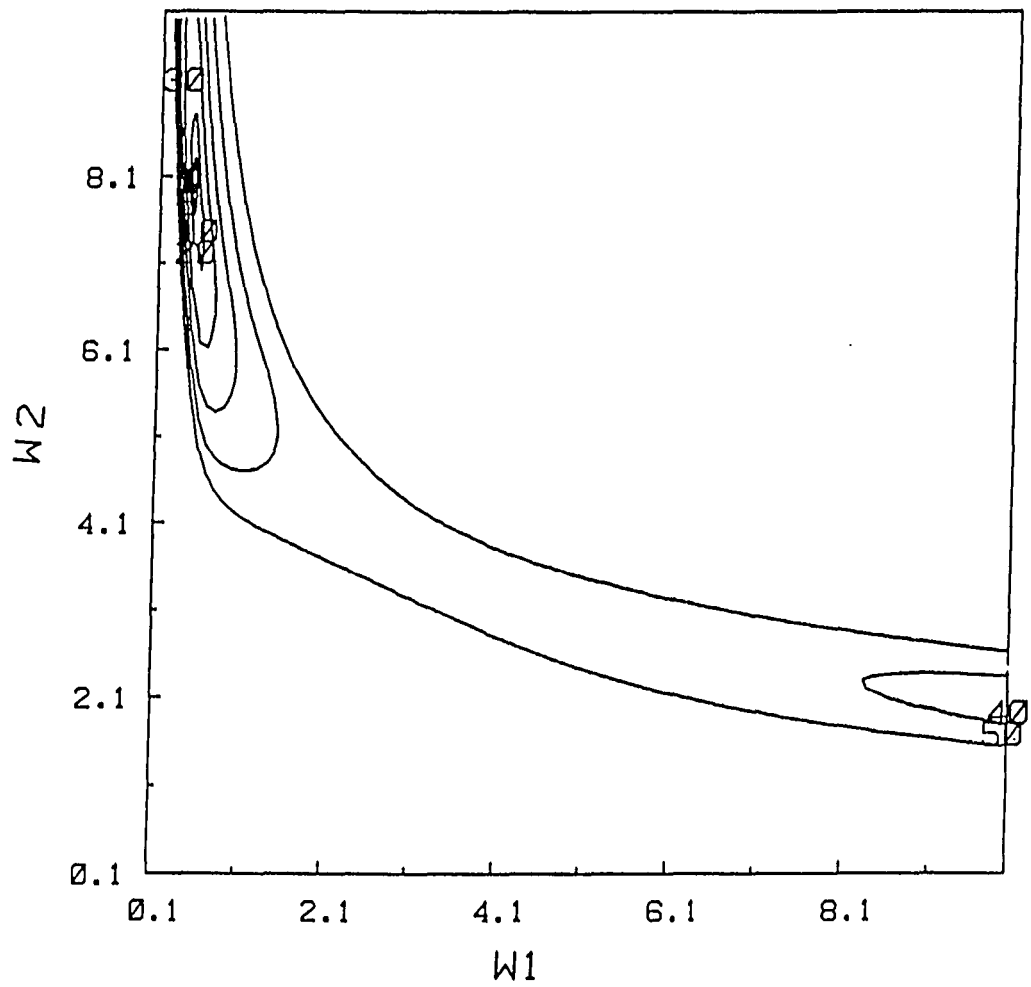

Figure 3.16 Contour plots of S versus W_1 and W_2 for the [0.5,8.0] case with the asymmetric power pattern of Figure 3.15. The sensor location is at 53 mm.

$[W_1,W_2]$ space for this problem. It shows that the second minimum point still remains but has become a local rather than a global minimum, and it has moved to the right. Second, the boundary conditions were changed to be asymmetric; at the left hand side the boundary temperature was fixed at 37 °C instead of 40 °C, and at the right hand side the boundary temperature was kept fixed at 40 °C. Figure 3.17 plots the steady-state temperature fields for the symmetric and asymmetric boundary condition cases with the same perfusion [0.5,8.0] and uniform power. Curve A denotes the symmetric boundary condition case and Curve B the asymmetric boundary condition case. Figure 3.18 plots the transient decay temperature difference between these two cases for the sensor location of 30 mm. Figure 3.19 plots the corresponding contour values of S in the $[W_1,W_2]$ space. It shows that the second global minimum point has again become a local minimum point. Because the effect of the boundary condition on the temperature measurements away from the boundary is small, the S contours for the case with the sensor at 53 mm are similar to Figure 3.5.

INVERSE CASE SOLUTIONS

Because of the existence of the local minima, any inverse solution for the perfusion vector may converge to the wrong solution (i.e., to a local minima), rather than the true one (global minimum). In particular, the final solution of the perfusion vector from the estimation algorithm can be easily trapped into, and converge to, the second minimum point if the initial perfusion vector is near the second minimum point. To illustrate this effect with a more practical,

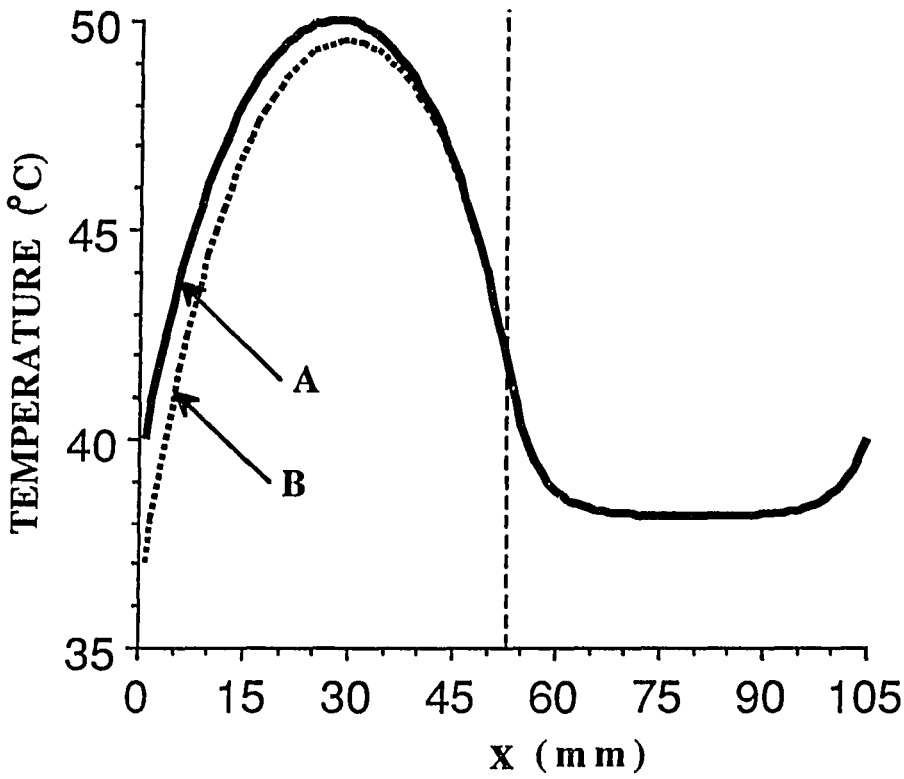

Figure 3.17 Steady-state temperature fields for the [0.5,8.0] with a uniform power but (A) symmetric boundary conditions; T(x=0) = T(x=L) = 40 °C, (B) asymmetric boundary conditions; T(x=0) = 37 °C, and T(x=L) = 40 °C.

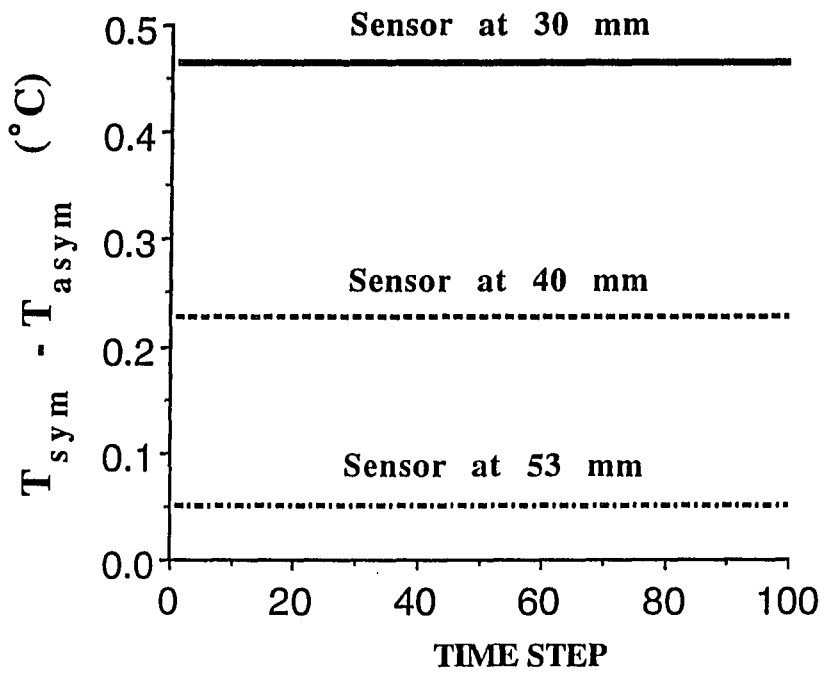

Figure 3.18 Temperature difference of the transient decay responses between the symmetric boundary conditions and the asymmetric boundary conditions at three sensor locations of 30, 40, and 53 mm for the [0.5,8.0] case.

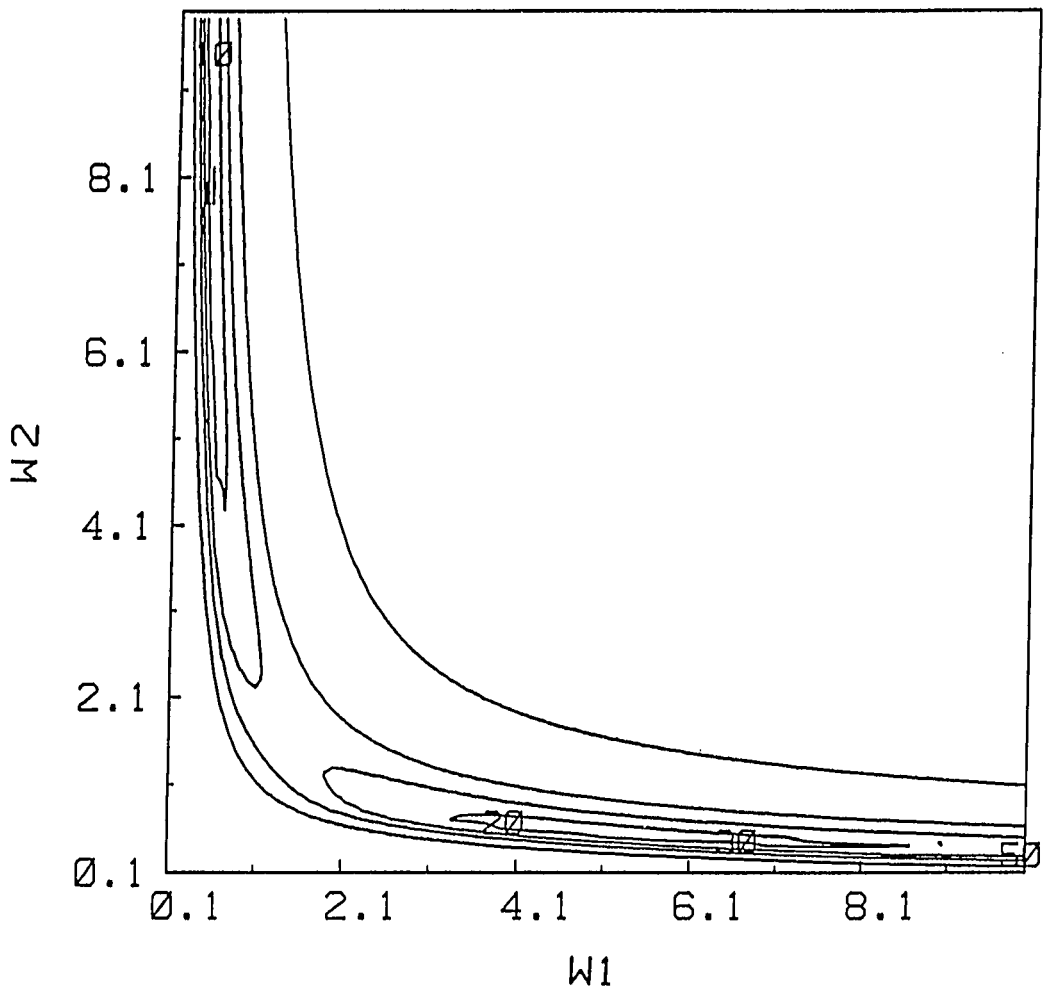

Figure 3.19 Contour plots of S as a function of W_1 and W_2 for the [0.5,8.0] case with the asymmetric boundary conditions of Figure 3.18. The sensor location is at 53 mm.

clinically realistic problem, the three-dimensional, seven zone model shown in Figure 3.1 was used to study the effects of the multiple minima. This model has also been used in previous studies to simulate a central tumor (zone 4) surrounded by normal tissue (7,8). The measurement locations were fixed at the centers of each perfusion zone. The perfusion vector was created by a random number generator which gave a perfusion vector of [0.18,0.26,0.25,0.92,0.32,0.04,1.03] as discussed by Liauh (1988). The number of sensors used to input data to the inverse algorithm varied from one to seven. Geometric considerations alone reveal that multiple minima solutions exist for this model. Table 3.3 shows that there are 8 possible symmetric solutions for the perfusion vector to provide the same steady-state and transient power-off temperatures when only one sensor is used and the sensor is located at the central position (i.e. in the center of zone 4). It is also clear that when the number of sensors increases, the number of minima will decrease. When running these inverse cases the magnitude of the regularization parameter (ϵ) was selected as 10^{-5} to avoid obtaining a singular matrix and distorting the original problem too much (Liauh 1988). The zero initial guess method (Liauh 1988) was first used to start the algorithm. For each case, the corresponding zones with sensors are listed in Table 3.4. GM represents a successful case which converged to the global minimum; LM represents a case which converged to a local minimum caused by the geometric symmetry of the perfusion pattern (the numbers in parenthesis indicate the two geometrically symmetric regions which had interchanged perfusion magnitudes); DIV indicates that the solution

Table 3.3 Eight possible global minimum points for the three-dimensional, 7 zone model as the sensor at the center point of the fourth zone shown in Figure 3.1

POSSIBLE SOLUTION	PERFUSION W_i (kg/m^3-s)						
	W_1	W_2	W_3	W_4	W_5	W_6	W_7
1	1	2	3	4	5	6	7
2	1	2	5	4	3	6	7
3	1	6	3	4	5	2	7
4	1	6	5	4	3	2	7
5	7	2	3	4	5	6	1
6	7	2	5	4	3	6	1
7	7	6	3	4	5	2	1
8	7	6	5	4	3	2	1

Table 3.4 Results of estimation searches using the zero initial guess method for cases with seven, six, four, three, two, and one sensors applied to a three-dimensional, seven zone model (see Figure 1d). The true perfusion vector is [0.18,0.26,0.25,0.91,0.32,0.04,1.03]. The applied power was uniform at 20,150 W/m^3 and the transient sampling time steps was 98. GM represents a successful case which converged to the global minimum for which the maximum temperature difference at all finite difference nodes between the true and predicted temperature fields is less than 1 °C; LM represents the cases which converged to a local minimum caused by symmetry for which the solutions had differences larger than 1 °C; DIV indicates a case for which the search was diverging after 25 iterations; SP indicates a case for which the search converged to a saddle point.

NUMBER OF SENSORS	CORRESPONDING ZONES WITH SENSORS	INITIAL SOLUTION SUCCESS
7	1-2-3-4-5-6-7	GM
6	1-2-3-5-6-7	GM
5	1-3-4-5-7	LM(2,6)
4	1-2-3-4	GM
4	1-3-5-7	LM(2,6)
3	1-2-3	GM
3	1-4-7	LM(2,6)
2	1-2	GM
2	1-3	DIV
2	1-4	GM
2	1-5	LM(2,6)
2	1-6	GM
2	1-7	DIV

Table 3.4 (continued)

NUMBER OF SENSORS	CORRESPONDING ZONES WITH SENSORS	INITIAL SOLUTION SUCCESS
2	2-3	LM(1,7)
2	2-4	GM
2	2-5	LM(1,7)
2	2-6	LM(1,7)
2	2-7	GM
2	3-4	DIV
2	3-5	LM(1,7)
2	3-6	LM(1,7)
2	3-7	LM(2,6)
2	4-5	LM(1,7),(2,6)
2	4-6	LM(2,6)
2	4-7	GM
2	5-6	LM(1,7)
2	5-7	LM(2,6)
2	6-7	GM
1	1	DIV
1	2	DIV
1	3	DIV
1	4	SP
1	5	DIV
1	6	LM(1,7)
1	7	SP

search had diverged away from the true solution after 25 iterations (and it was then terminated to save CPU time); and SP denotes that the solution had converged to a saddle point (i.e. a point located in one of the long, narrow troughs that contain the global minima and a local, symmetric minimum). All cases that are shown as local minima LM using the zero initial guess method were turned into successful (GM) cases when symmetry knowledge was used to restart the estimation algorithm. In all cases that were diverging failures (DIV) or saddle point convergences (SP) using the zero initial guess method, a successful search solution was always obtained when (a) an initial guess that was close to the true solution was used, and (b) knowledge of symmetry was utilized. That is, all cases in Table 3.4 could be turned into successful searches that converged to the global minimum when knowledge of the problems geometric symmetry was used. Other cases showing the convergence of the estimation algorithm to symmetric local minima are given by Liauh (1988).

DISCUSSION

It is clear from the present results that multiple minima (and saddle points) exist in the inverse hyperthermia temperature estimation problem, and that their presence can cause inverse algorithms to converge to an incorrect local minimum rather than to a true global minimum. These minima are present due to the symmetries that exist in the geometry of the perfusion pattern model used in the inverse algorithm. Any perfusion model which has a geometrically symmetric pattern will have multiple minima. This is true even if much

more complex perfusion models are used than the piecewise constant values used in this study. For example, Figure 3.20a (top) shows a linearly varying perfusion curve which would be indistinguishable from its symmetric image (Figure 3.20a, bottom) if a thermocouple were located at the central position (i.e. two global minima would exist for this perfusion pattern at the central sensor position). As the sensor position moves, the second global minimum would again become a local minimum which could entrap an inverse algorithm. Similarly, the sensor located in the center of Figure 3.20b would have difficulty in distinguishing between the two possible arrangments (3.20b, top and 3.20b, bottom) of the geometrically irregular and unsymmetric perfusions in region 1 (W_1) and 2 (W_2). Again, a local minima would be present. These multiple minima can be global minima if the temperature sensors are located exactly on points (or lines/or planes) of symmetry, and they will be local minima if they are not located on them.

While introducing asymmetries into the inverse problem (i.e., using asymmetric thermocouple positions, power deposition patterns, and/or boundary conditions as discussed earlier) can help in the inverse problem solution, they cannot eliminate it. Thus, when applying inverse methods, one must be aware of any symmetries present in the blood perfusion pattern used to model the actual tumor/normal tissue perfusion patterns. Fortunately, knowledge of the cause of the multiple minima can be used to avoid having an inverse solution being trapped by a local minima. That is, once a solution has been found, its mirror image can be used as a new initial guess. For example, all

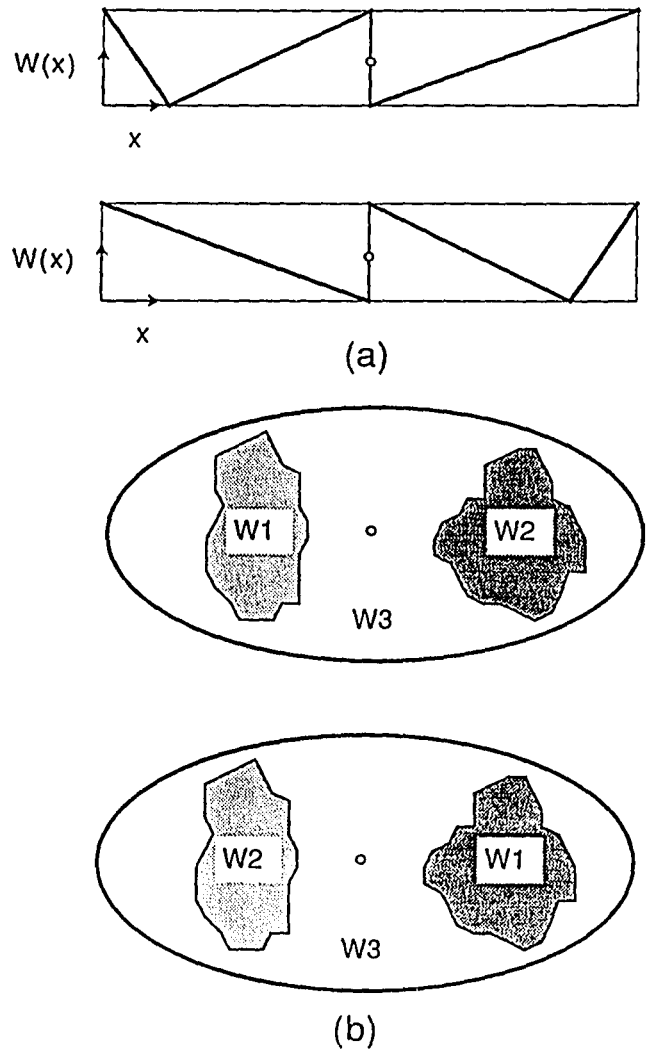

Figure 3.20 Schematic diagrams of more complex perfusion pattern models which could still contain multiple minima.

the local minimum solutions found due to symmetry in Table 3.4 were easily converted to true global minimum solutions through knowledge of the geometric symmetries in the problem. Knowledge of these symmetries is particularly important since the optimal sensor location appears to be those at (or close to) boundaries between regions so that maximum information is obtained about the perfusion field. These optimal locations not only contain the most directional information, but they also create a more robust S space in which to find the global minima. That is, the asymmetric thermocouple locations with the sensors located in the centers of the perfusion zones create long narrow channels (see Figures 3.5, 3.6, and 3.7) in which it is easy to determine the local perfusion value, but difficult to obtain the correct perfusions in neighboring regions due to the shallowness of the troughs in the directions orthogonal to the local perfusion direction.

It should also be noted that previous studies by Clegg et al., 1988 and Liauh 1988, which did not make use of knowledge of the multiple minima caused by symmetry, indoubtedly had cases which converged to a local minimum, which did a poor job of predicting the complete temperature fields. Some of those cases could have been converted into global minima using the approach proposed in the present study. Thus, the results in the previous studies could have been improved in terms of the number of cases which could be successfully analyzed by the inverse algorithm.

3.2 JACOBIAN FORMULATION

Three methods have been proposed to estimate the elements in the Jacobian matrix. As described previously, the influence coefficient method uses small perturbations from the latest estimate for the parameters to approximate the sensitivity coefficients. For the sensitivity equation method, the elements in the Jacobian matrix are obtained by solving a set of sensitivity equations. The last method is the adjoint formulation which utilizes integral equations with kernels which are derived from the governing partial differential equation. Since the computational efforts of evaluating the sensitivity coefficients for the sensitivity equation method and for the influence coefficient method are theoretically very close from the analysis from Chapter 2, the comparison of the performance of these two methods will be made later to verify the analysis. As pointed out previously, the adjoint method has the advantage of requiring fewer solutions of the bioheat transfer equation to estimate the Jacobian than does the influence coefficient method when the number of measurement sensors (N_s) is significantly smaller than the number of unknown parameters (N_p). Thus, it could be a preferable method to use in hyperthermia applications where the number of sensors is strictly limited by patient considerations. However, the adjoint method requires that CPU time intensive convolutions be numerically evaluated. The performance of the adjoint method is compared to that of the influence coefficient method for several test cases. A general rule is obtained to provide a guideline to determine if the adjoint formulation or the influence coefficient method will be faster for

given values of N_p and N_s. The technique used to develop this general rule is applicable to evaluating potential applications of other numerical schemes.

To obtain the transient solutions of the adjoint variables, the same double precision explicit finite difference scheme used for the temperature solver is also used for equation (2.12). Equation (2.12) is similar to equation (1.1) except there is no power term (i.e. Q=0), there are zero boundary conditions, and there is a Dirac Delta initial condition. Thus, the computational time (τ_{FDA}) for solving equation (2.12) is close to the computational time (τ_{EFD}) from equation (C.4) in Appendix C. In solving equation (2.12), the Dirac Delta initial conditions are numerically approximated by setting the initial condition of ϕ_I to zero everywhere except at $x=x_I$, $y=y_I$, $z=z_I$, where ϕ_I is set to be $1/(\Delta x*\Delta y*\Delta z)$, where Δx, Δy, and Δz are the finite difference spacings in the x, y, and z directions, respectively.

Two different parameterizations of the piecewise constant (zonal) blood perfusion field are considered. In the first, the blood perfusion is taken to be constant over each of the seven blocks or zones (shown in Figure 3.1). In the second, the blood perfusion is taken to be constant over each of the 27 equal-sized zones (shown in Figure 3.21). The magnitude of the applied power for each perfusion vector is chosen such that the maximum temperature over the domain is 50 °C. The magnitudes of the applied power and the perfusion vectors for the models considered are listed in Table 3.5.

To test the parameter estimation algorithm, the simulated temperature measurements from test cases shown in Table 1 are used

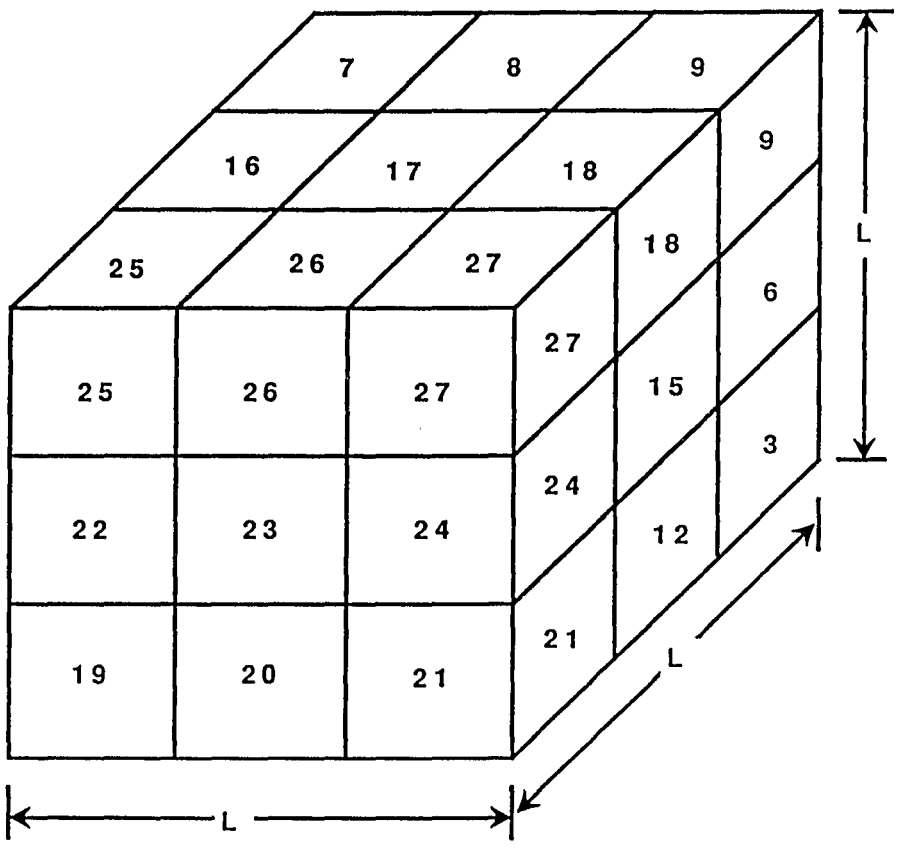

Figure 3.21 Schematic of the 27 perfusion zone models. The length L is equal to 10.5 cm.

Table 3.5 Blood perfusion vector, uniform applied power magnitude, and sampling time used in the three-dimensional, seven and twenty-seven zone models.

Perfusion Vector (kg/m^3-s) 7 Zone Model	Uniform Power (W/m^3)	Sampling Time (sec)
A. [0.5,0.5,0.5,0.0,0.5,0.5,0.5]	18,500	60
B. [8.0,8.0,8.0,0.0,8.0,8.0,8.0]	56,000	15
C. [0.8,0.5,0.2,0.0,0.2,0.5,0.8]	19,410	70
D. [0.18,0.26,0.25,0.92,0.32,0.04,1.03]	20,150	70
27 Zone Model		
E. Same as Case C	19,410	70
F. Random Perfusion	22,000	60

with both the adjoint and influence coefficient formulations of the inverse problems. The accuracy and computational efficiency of the two formulations are compared. The test problems are grouped into three sets. The first set tests the ability of the adjoint algorithm to reconstruct simple perfusion fields using noiseless data. The second set gives the comparison of the adjoint and the influence coefficient methods based on the CPU time per iteration. Finally, the relative performances of the adjoint and influence coefficient methods are compared in terms of their ability to solve the complete inverse problem for a perfusion field model that contains a large number of unknown parameters.

Verification of the Adjoint Formulation

The purpose of this set of test problems is to verify the ability of the adjoint formulation to accurately reconstruct the entire temperature field. For the first set of test problems, the seven zone perfusion model (see Figure 3.1) is used. No measurement noise is added. Two test problems are considered using the perfusion fields listed as Cases A and B in Table 3.5. Note that the average perfusion for Case A (a low perfusion case) is significantly less than for Case B (a high perfusion case). Four sensor locations are used, with the sensors taken to be located at the centers of symmetric zones 1, 3, 5 and 7 (see Figure 3.1). The estimated perfusions as a function of iteration number for the adjoint formulation are shown in Figures 3.22 and 3.23. Due to the symmetry of the perfusion patterns of Table

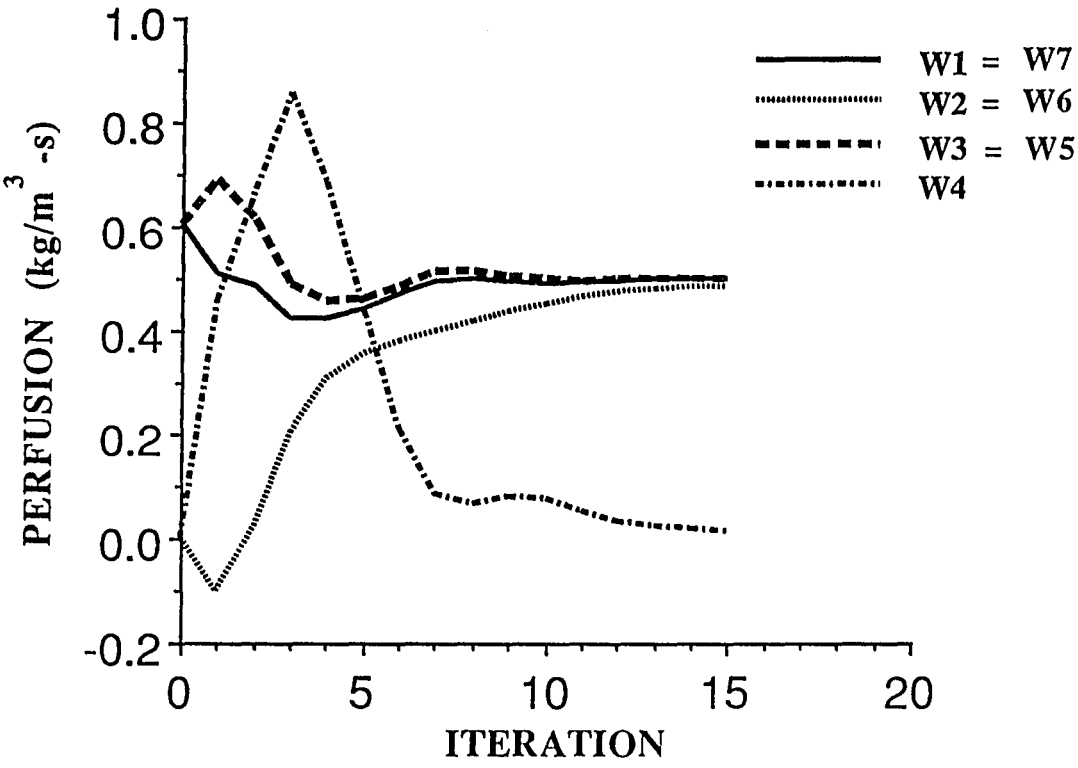

Figure 3.22 Estimated perfusions as a function of iteration number for the adjoint formulation for the 7 zone model with low perfusion pattern of case A in Table 3.5.

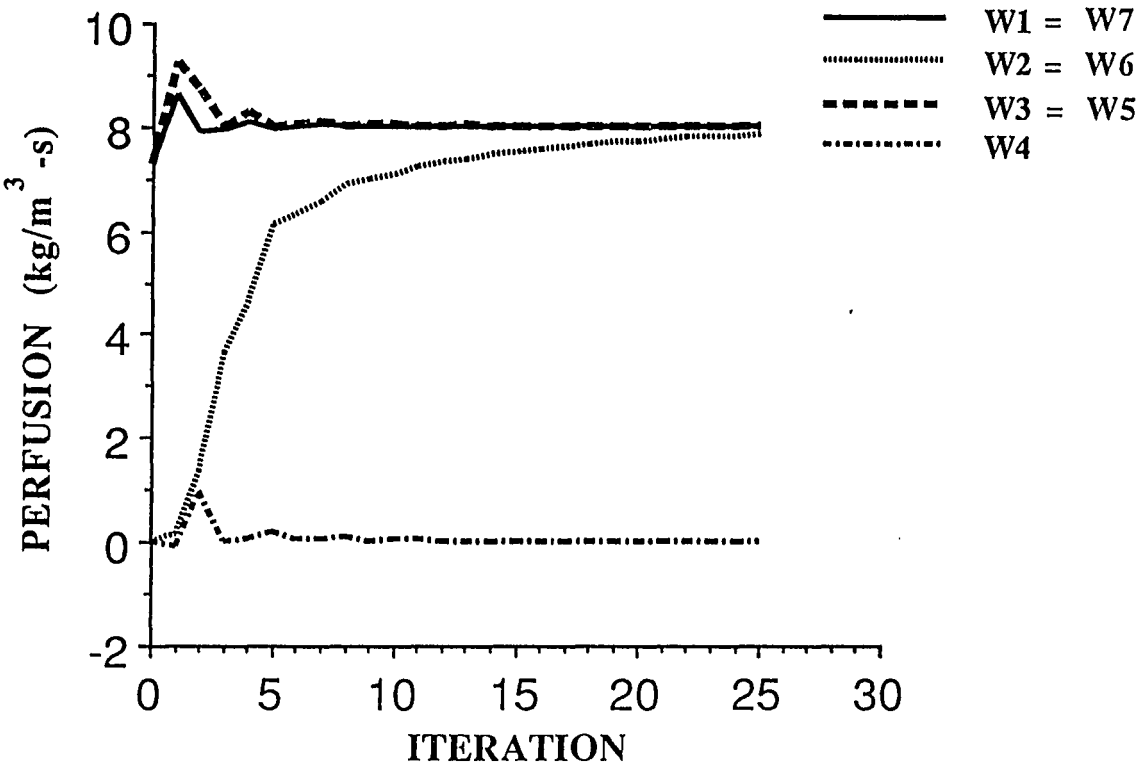

Figure 3.23 Estimated perfusions as a function of iteration number for the adjoint formulation for the 7 zone model with high perfusion pattern of case B in Table 3.5.

3.5, and of the initial estimate of the perfusion values, the following equalities hold in these graphs; $W_7=W_1$, $W_6=W_2$, and $W_5=W_3$ (see Figure 3.1). The regularization parameter was set to 1.0 for the low magnitude perfusion pattern case and to 0.0001 for the high magnitude case (Liauh 1988). The results of this test problem show that the adjoint method algorithm does converge to the correct solution (see Table 3.5, cases A and B) for this ideal inverse case.

Comparison of Jacobian Matrix Formulation CPU Time

The original motivation for this work was to develop the adjoint formulation because it had the potential of being computationally more efficient than the influence coefficient or sensitivity equation method when applied to problems with the number of measurement sensors less than the number of unknown parameters. To test this potential, two test problems (the 7 and 27 zone models shown in Figures 3.1 and 3.21, respectively) are considered in which the ratio of the number of measurement sensors to the number of unknown parameters is decreased by decreasing N_s. For both models, the perfusion fields Case C in Table 3.5 are identical. That is, zones 1 through 9 of the 27 zone model are assigned the same perfusion as zone 1 of the 7 zone model, etc. For this perfusion field with the input time interval of 60 seconds and the number of sampling time steps (N_t) of 98, the values of κ and N_{Iter} were determined from the results of the computer programs to be 2 and 63, respectively. Then, from equation (2.26), the BCOE value of χ for the problems and algorithms used here is

$$\chi = \frac{1 + 3.9N_s}{1+N_p} \quad . \tag{2.27}$$

Note that this equation gives an approximate crossover point (χ=1) of $N_s/N_p \simeq 1/4$.

The first comparison of the performance of the adjoint formulation and the influence coefficient method is simply based on the computational time per iteration required to calculate the elements of the Jacobian matrix. Figure 3.24 shows the CPU time needed to form a Jacobian matrix as a function of N_s for the 7 and 27 zone models. Figure 3.24 illustrates that when the number of measurement locations decreases, the CPU time required to form a Jacobian matrix is almost invariant for the influence coefficient method, and it decreases linearly for the adjoint method, as expected from the theory.

Figure 3.25 shows the value of χ as a function of N_s/N_p for the 7 and 27 zone models for both the influence coefficient and adjoint methods. These results demonstrate that the experimental values of χ for both the 7 and 27 zone models follow equation (2.27) well, which shows that the basic computer operation approach used to calculate the computational time required to form a Jacobian matrix for the adjoint and influence coefficient methods (see equations (2.20) and (2.21)) agrees well with the subroutine program time values. The small differences between the basic computer operation equation and subroutine program values are partly due to the approximation made to obtain equation (2.27). This agreement illustrates that using the

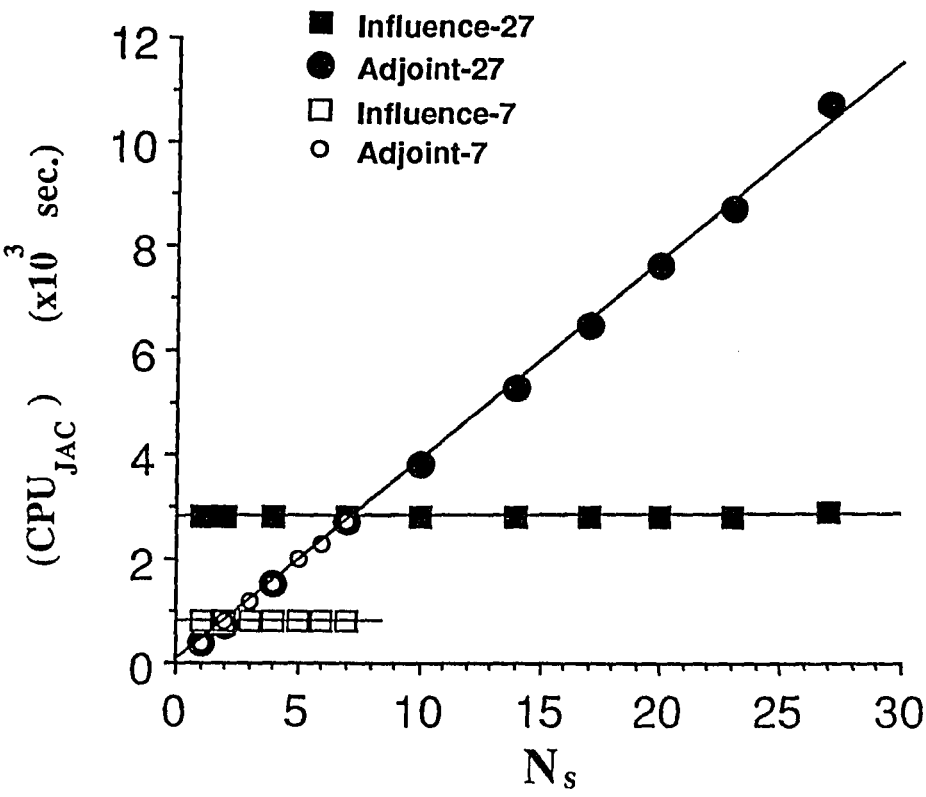

Figure 3.24 Values of the CPU time required to form a Jacobian matrix for the 7 zone and the 27 zone perfusion models as a function of the number of measurement sensors. The perfusion field for these two models is case C in Table 3.5.

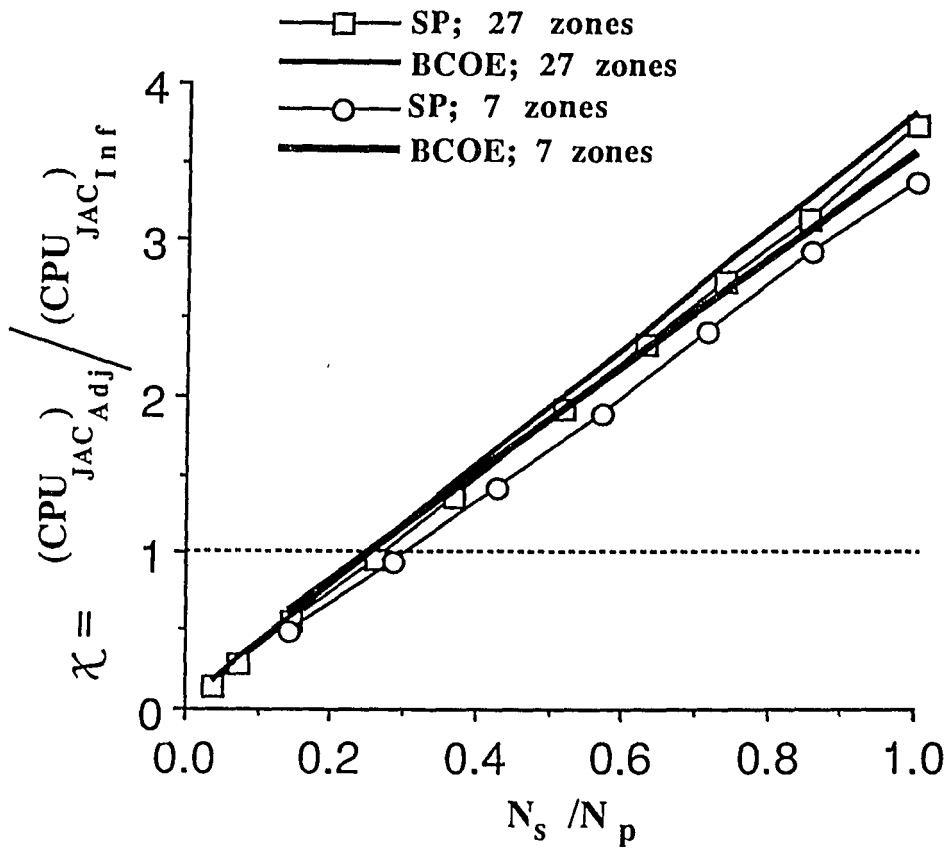

Figure 3.25 Basic computer operation equation (BCOE) and subroutine program (SP) values of χ as a function of N_s/N_p for the 7 zone and the 27 zone perfusion models. The perfusion field for these two models is case C in Table 3.5.

basic computer operation approach is a valid method of comparing different computational methods. Figure 3.25 also demonstrates that there is a crossover point of N_s/N_p at which both methods require the same time to form the Jacobian matrix. When the number of measurement sensors is small (i.e. small values of N_s/N_p), the adjoint formulation is faster than the influence coefficient.

Success of the Inverse Algorithms

While the previous results were concerned with the verification of the adjoint formulation and the comparison of the CPU time required for the two methods to evaluate the Jacobian elements, the present section presents results from using those methods in the complete inverse problem solution. To do this several inverse cases are considered with different numbers of sensors for both the 7 and 27 zone models. For the 7 zone model, the corresponding perfusion vectors are denoted C and D in Table 3.5. The random pattern (case D) is generated using a random number generator with the mean perfusion the same as for case C. When four sensors are used, they are located at the centers of zones 1, 2, 3, and 4; when three sensors are used, they are located at the centers of zones, 1, 2, and 3; and when two sensors are used, they are located at the center of zones 1 and 2.

The total sampling period and the power levels used for these test problems for the 27 zone model are listed under Case E and F in Table 3.5. When 27 sensors are used, they are centered in each zone; when 14 sensors are used, they are centered in the odd numbered zones; and when 7 sensors are used, they are centered in zones 5, 11, 13, 14,

15, 17, and 23 (see Figure 3.21). For the random perfusion case, the perfusions are assigned using a uniform random number generator, with a constraint of having a mean perfusion of 3/7 (kg/m^3-s), which equals the average value of the perfusion vector of Case C. Note that the intervals of the sampling time step for the symmetric and random perfusion patterns are 70 and 60 seconds, respectively, as shown in Table 3.5. This is because the perfusion of the central zone for the symmetric perfusion pattern is zero, and thus the corresponding transient power-off temperatures decay slower. For both the 7 and 27 zone models, noise levels of 0.0, 0.2, and 1.0 °C are added to the measurements and the regularization parameter (ϵ) is set to 1.0 (Liauh 1988). Even in the absence of noise, a non-zero regularization parameter must be used since the nonlinear parameter estimation problem is ill-conditioned, especially when the number of sensors is much less than the number of unknown parameters. In several test cases, the estimated perfusion fields gave corresponding temperature fields that are not within 1 °C of the true temperature fields. The final estimated perfusion field for these cases either converged to the wrong solution (denoted by ERR) or was diverging away from the correct solution after 25 iterations (denoted by DIV). Cases in which the temperature fields converged to within 1 °C of the true field and the estimated perfusion field converged to the correct solution are denoted by CON. The total CPU time was the time needed to run the program from the input to the output, not just the time to form the Jacobian matrix.

To compare the overall performance for the influence coefficient and adjoint methods, the total CPU time and the accuracy of the reconstruction are considered. All tissue properties and conditions were the same for both methods, as were the initial guesses of the perfusions and the sensor locations. Table 3.6 shows the resulting performance for both methods for the 7 zone model with the perfusion pattern of case C in Table 3.5. The performance includes the convergence, the relative CPU time, and the number of iterations for both methods. All CPU times are related to the total CPU time required for the influence coefficient method for the case of $N_s=N_p$ and no noise. Tables 3.7a and 3.7b show the resulting performance for the 27 zone model with the perfusion pattern of cases E and F, respectively, in Table 3.5.

The sensitivity equation method is investigated in addition to the influence coefficient method and the adjoint formulation in order to make a more complete study of the formation of the Jacobian matrix. As can be seen from the derivation of the sensitivity equation method, one must solve the partial differential equation N_p+1 times, which is the same number for the influence coefficient method. Several identical cases for the 7 zone model with the perfusion pattern of case C in Table 3.5 were tested by using the sensitivity equation method. Table 3.8 shows the results for the influence coefficient and sensitivity equation methods with the identical conditions such as the initial guess, the number of time steps, the sensor locations, etc., except the way to form the Jacobian matrix. It illustrates that the computational efforts of calculating the sensitivity coefficients for

Table 3.6 Relative CPU times for the 7 zone model with the perfusion pattern of case C in Table 3.4. INF indicates the influence coefficient method and ADJ the adjoint formulation. CON denotes a successful case in which the maximum difference between the exact and the predicted temperature fields is less than 1 °C at all finite difference nodes. ERR and DIV denote cases which do not satisfy this 1°C criterion and are either converging to the wrong perfusion vector or diverging away from the correct solution after 25 iterations. *For these two cases, the maximum temperature differences for ERR* and CON* are 1.12 and 0.97 °C, respectively. **All CPU times are relative to the total CPU time for the 7 sensor, no noise case using the influence coefficient method. The magnitude of the regularization parameter (ϵ) is equal to 1.

N_p	N_s	Noise Level (°C)	Convergence		Relative CPU Time**		Number of Iterations	
			INF	ADJ	INF	ADJ	INF	ADJ
7	7	0.0	CON	CON	1.0	4.3	4	6
7	7	0.2	CON	CON	1.0	4.3	4	6
7	4	0.0	CON	CON	1.8	9.5	8	22
7	4	0.2	CON	ERR	2.5	9.0	11	21
7	3	0.0	CON	CON	3.0	5.0	14	15
7	3	0.2	ERR	ERR	3.0	5.5	13	16
7	2	0.0	CON	CON	4.0	4.5	18	19
7	2	0.2	ERR*	CON*	3.5	4.8	16	18

Table 3.7a Relative CPU times for the 27 zone model with the perfusion pattern of case E in Table 3.5 for the influence coefficient method and the adjoint formulation. (See Table 3.6 for explanation of abbreviations)

N_p	N_s	Noise Level (°C)	Convergence		Relative CPU Time**		Number of Iterations	
			INF	ADJ	INF	ADJ	INF	ADJ
27	27	0.0	CON	CON	1.0	4.3	4	5
27	27	1.0	CON	CON	1.0	5.2	4	6
27	14	0.0	CON	DIV	2.9	11.6	12	25
27	14	0.2	CON	DIV	3.2	11.7	15	25
27	14	1.0	ERR	DIV	3.9	11.8	16	25
27	7	0.0	CON	DIV	2.4	5.9	10	25
27	7	1.0	ERR	DIV	3.2	5.8	13	25

Table 3.7b Relative CPU times for the 27 zone model with the perfusion pattern of case F in Table 3.5 for the influence coefficient method and the adjoint formulation. (See Table 3.6 for explanation of abbreviations)

N_p	N_s	Noise Level (°C)	Convergence		Relative CPU Time**		Number of Iterations	
			INF	ADJ	INF	ADJ	INF	ADJ
27	27	0.0	CON	CON	1.0	7.9	4	6
27	27	1.0	CON	CON	1.0	7.9	4	6
27	14	0.0	ERR	DIV	2.4	17.3	10	25
27	14	1.0	ERR	DIV	3.0	17.3	12	25
27	7	0.0	ERR	ERR	1.3	5.7	5	16
27	7	1.0	ERR	ERR	4.7	8.6	19	24

Table 3.8 Relative CPU times for the 7 zone model with the perfusion pattern of case C in Table 3.5 for the influence coefficient method (INF) and the sensitivity equation method (SEN). *For these two cases, the maximum temperature differences for ERR* are 1.12 and 1.08 °C, respectively. (See Table 3.6 for explanation of abbreviations)

N_p	N_s	Noise Level (°C)	Convergence		Relative CPU Time**		Number of Iterations	
			INF	SEN	INF	SEN	INF	SEN
7	7	0.0	CON	CON	1.0	1.1	4	4
7	7	0.2	CON	CON	1.0	1.1	4	4
7	4	0.0	CON	CON	1.8	2.3	8	9
7	4	0.2	CON	CON	2.5	2.7	11	11
7	3	0.0	CON	CON	3.0	3.7	14	15
7	3	0.2	ERR	ERR	3.0	3.1	13	13
7	2	0.0	CON	CON	4.0	4.3	18	18
7	2	0.2	ERR*	ERR*	3.5	4.0	16	17

the sensitivity equation method and for the influence coefficient method are almost the same.

DISCUSSION

Tables 3.6 and 3.7 illustrate that the total CPU time required for the adjoint formulation is always greater than that for the influence method, even for the cases with $N_s/N_p < 1/4$, which gives χ less than 1. Such cases would be expected to have lower total CPU times for the adjoint formulation, based on Jacobian calculation times alone. However, this is not the case because the total number of iterations for the adjoint method is always greater than that for the influence coefficient method. There are two main reasons for this phenomenon, both related to the adjoint method for calculating the Jacobian. First, the adjoint formulation estimates the coefficients in the Jacobian matrix through an approximate integral approach which is appropriate for the original differential form of the bioheat transfer equation. In contrast, the influence coefficient approach uses the finite difference approximation for the bioheat transfer equation directly to estimate the elements in the Jacobian. Even though both methods result in approximate estimates, the influence method may give approximations more appropriate for the finite difference algorithm actually used in the inversion process. The second and possibly more important disadvantage of the adjoint formulation was that integration errors associated with the numerical integration of equation (2.17) are large. We found that large integration errors existed at small t_j due to the quadratic errors associated with the Dirac Delta function

used for the initial conditions on the adjoint variables. (Note that using higher order quadrature reduces the integration error somewhat, but significantly increases the CPU time.) Due to these two reasons, the estimated perfusion vectors (which are determined by the Jacobian--see equation (2.28)) for the adjoint method go in directions which are not pointed as directly to the correct solution as are the influence coefficient vectors. As a result, the total number of iterations for convergence for the adjoint formulation is always greater than that required for the influence coefficient method.

This misalignment of the perfusion vector estimates also affects the accuracy of the final solution. As can be seen in Tables 3.6 and 3.7, the inverse solutions of the adjoint formulation are almost always less accurate than that of the influence coefficient method (except for one case, where it turns out that the maximum difference between the exact and the predicted temperature fields for the influence coefficient and adjoint methods are 1.12 and 0.97 °C, respectively). Table 8 shows the computational times and the accuracy of the reconstruction for the influence coefficient and sensitivity equation methods are close. This occurs because both of them require to solve N_p+1 numerical solutions for the partial differential equations. These equations, the sensitivity equations (2.5) and the bioheat transfer equation (1.1) are similar.

Tables 3.6, 3.7, and 3.8 show that the performance of all three methods is degraded, as expected, when additive measurement noise is considered (Clegg, et al., 1988, Liauh 1988, Liauh, et al. 1991). It is also of interest to note that for those convergent cases with and

without noise, the smallest successful values of N_s/N_p are about 1/2 and 1/4, respectively, which are always greater than or close to the critical value ($N_s/N_p \simeq 1/4$) at the temporal crossover point in Figure 3.25. That is, the crossover point in the time domain $N_s/N_p \simeq 1/4$ where $\chi = 1$, is very close to the crossover point from successful to non-successful inversions.

Finally, it should be noted that the results presented here are based solely on simulated hyperthermia treatments; that is, any model mismatch problems present in the clinic are not taken into account. These model mismatch problems may or may not effect the comparative temporal performance of the influence coefficient method and the adjoint formulation in terms of total CPU time. That is, while any model mismatch will not affect the times required to calculate the Jacobians, it may affect the directions in which the estimated perfusion vectors are sent, and thus alter both the number of iterations of both techniques and their ultimate accuracies. Therefore, the adjoint formulation may still have potential applications in clinical situations.

3.3 SEMI-LINEARITY

To further improve the performance of the estimation algorithm by using the influence coefficient method, well controlled numerical experiments generating three-dimensional temperature fields from a limited number of temperature sensor locations were used. A three-dimensional, seven zone model identical to Figure 3.1 was used for this study. Two perfusion patterns of cases C and D in Table 3.5 are

used; one with a symmetric pattern, and one with a random pattern created by a random number generator. The perfusion vector for the symmetric case studied has an average value of 3/7 $kg/m^3/s$. Thus, the perfusion vector for the random case was created with the same average value of 3/7 $kg/m^3/s$.

RESULTS

To simulate the clinical situations, cases in which the number of sensors was less than the number of unknown parameters, and cases with noisy temperature measurements were investigated. Several cases with different numbers of sensors and five noise levels are presented for the symmetric perfusion pattern (case C in Table 3.5) with the above seven values of $DELTA_1$. The numbers of sensors used in this study were 7, 4, or 3. For the 7 sensor case, there is a sensor for each zone. For the 4 sensor case, the sensors are in the zones 1, 2, 3, and 4, and for the 3 sensor case, they are in the zones 1, 2, and 3. No regularization was implemented (i.e., ϵ=0) because the problem was previously tested and shown not to be too ill-posed.

Results of the ratios of N_J/N_T, the relative CPU time, and the maximum difference between the true and predicted temperature fields are shown in Tables 3.9, 3.10, and 3.11, respectively, for the cases with 3 different sensor numbers, 5 noise levels, and 7 values of ERR_1. In the results presented, N_T represents the total number of iterations required to obtain the inversion solution, and N_J represents the number of calculations of the Jacobian matrix. First, Figure 3.26 illustrates the speed of the improved algorithm by plotting the

Table 3.9 Total iterations/number of calculations of the Jacobian matrix for the 7 zone model with a symmetric perfusion pattern.

DELTA 1		NOISE LEVEL (°C)					
		0.0	0.1	0.2	0.4	1.0	
	0.0	4/4	4/4	4/4	4/4	4/4	7 SENSORS
		5/5	5/5	5/5	5/5	6/6	4 SENSORS
		5/5	5/5	4/4	5/5	5/5	3 SENSORS
	0.01	4/4	4/4	4/4	4/4	4/4	
		5/4	5/5	5/5	5/5	6/6	
		5/5	5/5	4/4	5/5	5/5	
	0.1	4/3	4/3	4/3	4/3	4/3	
		5/4	5/4	5/4	5/4	6/5	
		5/4	5/4	4/4	5/3	5/4	
	0.5	4/2	4/2	4/2	4/2	5/2	
		13/1	13/1	13/1	14/1	17/1	
		10/2	8/2	7/2	7/2	5/3	
	1.0	25/1	25/1	25/1	25/1	25/1	
		13/1	13/1	13/1	14/1	17/1	
		21/1	15/1	12/1	7/2	11/1	
	5.0	25/1	25/1	25/1	25/1	25/1	
		13/1	13/1	13/1	14/1	17/1	
		21/1	15/1	12/1	12/1	17/1	
	10.0	25/1	25/1	25/1	25/1	25/1	
		13/1	13/1	13/1	14/1	17/1	
		21/1	15/1	12/1	12/1	17/1	

Table 3.10 Relative total computational times for the 7 zone model with a symmetric perfusion pattern. All CPU times are relative to the total CPU time for the 7 sensor, no noise case with $DELTA_1$ of 0.

		NOISE LEVEL (°C)					
		0.0	0.1	0.2	0.4	1.0	
DELTA 1	0.0	1.0	1.01	1.02	1.01	1.01	7 SENSORS
		1.24	1.24	1.24	1.27	1.47	4 SENSORS
		1.24	1.27	1.01	1.26	1.26	3 SENSORS
	0.01	1.02	1.0	1.01	1.01	1.01	
		1.03	1.24	1.24	1.24	1.47	
		1.22	1.25	1.01	1.27	1.27	
	0.1	0.80	0.79	0.79	0.79	0.8	
		1.03	1.06	1.03	1.03	1.26	
		1.02	1.02	1.01	0.82	0.82	
	0.5	0.59	0.81	0.58	0.6	0.61	
		0.64	0.64	0.63	0.69	0.75	
		0.75	0.69	0.86	0.67	0.67	
	1.0	1.01	1.4	1.0	1.02	1.01	
		0.63	0.63	0.63	0.68	0.75	
		0.89	0.7	0.78	0.66	0.78	
	5.0	1.0	1.39	1.01	1.01	1.01	
		0.65	0.63	0.63	0.67	0.75	
		0.89	0.71	0.78	0.6	0.75	
	10.0	1.04	1.39	1.02	1.03	1.01	
		0.66	0.63	0.63	0.69	0.75	
		0.89	0.69	0.78	0.6	0.76	

Table 3.11 Maximum difference between the true and predicted temperature fields for the 7 zone model with a symmetric perfusion pattern.

		NOISE LEVEL (°C)					
		0.0	0.1	0.2	0.4	1.0	
DELTA 1	0.0	0.001	0.004	0.009	0.019	0.049	7 SENSORS
		0.000	0.399	0.812	1.662	4.082	4 SENSORS
		0.002	2.004	2.975	4.943	9.821	3 SENSORS
	0.01	0.001	0.004	0.009	0.019	0.049	
		0.000	0.399	0.812	1.662	4.082	
		0.002	2.004	2.975	4.943	9.821	
	0.1	0.001	0.004	0.009	0.019	0.049	
		0.000	0.399	0.807	1.647	4.084	
		0.001	2.007	2.975	4.912	9.821	
	0.5	0.012	0.015	0.018	0.024	0.039	
		0.173	0.369	0.736	1.453	3.494	
		0.099	2.134	3.031	4.814	9.698	
	1.0	2.182	2.232	2.348	2.569	3.179	
		0.173	0.369	0.736	1.453	3.494	
		0.392	2.327	2.995	4.814	8.953	
	5.0	2.182	2.323	2.348	2.569	3.179	
		0.173	0.369	0.736	1.453	3.494	
		0.392	2.327	2.995	4.814	8.953	
	10.0	2.182	2.323	2.348	2.569	3.179	
		0.173	0.369	0.736	1.453	3.494	
		0.392	2.327	2.995	4.814	8.953	

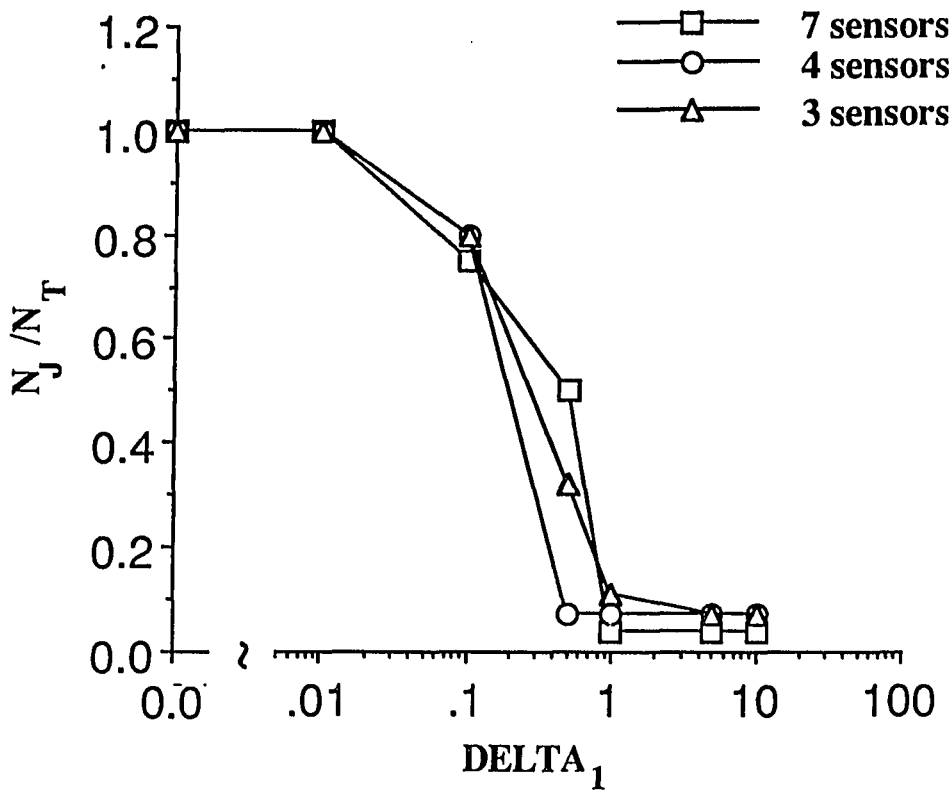

Figure 3.26 Values of the ratio (N_J/N_T)of the number of calculation of the Jacobian matrix to the total number of iterations as a function of $DELTA_1$ for the 7 zone model with a symmetric perfusion pattern and 7, 4, and 3 sensors.

average value of N_J/N_T as a function of $DELTA_1$ for the 7, 4, and 3 sensor cases. The average values are for the five noise levels. Next, to further illustrate the speed of the semi-linear algorithm, Figure 3.27 plots the average relative computational time as a function of $DELTA_1$ for the 7, 4, and 3 sensor cases. All relative CPU times are related to the total CPU time for the 7 sensor, no noise case with $DELTA_1$ of 0. Finally, to illustrate the accuracy of the improved algorithm Figure 3.28 plots the total number of successful cases versus the value of $DELTA_1$. The total number of successful cases is the sum of all cases in which the maximum error between the reconstructed and true steady-state temperature fields is less than 1.0 °C (Liauh 1988). The maximum number for this variable is five, from the five noise levels. From Figures 3.26, 3.27, and 3.28 the optimal value of $DELTA_1$ for this symmetric perfusion pattern is close to 0.5 since this value decreases the computational time significantly without losing many successful cases. With this optimal value of $DELTA_1$, the computational times required will be reduced by close to 40%.

To extend the results from the symmetric perfusion pattern, a random perfusion pattern was generated to check the existence and value of the optimal value of $DELTA_1$. It has been shown that when the perfusion is random, this inverse problem becomes more ill-posed (Liauh 1988). To reduce the ill-posedness of the inverse problem, Tikhonov regularization of order zero was implemented. The magnitude of the regularization parameter (ϵ) was selected to be 0.00001 (Liauh 1988). The computational time required to obtain the final solution

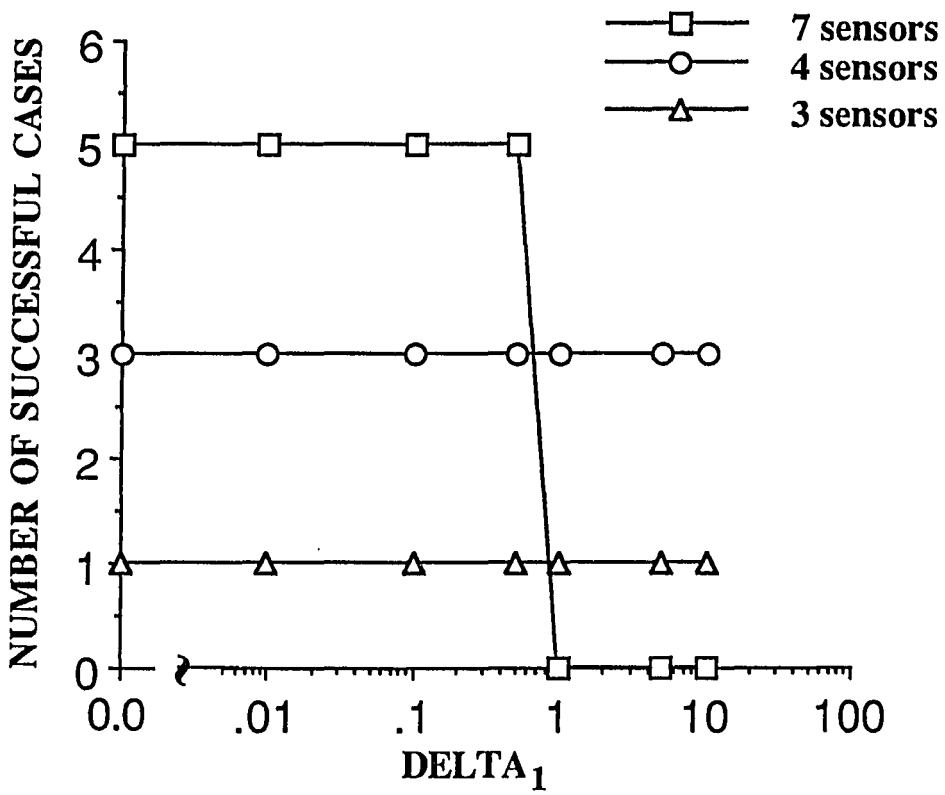

Figure 3.27 Number of Successful cases as a function of $DELTA_1$ for the 7 zone model with a symmetric perfusion pattern and 7, 4, and 3 sensors.

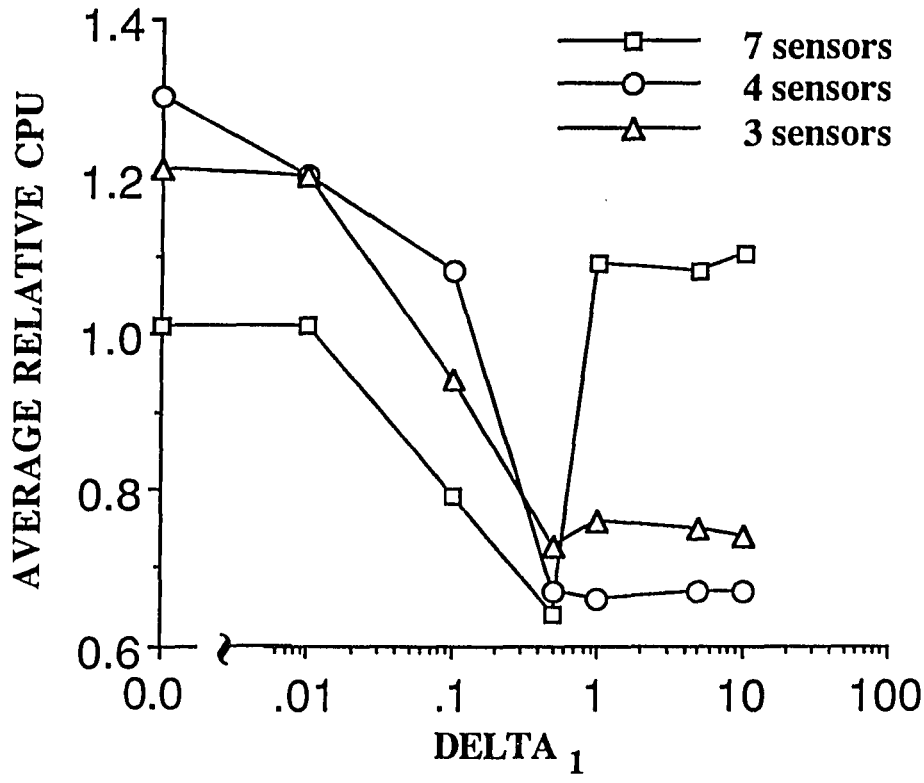

Figure 3.28 Average relative CPU time as a function of $DELTA_1$ for the 7 zone model with a symmetric perfusion pattern and 7, 4, and 3 sensors.

and the maximum difference between the true and predicted temperature fields for the 4 sensor case with three noise levels (0.0, 0.4, 1.0 °C) and six values of $DELTA_1$ (0.01, 0.1, 0.5, 1.0, 5.0, and 10.0) are listed in Table 3.12. The sensors are located at the centers of the first, third, fifth, and sixth zones (see Figure 3.1). Figure 3.29 plots the average computational time and the total number of successful cases as a function of $DELTA_1$ for this random perfusion pattern. The optimal value for $DELTA_1$ is also 0.5, the same as for the symmetric perfusion pattern.

DISCUSSION

To explain why this semi-linear approach works, Figures 3.30a, b, and c plot the estimated perfusions as a function of iteration number for the cases with $DELTA_1$ equal to 0.0, 0.5, and 1.0, respectively, for the 7 sensor case without noise. (Note that due to the symmetry of the perfusion patterns of Table 3.5, and of the initial estimate of the perfusion values, the following equalities hold in Figure 3.30; $W_7=W_1$, $W_6=W_2$, and $W_5=W_3$.) Theoretically, when an estimated perfusion vector is close to the true value, the corresponding Jacobian matrices evaluated by an influence coefficient method are close to one another. Hence, it is not necessary to reevaluate the Jacobian matrix in order to obtain the true solution. Figure 30a shows the estimated perfusions for each iteration for the case with 7 sensors when the problem was assumed to be totally nonlinear (when $DELTA_1 = 0.0$). From Table 3.9, the number of calculations of the Jacobian matrix is 4, which is identical to the

Table 3.12 Results of the 7 zone model with a random perfusion pattern with 4 sensors; (a) Maximum difference between the true and predicted temperature fields; (b) relative total computational times. All CPU times are relative to the total CPU time for the no noise case with ERR_1 of 0.

		NOISE LEVEL (°C)		
		0.0	0.4	1.0
DELTA 1	0.0	0.0	0.75	2.22
	0.01	0.0	0.76	2.21
	0.1	0.0	0.79	2.17
	0.5	0.07	0.98	1.92
	1.0	0.36	1.12	2.16
	5.0	0.36	1.11	2.16
	10.0	0.36	1.11	2.16

(a)

		NOISE LEVEL (°C)		
		0.0	0.4	1.0
DELTA 1	0.0	1.0	1.04	1.03
	0.01	1.0	1.0	0.99
	0.1	0.83	0.85	0.67
	0.5	0.65	0.56	0.46
	1.0	0.48	0.46	0.43
	5.0	0.48	0.45	0.42
	10.0	0.48	0.45	0.41

(b)

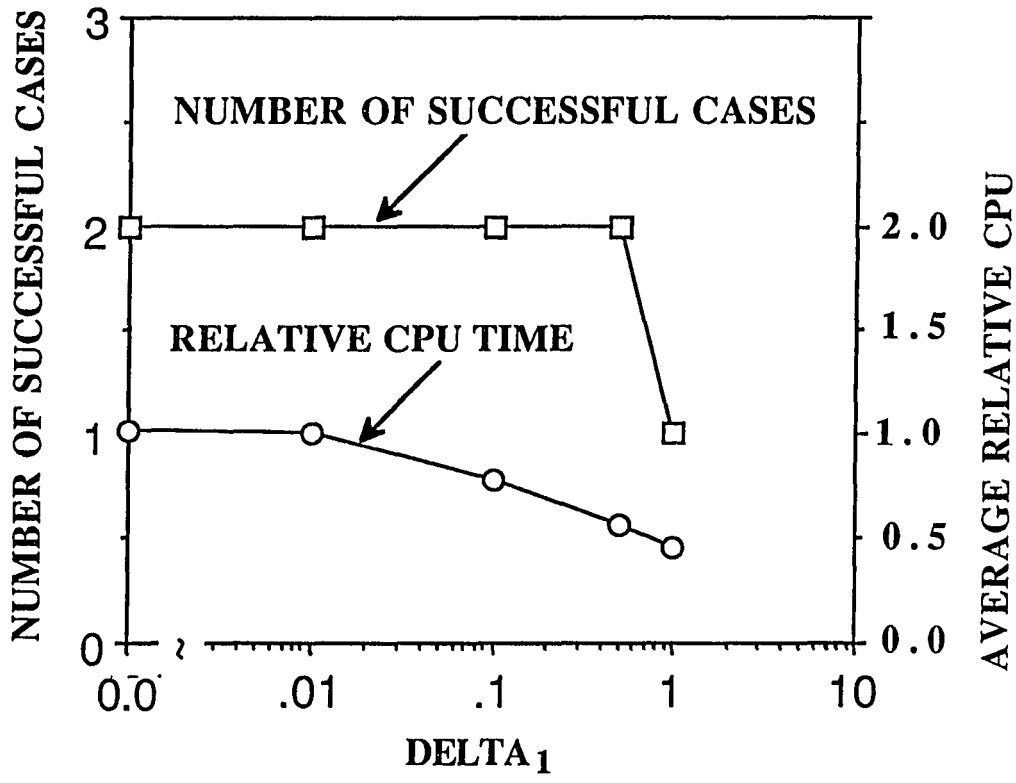

Figure 3.29 Number of successful cases and average relative CPU time as a function of $DELTA_1$ for the 7 zone model with a random perfusion pattern and 4 sensors.

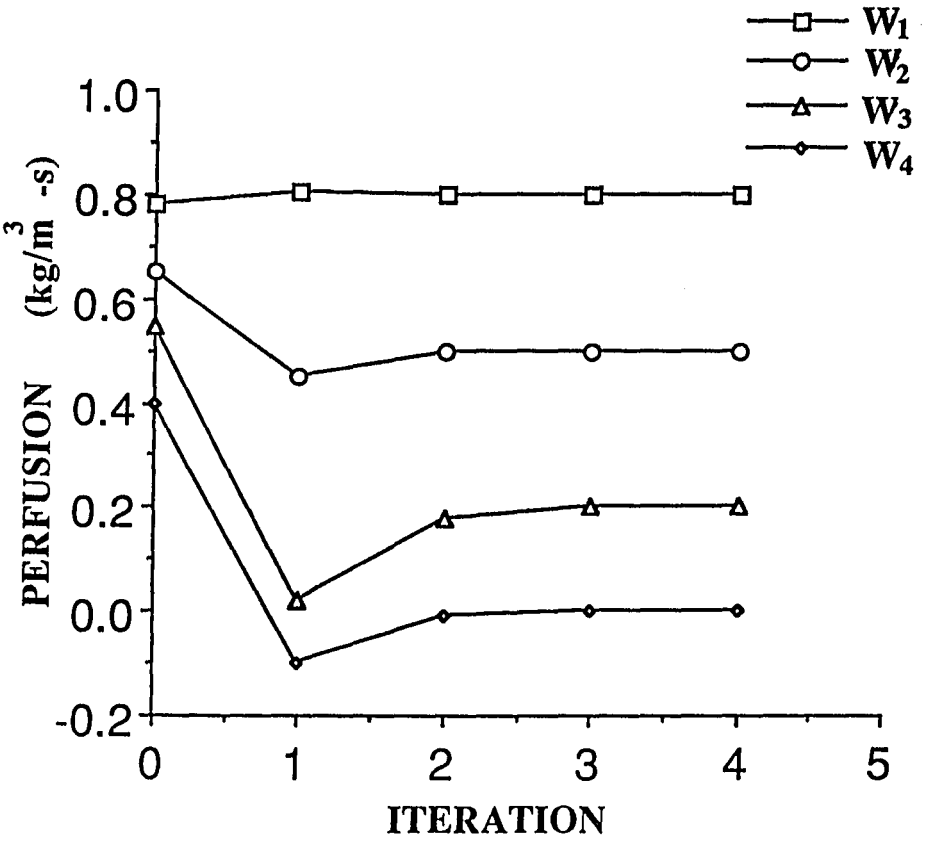

Figure 3.30a Estimate of perfusion as a function of iteration for the 7 zone model with a symmetric perfusion pattern and 7 sensors for $DELTA_1$ of 0.0.

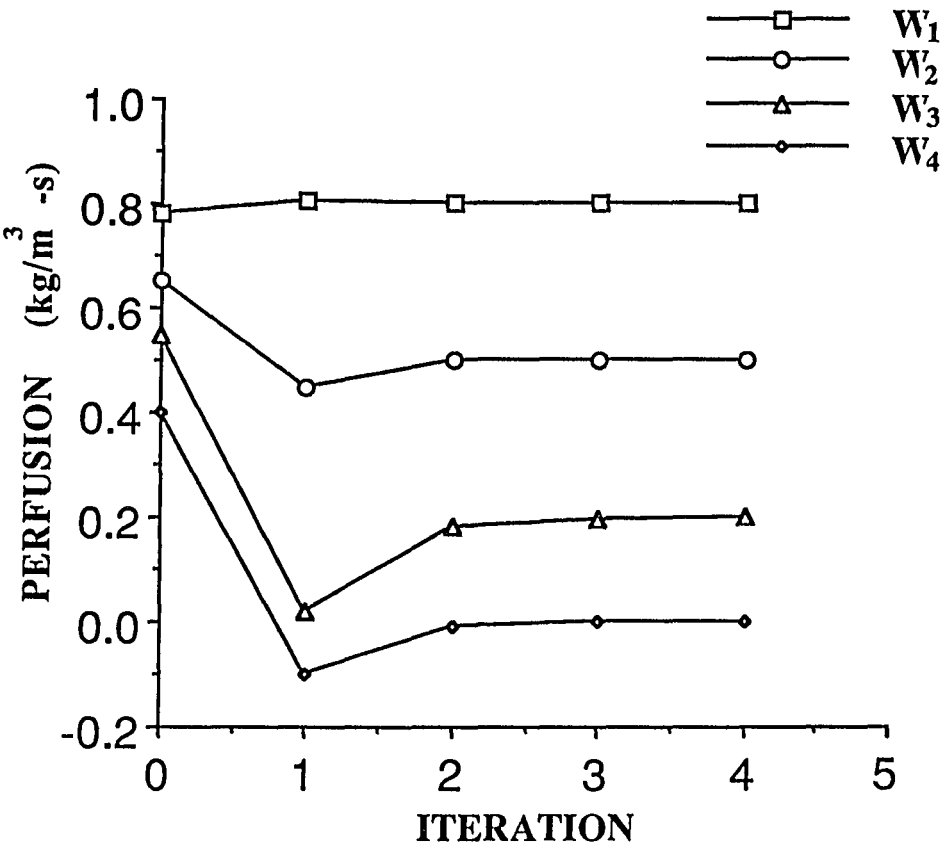

Figure 3.30b Estimate of perfusion as a function of iteration for the 7 zone model with a symmetric perfusion pattern and 7 sensors for $DELTA_1$ of 0.5.

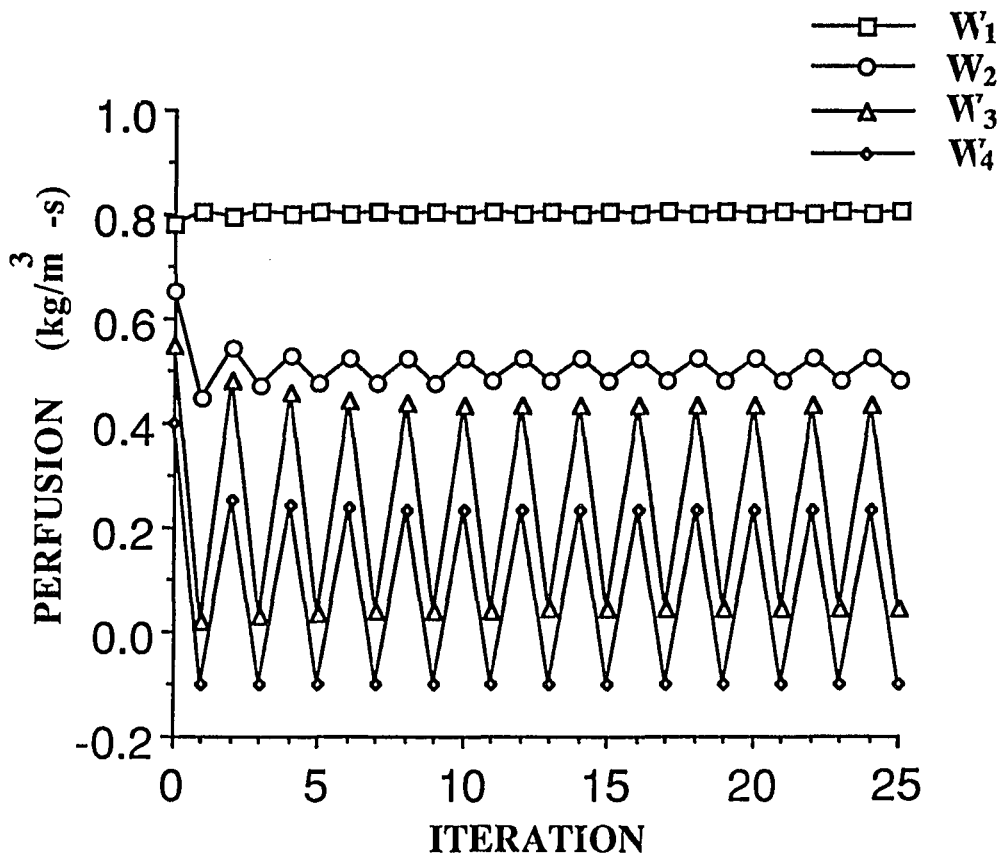

Figure 3.30c Estimate of perfusion as a function of iteration for the 7 zone model with a symmetric perfusion pattern and 7 sensors for $DELTA_1$ of 1.0.

total number of iterations. When the optimal $DELTA_1$ of 0.5 shown in Figure 3.26 was used, Figure 30b shows the resulting estimated perfusions for each iteration. From Table 3.9, the number of calculations of the Jacobian matrix is 2 for this 7 sensor case with $DELTA_1$ of 0.5. Figures 3.30a and 3.30b reveal that the Jacobian matrix at the second iteration for the case with $DELTA_1$ of 0.5 is close to the rest of the Jacobian matrices after the second iteration for the totally nonlinear case. When a nonlinear problem is assumed to be linear, the final estimate will depend upon the starting point for the search algorithm. As seen from Figure 3.30c for the same case with $DELTA_1$ of 1.0, the resulting estimated perfusions are oscillatory when the search algorithm just used the first Jacobian matrix. This occurs because the linear approximation fails at the starting point for this case. It can be seen from Figure 3.30b that the validality of the linear approximation works if the initial perfusion guess is chosen as the second perfusion vector.

To further investigate the effect of the initial guess of the perfusion vector, some observations are made from Tables 3.9, 3.10, and 3.11. As seen from Table 3.10, the relative CPU time for the 7 sensor case is greater than that for the 4 or 3 sensor case when $DELTA_1$ is greater than 1.0. This occurs because the perfusion estimates are oscillatory for the 7 sensor case (see Figure 3.30c). When the search direction given by the first Jacobian matrix deviates from the correct direction, the final perfusion vector will never converge to the true solution, even though the initial guess is close to the true solution. This phenomena can be seen from Figure 3.30c, in

which the initial guess [0.79, 0.65, 0.54, 0.4, 0.54, 0.65, 0.79] is close to the true values (see Table 3.5), but the final estimated perfusion is oscillatory for the 7 sensor case with $DELTA_1$ of 1. Unlike the 7 sensor case, the final estimated solution for the 4 or 3 sensor case with the same value of $DELTA_1$ converges to the true solution, even though the initial guess perfusion vector has some zero perfusions for the zones without sensors. Figures 3.31a and 3.31b plot the estimated perfusions as a function of the iteration number for the cases with 4 and 3 sensors, respectively, with $DELTA_1$ of 1. Figures 3.30c and 3.31 illustrate that the search direction pointed by the first Jacobian matrix for the 4 or 3 sensor case is more accurate than that for the 7 sensor case. By using the same first Jacobian matrix for the 4 sensor case, Figure 3.32 plots the estimated perfusions as a function of iteration number for the 7 sensor case, and it shows the successful estimation.

3.4 MODEL MISMATCH PROBLEM

The results of a study of the effects of mismatch between the actual tumor and the simulated model are presented in this section. For this study, simple one-dimensional model mismatch cases were studied. The perfusion field of the actual tumor was specified as a known function of space, but the perfusion term of the simulated tumor was approximated by a piecewise constant, i.e., the whole domain was divided into several zones in each of which the magnitude of the perfusion was constant, but was variable from zone to zone. The simple

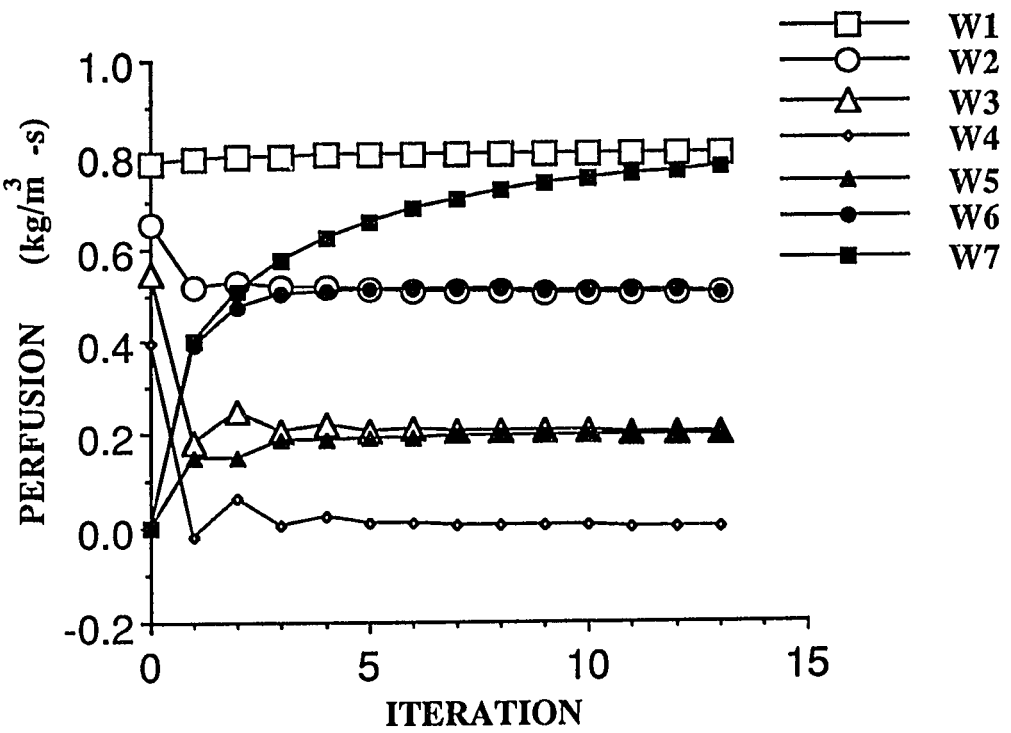

Figure 3.31a Estimate of perfusion as a function of iteration for the 7 zone model with a symmetric perfusion pattern and $DELTA_1$ of 1.0 for the cases with 4 sensors.

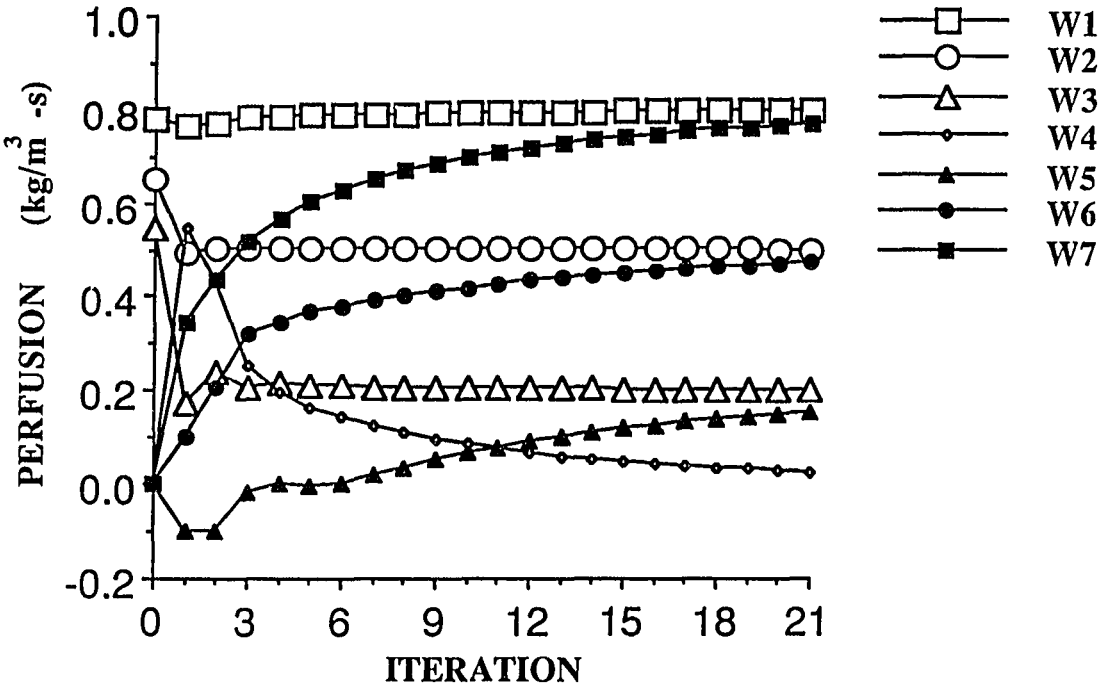

Figure 3.31b Estimate of perfusion as a function of iteration for the 7 zone model with a symmetric perfusion pattern and $DELTA_1$ of 1.0 for the cases with 3 sensors.

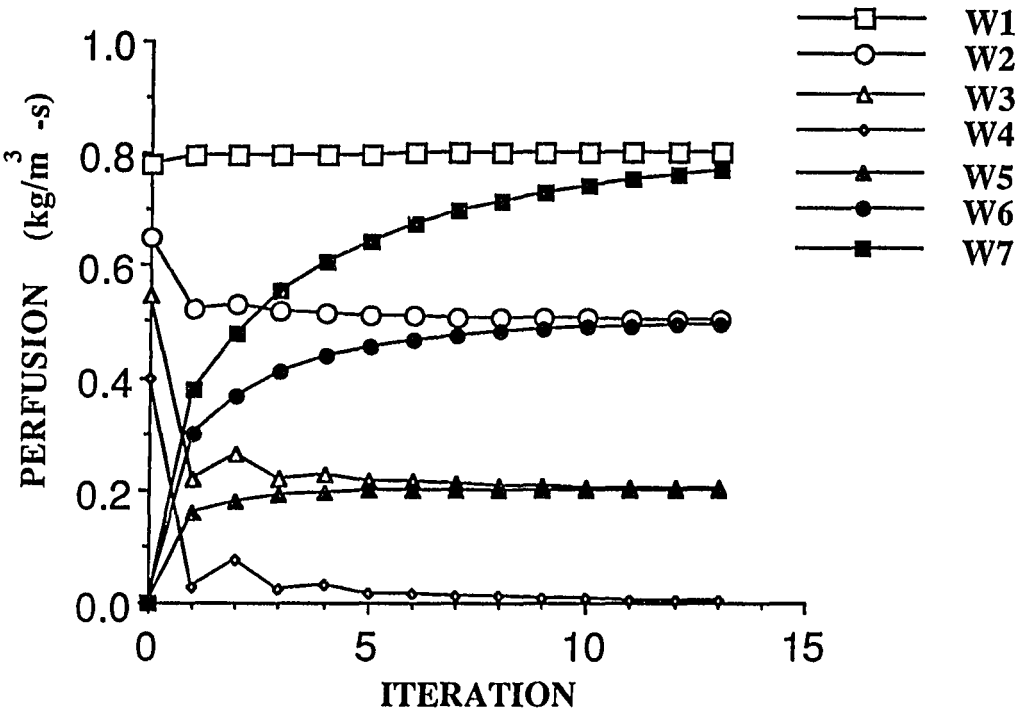

Figure 3.32 Estimate of perfusion as a function of iteration for the 7 zone model with a symmetric perfusion pattern, 7 sensors, and $DELTA_1$ of 1.0. But the initial guess of perfusion vector is the same as the 4 sensor case.

one-dimensional model has been used in order to determine basic, fundamental principles which can then be applied to more practical three-dimensional models.

ONE-DIMENSIONAL RESULTS

Model mismatch was caused by the discretization of a perfusion field into several discrete zones. Figure 3.33 shows the perfusion distributions in the direct (or real) case as a linear function, and a parabolic function, respectively. The linear perfusion function takes the form $W(x) = 0.5 + 0.0714x$, which has $W = 0.5$ kg/m^3-s at x=0 mm, and $W = 8.0$ kg/m^3-s at x=105 mm. The parabolic function takes the form $W(x) = 0.5 + 360.53(x-53)^2$, which has $W = 8.0$ kg/m^3-s at x=1 or 105 mm, and $W = 0.5$ kg/m^3-s at x=53 mm. In an attempt to investigate the effects of using a zonal approach on the temperature fields (i.e., how many zones are good enough to describe the continuous perfusion field providing an accurate steady-state temperature field), several direct cases with different zone models were tested. For a certain zone model, the whole domain was divided into either one, two, three, four, five, or a higher number of equal-sized zones. The perfusion for each zone was assigned as either the average value of the true perfusion field in that zone (denoted by W_{avg}) or the function value at the center of that zone (denoted by W_{fun}). That is, the perfusion (W_i) for the i^{th} zone from x=a to x=b mm could be calculated as follows:

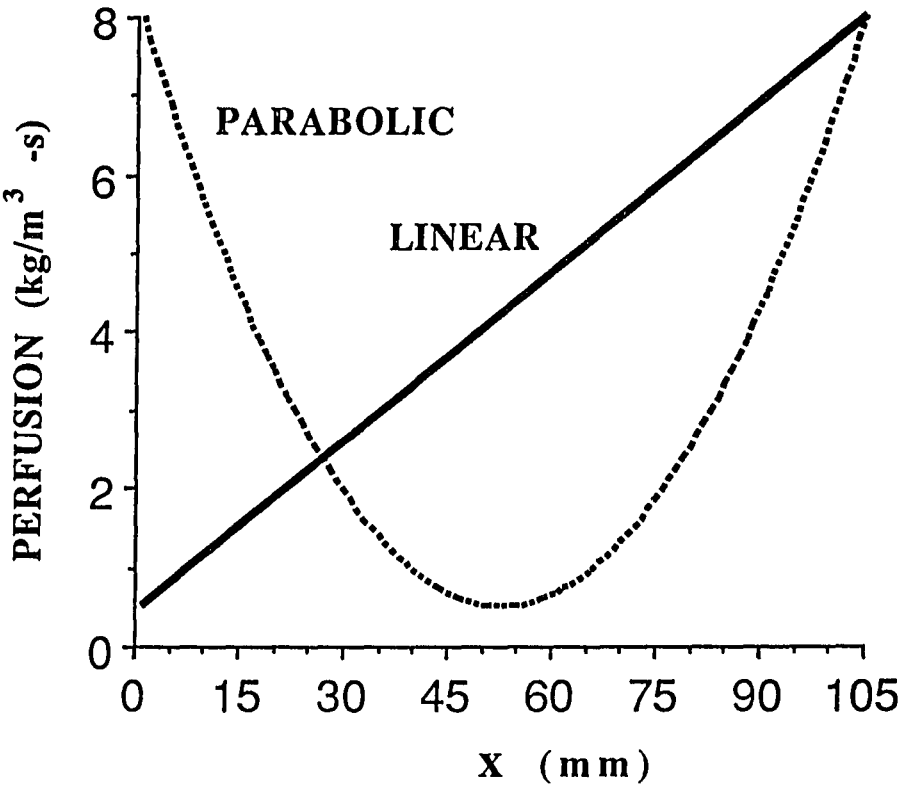

Figure 3.33 Two continuous perfusion fields as a function of x for the one-dimensional model.

$$W_i = W_{avg} = \frac{1}{b-a} \int_a^b W(x)\, dx$$

or

$$W_i = W_{fun} = W(x=\frac{a+b}{2}).$$

These average and function perfusions for different zone models for the linear and parabolic perfusion patterns are listed in Table 3.13.

First, Figure 3.34 shows the steady-state temperature fields for the true perfusion field and the different perfusion zone models with the average perfusions for the linear and parabolic cases. Figure 3.35 plots the temperature differences between the true and estimated (using the zonal approach) steady-state temperature fields for both continuous perfusion cases. Figures 3.34 amd 3.35 illustrate that the zonal approach is good enough to describe the perfusion field in terms of the accuracy of the temperature field (within 1 °C criterion) when the number of equal-sized zones is greater than 5 for the linear case. But for the parabolic case, the steady-state temperature field for the five zone model still can not satisfy the criterion. Because the perfusion variation for the parabolic case is greater than that for the linear case shown in Figure 3.33, more zones for the parabolic case will be needed to obtain an accurate steady-state temperature field. After increasing the number of zones, the minimum number of zones required to obtain an accurate temperature field is found to be 10 as shown in Figure 3.35b.

Second, it is desirable to know to which perfusion values the estimation algorithm will converge if the true continuous perfusion

Table 3.13 Average, function, and inverse (estimated) perfusions for 5 different zone models for the linear and the parabolic perfusion cases.

NUMBER OF ZONE	PERFUSION VECTOR (kg/m^3-s) LINEAR			PARABOLIC		
	W_{avg}	W_{fun}	W_{inv}	W_{avg}	W_{fun}	W_{inv}
1	4.25	4.25	4.147	3.0	0.5	0.879
2	2.375 6.197	2.375 6.197	2.304 6.155	3.0 3.05	2.375 2.522	1.894 2.006
3	1.726 4.25 6.774	1.726 4.25 6.744	1.745 4.218 6.751	4.165 0.767 4.165	3.898 0.5 3.898	3.523 0.553 3.523
4	1.365 3.312 5.188 7.063	1.365 3.312 5.188 7.063	1.437 3.289 5.183 7.043	4.972 1.125 1.102 4.875	4.938 0.969 0.969 4.718	4.851 0.864 0.835 4.613
5	1.221 2.736 4.25 5.764 7.279	1.221 2.736 4.25 5.764 7.279	1.255 2.724 4.244 5.758 7.271	5.485 1.816 0.593 1.816 5.485	5.393 1.723 0.5 1.723 5.393	5.459 1.587 0.463 1.587 5.459

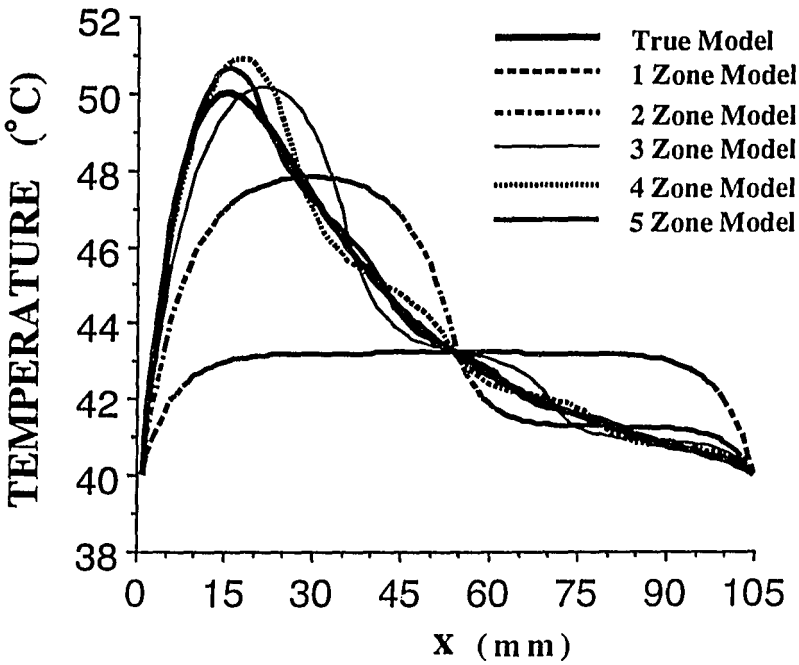

Figure 3.34a Steady-state temperature fields for the true model with a linear perfusion variation, and for the five different zone models.

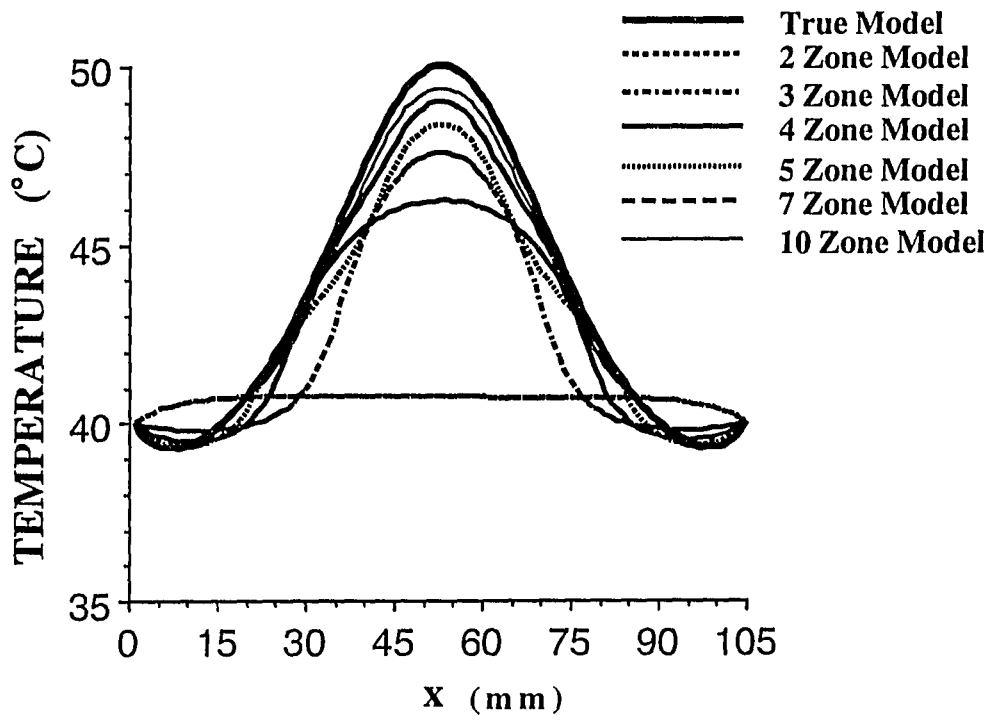

Figure 3.34b Steady-state temperature fields for the true model with a parabolic perfusion field, and for the six different zone models.

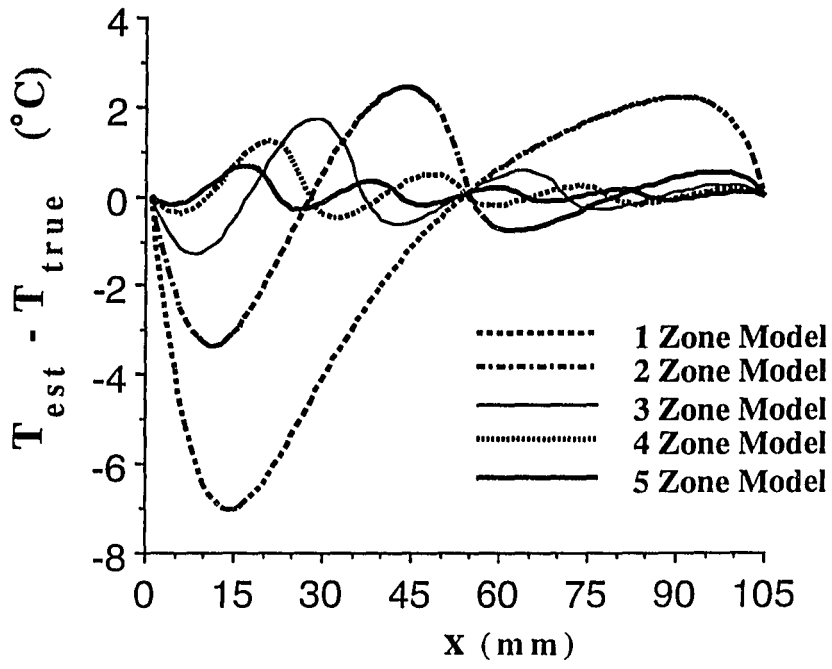

Figure 3.35a Differences between the estimated and true model temperatures for the perfusions of Figure 3.34a.

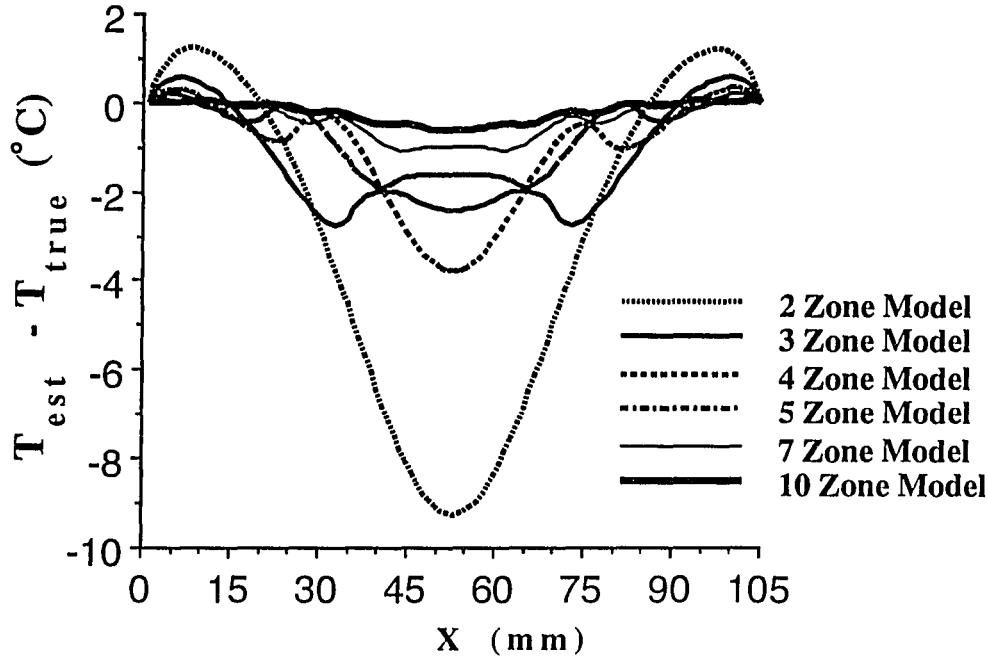

Figure 3.35b Differences between the estimated and true model temperatures for the perfusions of Figure 3.34b.

field was approximated by a piecewise perfusion field. To investigate this problem, the number of temperature sensors used for the estimation algorithm was identical to the number of perfusion zones and their locations were selected at the centers of each zone. For example, the five equal-sized zone model used five sensors. The temperature measurements at these five sensor locations from the direct solutions without noise were used as input to the estimation algorithm. Then, the resulting inversion (or reconstruction) of the steady-state temperature field was compared with the true direct steady-state temperature field. The initial guess of perfusion for each zone was set to be an estimate of the overall tissue cooling coefficient (Roemer 1990). The resulting estimated perfusion within each zone is listed in Table 3.13. It shows that for the linear case the estimated perfusions are close to the function (or average) values of the exact function in those zones for different zone models. But for the parabolic case the estimated perfusions are close to the function perfusions, rather than the average values. Figure 3.36 plots the steady-state temperature fields for the five zone model with the true parabolic perfusion field and the average perfusion, function perfusion, and the estimated perfusion vectors. The final steady-state temperature field corresponding to the estimated perfusions for the 5 zone model is close to the true solution with a maximum temperature difference of 0.62 °C.

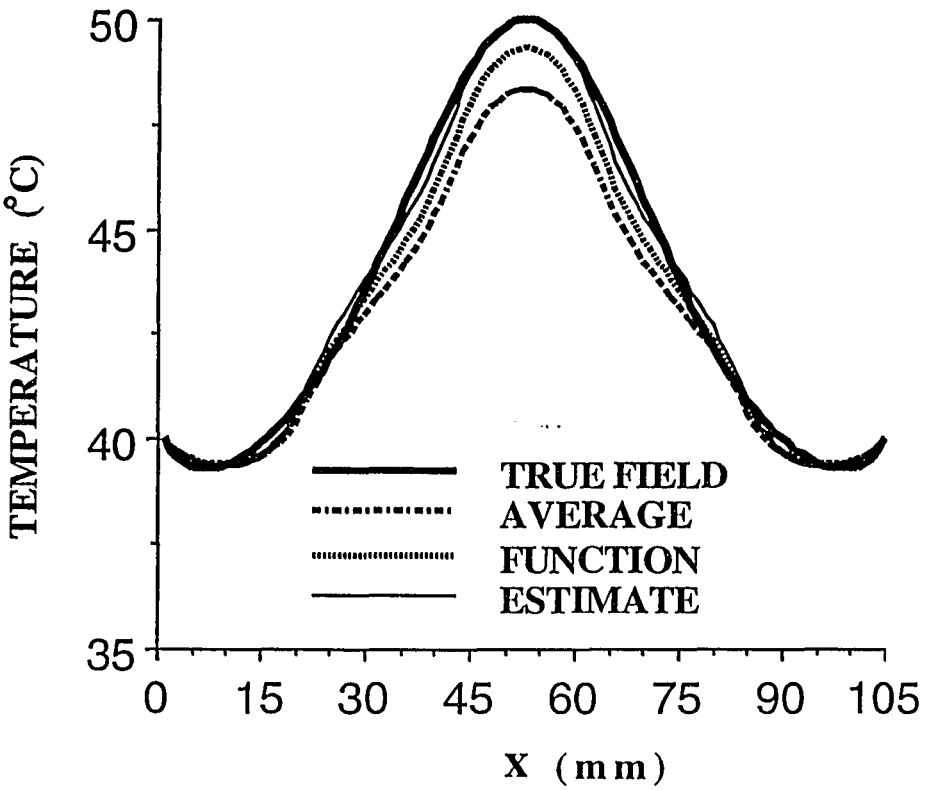

Figure 3.36 Steady-state temperature fields for the true parabolic case and for the average, function, and inverse perfusion fields for the 5 zone model.

DISCUSSION

When the perfusion field was approximated by a zonal approach using an equal-sized N zone model, the estimate of perfusion for each zone is dependent upon the sensor location in each zone. This can be seen from Table 3.13 for the parabolic case. The estimated perfusion vector is close to the function perfusion vector for any zone model. This is because the temperature response at a point is determined by its surrounding perfusions locally. Thus, when the optimization algorithm was used to minimize the objective function (S) in equation (2.2), the estimated perfusion vector is always close to the function vector, rather than the average one.

To further illustrate this phenomenon, a two zone model for the linear perfusion field was used. The number of sensors used was two but their locations were varied. Table 3.14 shows the resulting estimates of perfusion, the corresponding function perfusions, and the maximum difference between the true and predicted temperature fields for four sets of sensor locations. It shows that for a given zone model with the number of sensors equal to the number of zones, there exist some sensor locations which can obtain a better temperature reconstruction. Because there is model mismatch, it will not help to improve the accuracy of the reconstruction temperature field by increasing the number of sensors greater than the number of zones. Table 3.13 shows that the maximum temperature difference decreases as the number of zones increases. In addition, it has been shown the feasibility of accurately reconstructing the temperature for the cases with the number of unknown parameters (or the number of zones) greater

Table 3.14 Estimated and function perfusions for a two zone model with two sensors at different locations for the linear perfusion case.

SENSOR LOCATIONS (mm)	ESTIMATED PERFUSION (kg/m^3-s)		FUNCTION PERFUSION (kg/m^3-s)	
	W_1	W_2	W_1	W_2
27,80	2.304	6.155	2.375	6.197
20,90	1.940	6.842	1.870	6.918
10,97	1.542	7.284	1.149	7.423
46,60	3.426	4.983	3.745	4.750

than the number of sensors (Clegg et al. 1988, Liauh et al. 1991). Therefore, for a fixed number of sensors, the accuracy of the temperature reconstruction can be improved by increasing the number of zones.

3.5 IMPLEMENTATION OF POWER-ON TEMPERATURES

In an attempt to show the feasibility of utilizing the transient power-on temperatures as input data for the optimization algorithm to accurately estimate the blood perfusion and/or the parameters related to the applied power, several cases with either a uniform power field or an ultrasound power field were tested. First, the previous one-dimensional 2 zone (see Figure 3.2) and three-dimensional 7 zone (see Figure 3.1) models with a uniform power were selected to show the feasibility of using the power-on data to predict the blood perfusion and to reconstruct the steady-state temperature field. Second, a scanned focussed ultrasound power field was used to simulate treatments for the three-dimensional 7 zone model. It should be noticed that the blood perfusion field for this study was assumed not to change during the heating-up process, something which may occur in some clinical situations.

Like the case with the transient power-off data, an initial guess of blood perfusion is needed to start the parameter estimation procedure. From the results of the power-off study, a good initial guess of the unknown perfusion will help to obtain an accurate estimation. For this reason, the initial guess should be close to the true solution. Unlike previous investigators (Clegg, et al., 1988,

Liauh, et al, 1991, Roemer 1990) who used the transient decay temperatures to evaluate the local perfusion, an iterative scheme was developed in this dissertation (see Appendix B) to obtain an initial estimate for the local perfusion from the power-on temperatures. For the zones in which temperature measurements were available, an initial estimate of perfusion was assigned as the local effective perfusion ($W_{eff} = U/c_b$) for each zone. In this method, the general solution could be solved analytically (equation (B.3)). Equation (B.3) shows that the relationship between the temperature and the effective perfusion is nonlinear. Therefore, an iterative scheme was derived to optimize the effective perfusion by minimizing the difference between the measured and predicted temperatures. Like the previous cases using the transient power-off temperatures, for the zones without temperature measurements, the perfusions were initially set to zero.

UNIFORM POWER

The simulated hyperthermia treatments were created for the one- and three-dimensional cases. Like previous studies, the thermophysical properties of tissue were assumed constant and known, and the boundary and initial conditions were the same as before. The magnitude of the uniform power for the one-dimensional 2 zone model with a perfusion vector [0.5,8.0] kg/m^3-s was 36,800 W/m^3 shown in Table 3.1 and 14,910 W/m^3 for the three-dimensional 7 zone model shown in Table 3.5. To illustrate the general power-on temperature patterns, Figure 3.37 plots the transient power-on temperatures at seven sensor locations for the one-dimensional 2 zone model.

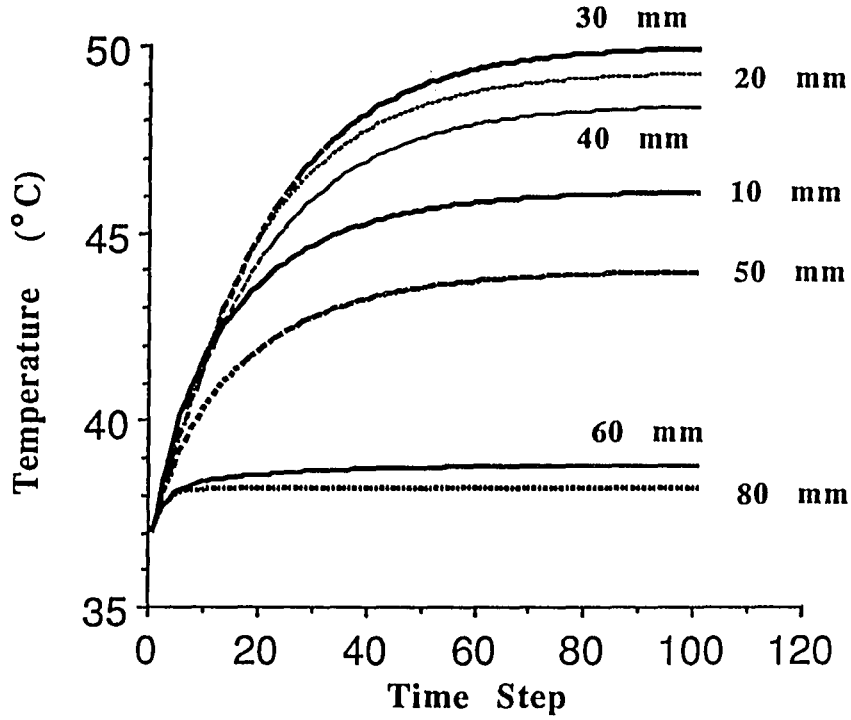

Figure 3.37 Transient power-on temperatures at 7 different sensor locations for the one-dimensional model with 2 equal-sized zones.

Figure 3.38 plots the maximum absolute difference between the true and predicted steady-state temperature fields as a function of the sensor location by using the zero initial guess method. The number of time steps was 56 and two noise levels were used, 0.0 and 0.2 °C.

This figure (see discussion section also) shows the general feasibility of using the transient power-on data for a simple one-dimensional 2 zone model. Next, a three-dimensional model with 7 zones was further investigated. The number of sensors used in this case was either 7, 4, or 3. For the case with seven sensors, they are located at the centers of zones. When four sensors are used, they are located at the centers of zones, 1, 2, 3, and 4, and for the three sensor case they are located at the center of zones 1, 2, and 3. Table 3.15 shows the resulting performance of the estimation algorithm using the transient power-on and power-off data for two different noise levels. It illustrates that the estimation algorithm has the same performance when using either the transient power-on or power-off temperature measurements.

SCANNED FOCUSED ULTRASOUND POWER

To simulate the real clinical situation during ultrasound hyperthermia treatments, where the applied power is a function of space rather than a uniform constant, a scanned focused ultrasound power field was created. In this study, the focussed ultrasound power distribution in the soft tissue was assumed to be well described by equation (2.31) if the soft tissue ultrasonic attenuation was given. One goal is to use the estimation algorithm to predict this attenuation coefficient from the power-on temperature measurements.

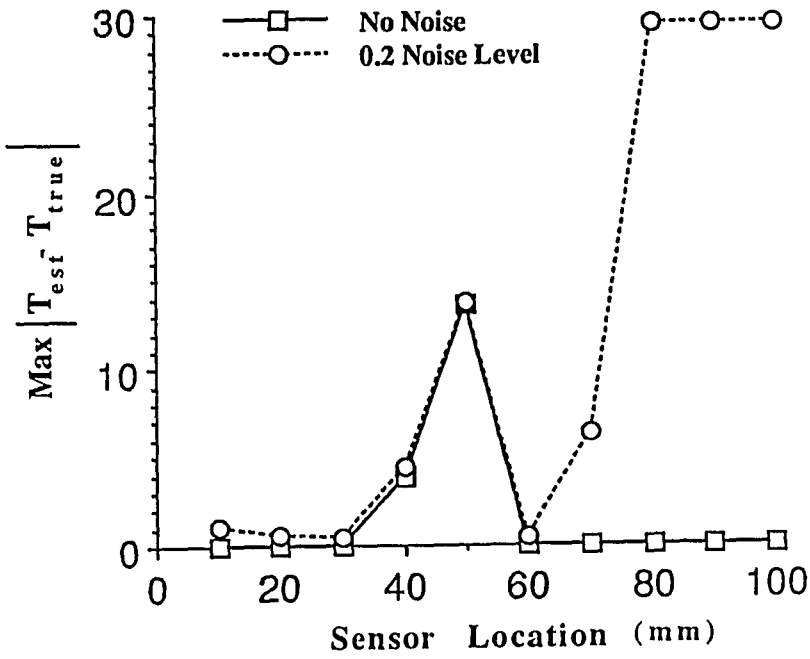

Figure 3.38 Maximum (absolute) difference between the true and predicted steady-state temperature fields as a function of sensor location for the 2 zone model using a zero initial guess for two noise levels.

Table 3.15 Maximum temperature difference between the true and estimated temperature field and the number of iterations for the three-dimensional model with a symmetric perfusion vector (see Table 3.5). ON indicates the case using the transient power-on data and OFF indicates the case using the transient power-off data. No regularization was used.

N_p	N_s	Noise Level (°C)	Accuracy (°C) Max$\lvert T_{ture} - T_{est} \rvert$ ON	OFF	Number of Iterations ON	OFF
7	7	0.0	0.00	0.00	4	4
7	7	0.2	0.02	0.01	5	4
7	4	0.0	0.00	0.00	6	8
7	4	0.2	0.71	0.62	9	11
7	3	0.0	0.00	0.00	8	14
7	3	0.2	4.92	1.09	26	13

Direct Case

A single transducer with a radius of curvature of 25 cm and a diameter of 7 cm was used to simulate the ultrasound power field. The frequency of the ultrasound wave was 1 MHz, and the distance between the skin surface and the transducer was 18.5 cm in the z direction. Figure 3.39 shows the contour plot of the absorbed power deposition pattern for the transducer focussed at 3 cm from the skin (i.e. the focal depth of 3 cm) of the tissue with the attenuation coefficient of 0.3527 (dB/cm-MHz) (Moros 1990). This absorbed power field was divided by its peak value and then rescaled such that the maximum was 100% at the peak.

For this stationary transducer, the effective absorbed power deposition at the focal plane is about 1.5 cm in diameter as shown in Figure 3.39. In order to elevate the temperatures for most of a large tumor region, the transducer was horizontally scanned. Figure 3.40 illustrates the schematic diagram of the simulated experimental setup showing the transducer orientation and scanning procedure. After the absorbed power deposition generated the single stationary transducer was evaluated, a program developed by Moros (1990) was used to calculate the average scanned focussed ultrasound power deposition for the same transducer scanning a circular path. This average power field was used to calculate the steady-state temperature field for the simulated hyperthermia treatment. Figures 3.41 and 3.42 plot the average scanned focussed ultrasound power depositions in the x-z plane at y=6 cm and the x-y plane at the focal depth plane for the case with a scanning diameter of 3 cm, respectively.

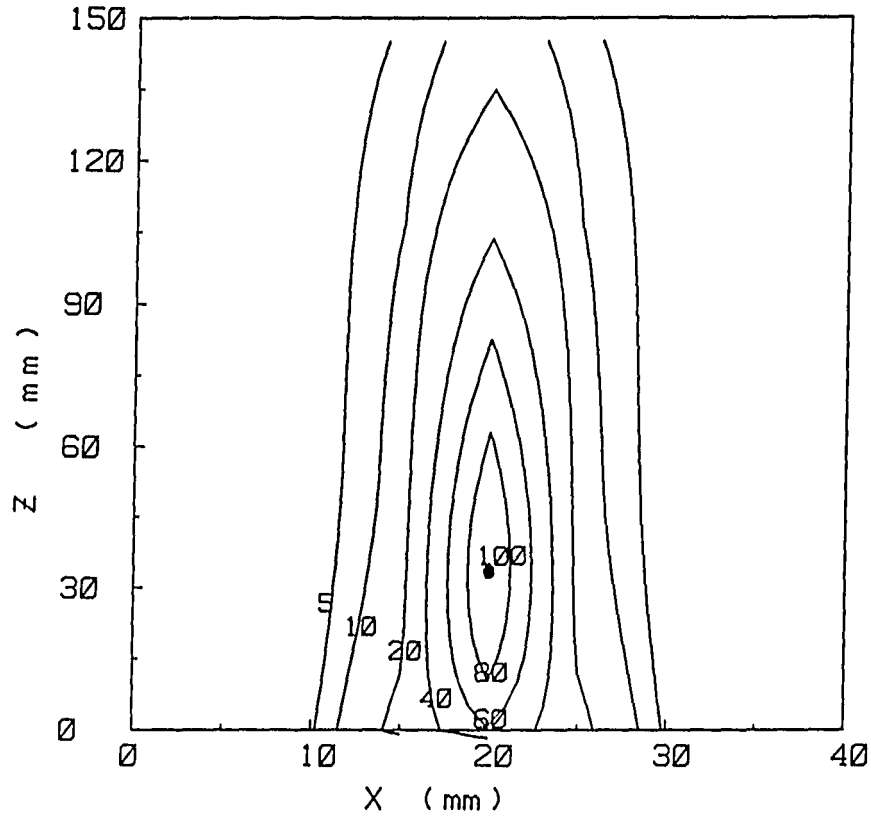

Figure 3.39 Contour plot of the absorbed power deposition pattern for the case with the focal depth of 30 mm from the skin.

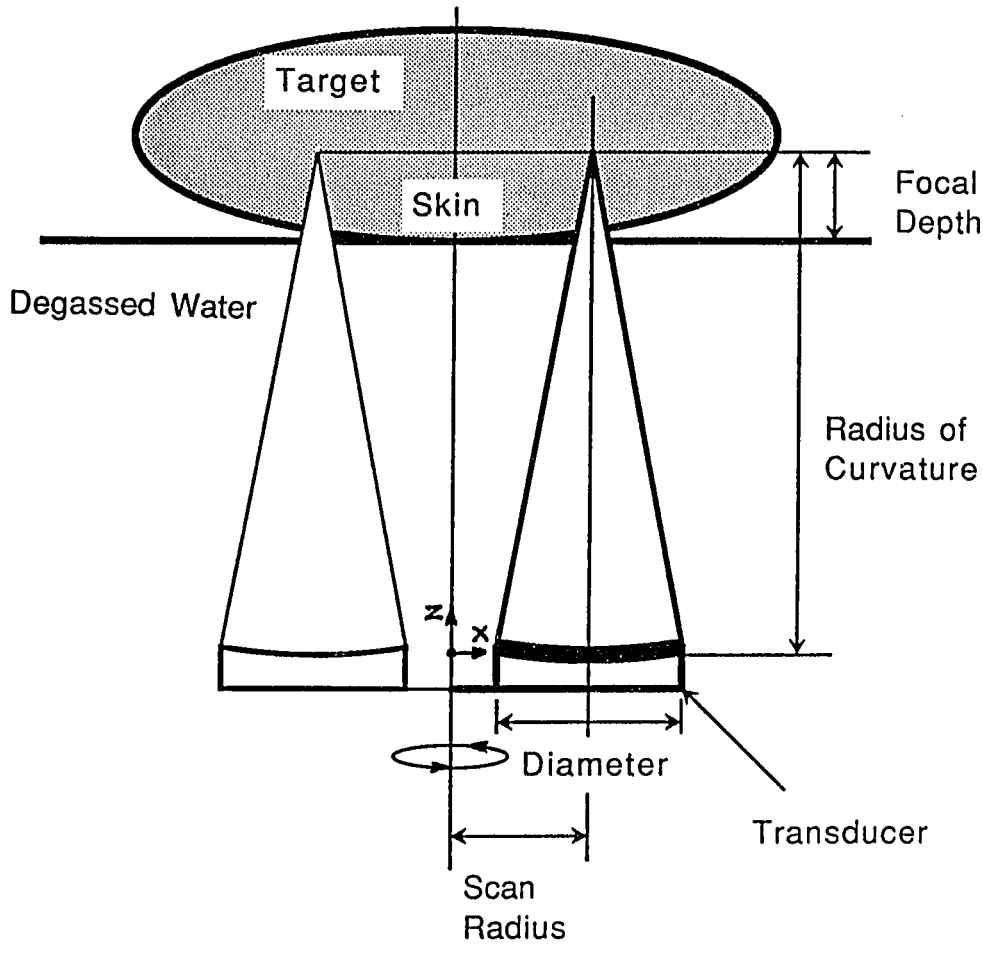

Figure 3.40 Schematic diagram of experimental setup showing the transducer orientation and scanning procedure. Figure not to scale.

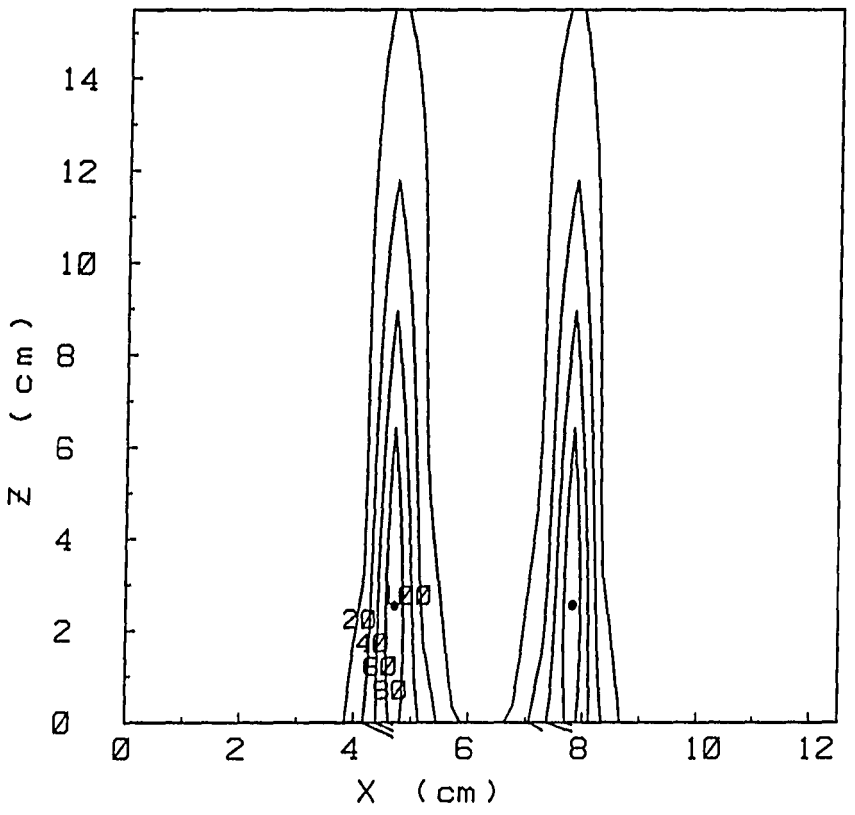

Figure 3.41 Average scanned focussed ultrasound power deposition in the x-z plane at y=6 cm.

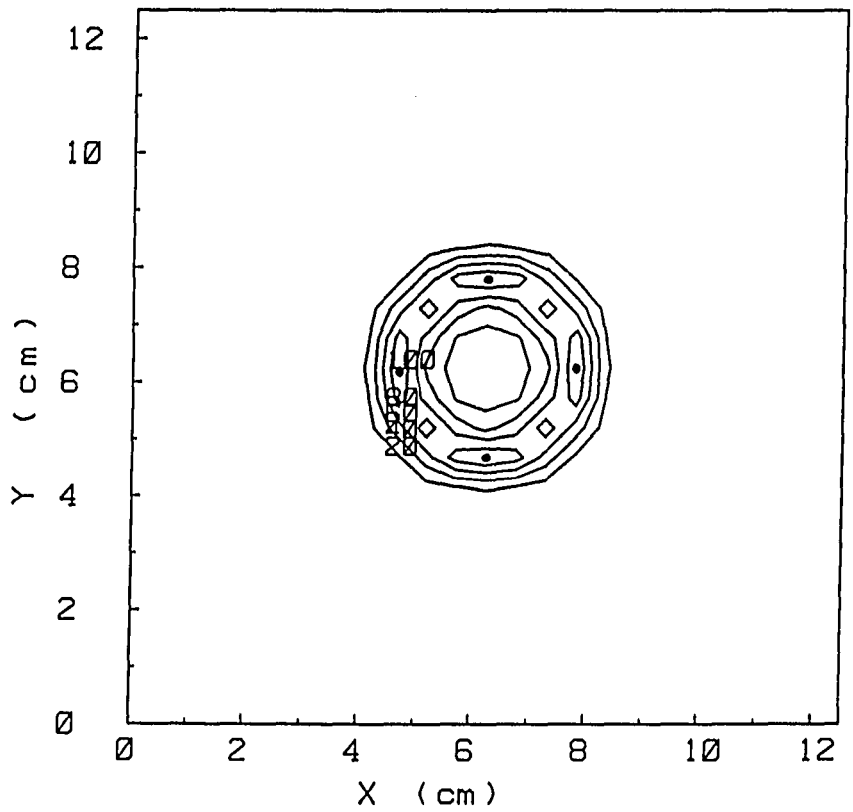

Figure 3.42 Average scanned focussed ultrasound power deposition in the x-y plane at the focal depth plane.

Inverse Case

For the inverse case, the attenuation coefficient (α) was assumed to be unknown and it was attempted to estimate its value by using a state and parameter estimation algorithm from a set of transient temperature measurements during simulated hyperthermia treatments. A set of measured temperatures was obtained from the solutions of the bioheat transfer equation using the average scanned focussed ultrasound power field (shown in Figures 3.41 and 3.42). The measured temperatures include the steady-state and transient power-on data at several sensor locations. To simulate future animal experiments (not to be performed in this dissertation study), the number of probes used in this study was 16. Each probe has 7 equal-spaced measurement points. Hence, the total number of measurement locations was 112. Figure 3.43 illustrates the schematic diagram for the proposed positions of the 16 probes for the future experiment.

First, a simple three-dimensional model with a uniform perfusion of 0.5 kg/m^3-s was used to show the feasibility of predicting the attenuation coefficient when the perfusion field was known exactly during the estimation procedure. The sampling time interval for this uniform perfusion case was 60 seconds. It should be noticed that in this study the only unknown parameter was the attenuation coefficient. Table 3.16 shows the resulting estimates of the attenuation coefficient by using all temperatures at 112 sensor locations for the cases with the number of time steps of 20, 10, and 2 for different perfusions (W). It shows that the predicted attenuation coefficient (μ_p) can be accurately estimated by a few transient power-

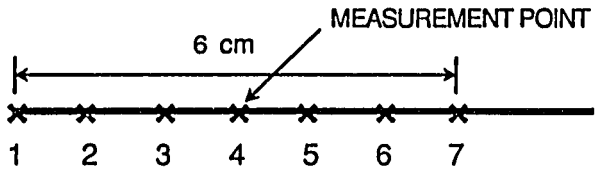

(a)

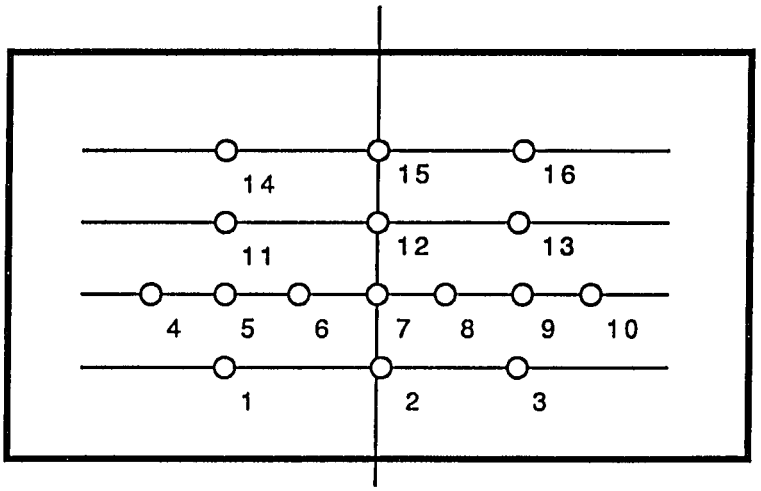

(b)

Figure 3.43 Schematic diagram for (a) the measured points for the 7 junction probe; (b) the layout of all 16 probes.

Table 3.16 Values of the predicted attenuation coefficient (μ_p) for different given perfusions (W) and the numbers of time steps (N_t).

W	0.5	0.5	0.5
N_t	20	10	2
μ_p	0.353	0.353	0.353

W	0.5	0.4	0.3	0.2	0.1	0.0	0.6	0.7	0.8	0.9	1.0
N_t	2	2	2	2	2	2	2	2	2	2	2
μ_p	0.353	0.351	0.349	0.347	0.345	0.344	0.355	0.356	0.358	0.360	0.362

on temperatures, providing the perfusion was known and the temperatures were noiseless. Furthermore, it is desirable to investigate the influence on the estimate of the attenuation coefficient when the perfusion was given with a wrong magnitude. Figure 3.44 plots the percent error between the true and predicted attenuation coefficients as a function of the given perfusion value for the cases with 112 sensor locations and without noise. The percent error was defined as the value of $[(\mu_p-\mu_{true})/\mu_{true}]\times 100\%$. The slope of the line in Figure 3.44 is approximated as 5 %/(kg/m^3-s); thus, the percent error is 0.5% when the given perfusion is 0.1 kg/m^3-s from the true perfusion (0.5 kg/m^3-s).

Next, both the attenuation coefficient and the magnitude of the uniform blood perfusion, which were unknown parameters, were estimated from the transient power-on temperatures. Table 3.17 shows the resulting estimates of the perfusion and the attenuation coefficient for the cases with 112 sensors with 80 transient power-on data with three noise levels (0.0, 0.1, and 1.0 °C). It shows the uniform perfusion and the attenuation coefficient can be accurately estimated by using 112 sensors even though the temperature measurements contain large noise (1.0 °C).

Finally, a more complicated three-dimensional model with a nonuniform perfusion field was tested. The real perfusion field was a piecewise constant vector [0.2,0.8,0.3,0.1,0.6,1.0,0.5]. The above scanned focused ultrasound power was also used to simulate the treatments with 16 temperature probes (112 sensor locations). The sampling time interval for this perfusion vector was 30 seconds. For

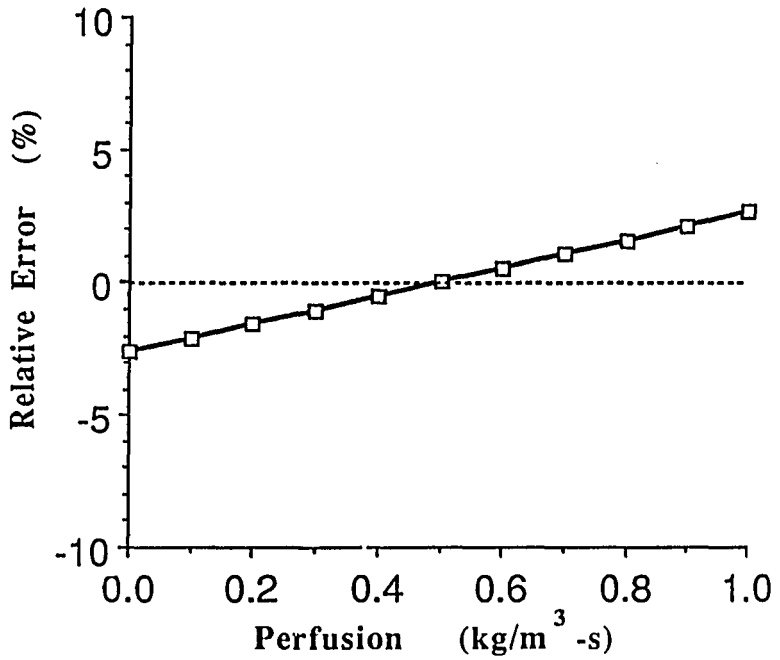

Figure 3.44 Percent error between the true and predicted attenuation coefficients as a function of the perfusion value.

Table 3.17 Estimate of the perfusion, the percent error of the estimated attenuation coefficient, and the maximum difference between the true and predicted steady-state temperature fields for the case with a uniform perfusion of 0.5 kg/m^3-s and a scanned focussed ultrasound power. Both the perfusion magnitude and the attenuation coefficient magnitude were estimated.

N_t	NOISE LEVEL (°C)	ESTIMATED PERFUSION (kg/m^3-s)	PERCENT ERROR FOR μ_p (%)	MAX. ERROR (°C)
80	0.0	0.5	0.0	0.0
80	0.1	0.499	0.08	0.004
80	1.0	0.496	0.88	0.045

this inverse case, the perfusion vector and the attenuation coefficient were unknown. Thus, the total number of unknown parameters was 8. Table 3.18 shows the resulting estimates of the perfusion vector and the attenuation coefficient for the cases using 112 sensor locations with two noise levels and two different time steps. Without noise the estimation algorithm always predicts the perfusion vector and the attenuation coefficient very accurately for the cases with N_t of 10 and 80. As can be seen from Table 3.18, the 1.0 °C noise level greatly degrades the performance of the estimation algorithm if the number of transient power-on data is small.

DISCUSSION

The reason for the failed temperature reconstruction for the case with the sensor close to the interface by using a zero initial guess method shown in Figure 3.38 is because of the existance of the multiple minima solutions. From the previous study of the multiple minima, two possible perfusion vectors, [0.5,8.0] and [8.0,0.5], will provide the same temperature responses at the sensor which is located at the symmetric point when the transient power-off temperatures were used. The same phenomena as seen in the previous multiple minima studies will occur in this case with the transient power-on temperatures. When the sensor was located near the interface, 40 or 50 mm for example, the estimation algorithm converged to the local minimum point because the initial guess was close to it. Using the symmetric knowledge obtained from the previous studies, the second estimated perfusion vector converged to the true perfusion values by

Table 3.18 Estimate of the perfusion vector, the percent error of the estimated attenuation coefficient, and the maximum difference between the true and predicted steady-state temperature fields for the case with the perfusion vector [0.2,0.8,0.3,0.1,0.6,1.0,0.5] (kg/m^3-s) and a scanned focussed ultrasound power.

N_t	NOISE LEVEL (°C)	ESTIMATED PERFUSION (kg/m^3-s) $[W_1,W_2,\ldots,W_7]$	PERCENT ERROR FOR μ_p (%)	MAX. ERROR (°C)
10	0.0	0.2,0.8,0.3,0.1,0.6,1.0,0.5	0.0	0.0
10	1.0	0.089,1.481,0.314,-0.02,0.536,0.991,0.436	-3.66	1.15
80	0.0	0.2,0.8,0.3,0.1,0.6,1.0,0.5	0.0	0.0
80	1.0	0.194,0.804,0.327,0.091,0.611,0.986,0.5	-0.45	0.06

using a second initial guess based on the first estimated perfusion vector. For instance, the first estimated perfusion vector was [2.24,0.44] from the initial guess [0.47,0.0] when the sensor was at 50 mm. Using a new initial guess [0.44,2.24], the final estimated perfusion vector converged to [0.5,8.0]. This study also shows that the performance of the estimation algorithm degrades when the power-on data contains additive noise.

For most of the successful cases when the maximum temperature difference between the true and the predicted temperature fields was less than 1 °C as shown in Table 3.15, the total computational time required for the case with the power-on data is less than that with the power-off data. This is due to two reasons. First, for the power-off case, there is a need to calculate the steady-state temperature field before evaluating the transient power-off temperature responses. On the other hand, for the power-on case, the entire temperature field before calculating the power-on temperature responses is given as a constant, uniform initial condition. Second, after calculating the transient power-on responses, the steady-state temperature field can be calculated faster by using the final transient power-on temperature field as an initial condition, rather than the given (original) initial condition for the same applied power.

Table 3.16 illustrates that the estimate of the attenuation coefficient is not sensitive to the variation of the perfusion field. This occurs because the temperature rise is dominated by the applied power at the beginning of the heat-up procedure. At this stage, the effect of the perfusion is not significant. Thus, the resulting

temperatures linearly increase with time as shown in Figure 3.37. In this situation, the attenuation coefficient can be accurately estimated without good knowledge of the perfusion field, even if the first two power-on temperatures were used. This is an encouraging result because it indicates that perhaps this technique can be used to accurately predict a power deposition during the ultrasound hyperthermia treatments even though the perfusion field is not accurately known. It should be noted that the number of time steps should be large in this period (i.e. the sampling time interval is small) in order to eliminate the effect of the noise which will occur during the treatments.

CHAPTER 4

CONCLUSIONS

In this dissertation the feasibility of using a (semi-linear) state and parameter estimation algorithm to optimize the perfusion and then predict the steady-state temperature field from a limited number of transient (power-on or power-off) temperature measurements has been shown for simulated hyperthermia treatments. Using one-, two-, and three-dimensional numerical simulation models, it is shown that multiple minima solutions exist for some inverse hyperthermia temperature estimation problems. A general strategy is obtained for (a) detecting when the inverse algorithm has converged to a local minimum, and (b) for using that knowledge to direct the search algorithm towards the global minimum. In forming the Jacobian matrix, the results show that the influence coefficient and sensitivity equation methods have the same performance and are preferable to the adjoint formulation. To further speed up the algorithm, a semi-linear approach is implemented. Results show that this improved state and parameter estimation algorithm decreases the total computational time required to accurately reconstruct complete hyperthermia temperature fields. The effects of the model mismatch have been presented for the

one-dimensional problem. From previous results, the feasibility of using sets of transient power-on temperatures as inputs for the state and parameter estimation algorithm to simultaneously reconstruct both the temperature and ultrasound power fields has been shown for the simulated ultrasound hyperthermia treatments.

4.1 MULTIPLE MINIMA

Multiple minima (and saddle points) exist in the inverse hyperthermia problem due to symmetries in the perfusion model used in the inverse algorithms. These minima are solely an artifact of the symmetries in the inverse case perfusion model and their existence is unrelated to the true perfusion present in any patient. Adding asymmetries to the problem can cause these minima to change from global to local, but does not eliminate them. Knowledge of their possible presence can be used in a multiple initial guess search strategy to aid in finding the true global minimum. The optimal sensor locations appear to be those at points of maximum symmetry (i.e. on perfusion zone boundaries).

4.2 JACOBIAN FORMULATION

The results show that when the ratio of the number of measurement sensors to the number of unknown parameters is smaller than a critical value (approximately 1/4), the adjoint formulation is faster (CPU time to form the Jacobian matrix) than the influence coefficient method. Unfortunately, for the problems investigated in this study the number of sensors needed to obtain enough information

to yield successful inverse solutions is such that the corresponding ratios are always larger than the critical values. Thus, while the adjoint method appears to be theoretically sound, the method suffers during its numerical implementation when compared to the influence coefficient method. The large CPU times associated with the numerical implementation of the adjoint method are a result of the CPU intensive integrations for evaluating the convolution over time. Additionally, the numerical errors associated with the integrals are significant, a factor which adversely affects the convergence rate and the ultimate success of the nonlinear parameter estimation procedure. Thus, the results show that the influence coefficient method was generally less CPU intensive overall for the problems considered. To be competitive with the influence coefficient method, faster and more accurate numerical integration techniques must be used and better early time finite difference approximations near the Dirac Delta initial conditions must be developed.

A more general result obtained from this study is that the basic computer operation equation approach is a valid method of comparing competing numerical techniques. The main value of this approach is that it allows comparisons of approaches based on the characteristics of their basic algorithms, and it does not require that the techniques be programmed and run, as does the subroutine program method. The technique is thus valid, general, and easy to use.

4.3 SEMI-LINEARITY

This paper presents the results of a new approach to use in the state and parameter estimation algorithm to decrease the total computational time while still accurately reconstructing the entire temperature field. The results indicate that there is an optimal choice of $DELTA_1$ such that the computational time required is minimum and the accuracy of the reconstruction remains. For the two perfusion patterns studied here, the optimal value for $DELTA_1$ is 0.5 without losing a large number of successful cases but reducing the computational time to 40% of the original time needed without implementing this semi-linear approach. From this study it can be concluded that when the average perfusion is low, the relationship between the temperature and the perfusion is quasilinear. Thus, this semi-linear scheme can be implemented to obtain a great improvement. For more complicated perfusion distributions, a comprehensive set of cases has to be studied before using the semi-linear scheme to improve the performance of the algorithm.

4.4 MODEL MISMATCH

From the model mismatch study, the accuracy of the reconstructed steady-state temperature field is apparently dependent upon a) the number of parameters (the number of perfusion zones) that are optimized, b) the maximum and minimum perfusions in the zones, and c) the number of temperature sensors and their locations. The minimum number of zones is five for the linear perfusion field and 10 for the parabolic perfusion field to obtain the direct steady-state temperature fields within 1.0 °C accuracy. In these cases, the

difference between the maximum and minimum perfusions within each zone is about 2.0 kg/m^3-s. It has been shown that the number of zones for the zonal approach is crucial to determine the accuracy of the reconstruction. Moreover, if the zonal approach is not good enough to describe the real perfusion field, increasing the number of sensors to become greater than the number of zones will not help to obtain more accurate reconstructions.

4.5 POWER-ON DATA

The preliminary results of the one-dimensional case using transient power-on temperatures show that the same phenomena as from the previous multiple minima study exist as when using transient power-off temperatures. Therefore, the same strategy developed for the multiple minima study can be applied for the power-on cases. Second, the results reveal that the total computational time required for the case with the power-on data is generally less than that using the power-off data. Finally, the attenuation coefficient can be accurately predicted by the estimation algorithm using the first few power-on temperature measurements even when the perfusion field is not accurately known.

4.6 FUTURE WORK

Although the results from the above simulations are promising, much work is still necessary before implementing the estimation algorithm in the clinic. Some recommendations for future work follow:

(1) Direct case studies of various perfusion parameterizations should be performed to determine how many parameters are enough to describe the real perfusion field before the estimation algorithm is used to predict them. Presently, several techniques, such as Xenon uptake, radioactive tracers or colored microspheres, can provide information about the real perfusion field. By using either the polynomial approximation (e.g., a cubic spline function) or the zonal approach to fit these data, the question arises is, how many polynomials (spline functions) or perfusion zones are needed to accurately describe the real perfusion field?

(2) As was previously pointed out by several investigators, Pennes' bioheat transfer equation cannot describe the temperature field accurately when large blood vessels are present. If there is a good thermal model for hyperthermia which includes the existence of blood vessels, it is desirable to use the estimation algorithm to predict some blood vessel parameters present in the thermal model, e.g., the velocities in the blood vessels.

(3) As seen from the previous results of the model mismatch for the one-dimensional model, the optimal sensor location exists but it is related directly with the model mismatch. Before investigating the optimal sensor location problem, more studies about the effects of the model mismatch on the estimation algorithm should be systematically studied.

(4) From the power-on study, the scanned focused ultrasound power field could be accurately predicted when the attenuation coefficient of the tissue was accurately estimated by the estimation algorithm. Some sensitivity studies have to be done to obtain what terms or conditions will have greatest effects on the inverse solutions. For example, the effects of the sensor locations, the boundary conditions, the position of focal depth, etc. From these studies, it will provide information about which terms or conditions should be measured carefully during the animal experiments or patient treatments.

(5) A sequential estimation can be developed to predict the blood perfusion by using the transient power-on data.

(6) In order to deal with more complicated problems, a vectorized program should be developed for the parallel (or vectorized) computer systems when the number of unknown parameters is large.

APPENDIX A

PENETRATION DEPTH

To quantitively understand the reason why the state and parameter estimation algorithm can more easily predict the temperature fields for the models with low perfusion patterns the following analysis is given. First, we consider a simple one-dimensional problem (shown in Figure A.1a) with a constant boundary temperature (T_b) at the boundary x=a and a semi-infinite, homogeneous domain ($a \leq x \leq \infty$) governed by the bioheat transfer equation. For a situation without applied power the governing equation for the steady-state temperature field is

$$\frac{d^2T}{dx^2} - \alpha^2(T-T_a) = 0 \qquad (A.1)$$

where $\alpha^2 = (Wc_b)/k$. The general solution is written as

$$T-T_a = C_1e^{-\alpha x} + C_2e^{\alpha x} \qquad (A.2)$$

where C_1 and C_2 are constant values. Plugging the boundary condition

$$T(x) = T_b \text{ as } x = a \ (= 0),$$

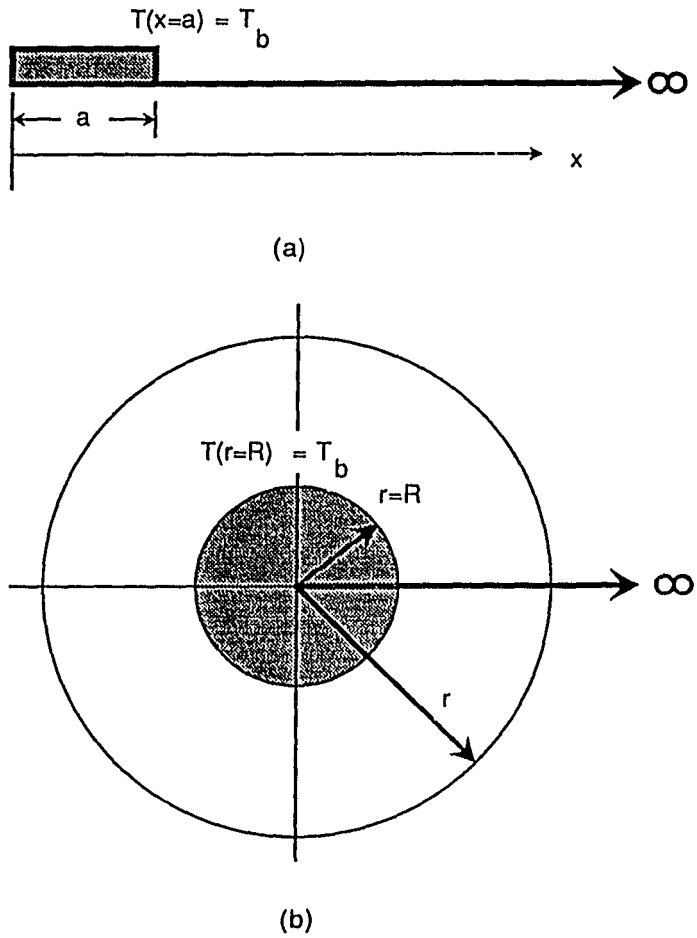

Figure A.1 Schematic diagram for (a) the one-dimensional cartesian model with a semi-infinite domain; (b) a sphere inside an infinite domain.

and T(x) is bounded as $x \to \infty$ into equation (A.2), the final solution is

$$\frac{T(x) - T_a}{T_b - T_a} = e^{-\alpha x} = e^{-x/(k/Wc_b)^{1/2}} \qquad (A.3)$$

The penetration depth is defined as the distance (x_p) such that $x_p = (k/Wc_b)^{1/2}$. Equation (A.3) shows that the penetration depth decreases as the perfusion W increases.

Based on equation (A.3), the sensitivity term $\partial T(x)/\partial W$, defined as the derivative of temperature with respect to the perfusion, is

$$\frac{\partial T(x)}{\partial W} = \frac{-x}{2}\left[\frac{c_b}{kW}\right]^{1/2}(T_b - T_a)\, e^{-x/(k/Wc_b)^{1/2}}$$

or

$$\frac{\partial}{\partial W}\left\{\frac{T(x)-T_a}{T_b-T_a}\right\} = \frac{\partial T^+}{\partial W}$$

$$= \frac{-x}{2}\left[\frac{c_b}{kW}\right]^{1/2} e^{-x/(k/Wc_b)^{1/2}} \qquad (A.4)$$

To quantify this effect, three test cases were chosen in which the values of blood perfusion (W) were 0.5, 4.0, and 8.0 kg/m^3-s. Figure A.2 plots the nondimensional temperature field as a function of x and Figure A.3 plots the sensitivity as a function of x.

Second, assume that there is a constant boundary temperature (T_b) on an inner spherical boundary at r=R located inside an infinite, homogeneous domain ($R \leq r \leq \infty$) (shown in Figure A.1b) governed by the bioheat transfer equation. For a situation without applied power the governing equation is

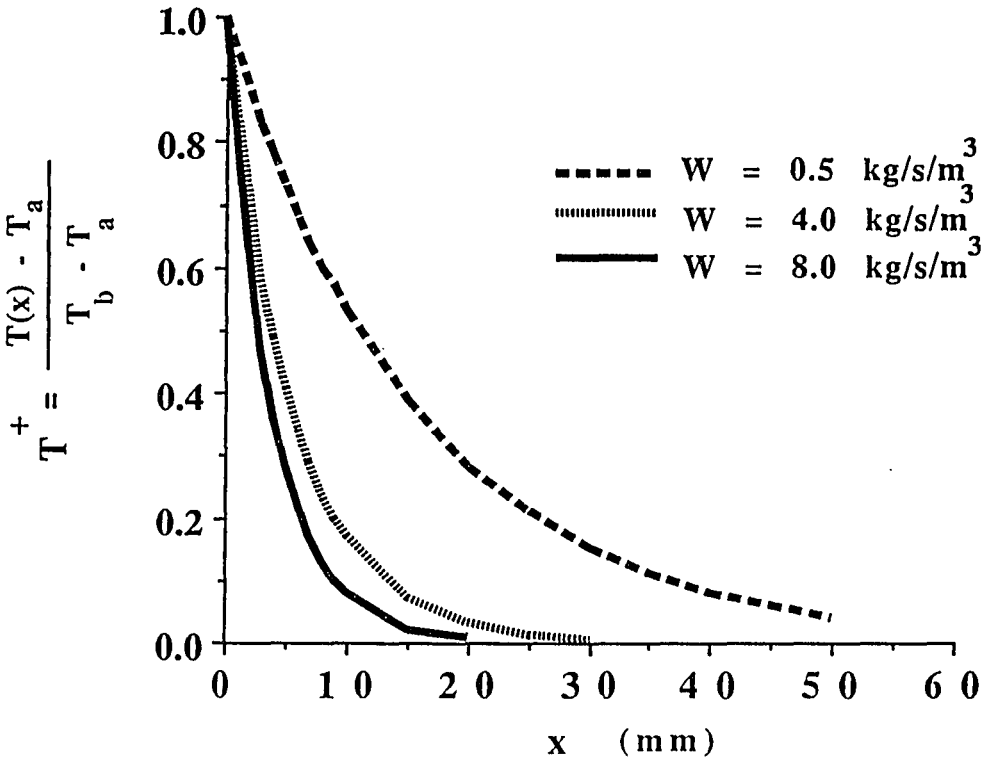

Figure A.2 Nondimensional steady-state temperature field

$T^+ = \frac{T(x)-T_a}{T_b - T_a}$ as a function of x for three perfusion values of 0.5, 4.0, and 8.0 for one-dimensional case.

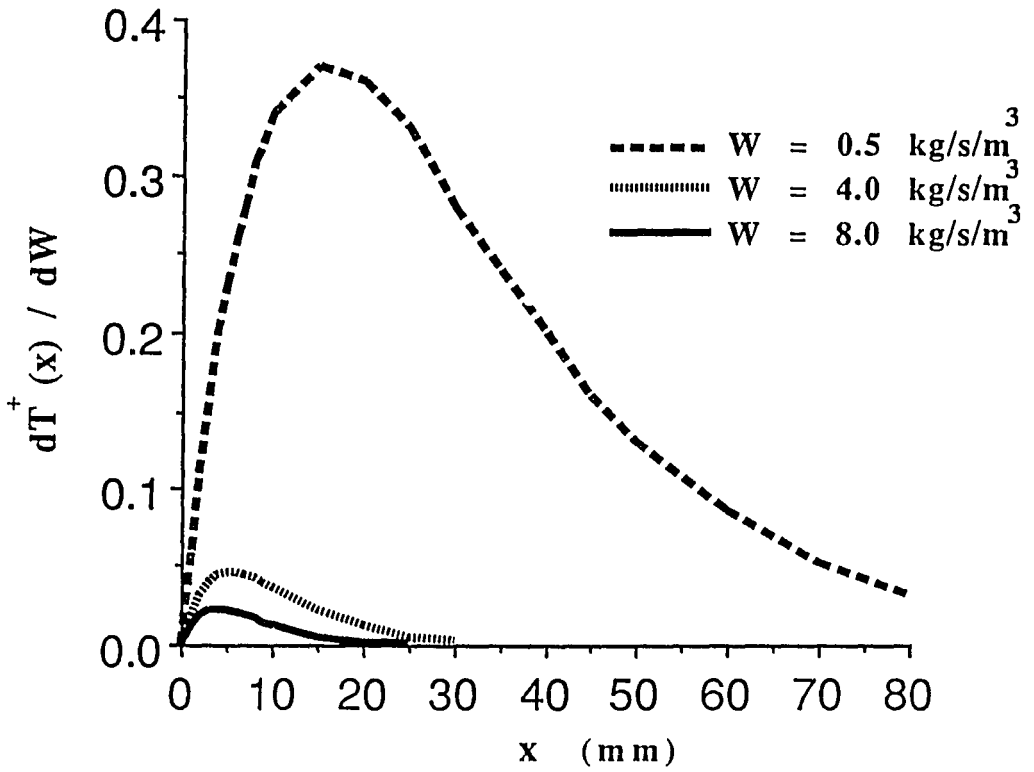

Figure A.3 Sensitivity dT^{+}/dW as a function of x for perfusion values of 0.5, 4.0, and 8.0 for the one-dimensional case.

$$\frac{d^2T}{dr^2} + \frac{2}{r}\frac{dT}{dr} - \beta(T-T_a) = 0 \qquad (A.5)$$

where $\beta=(Wc_b)/k$. The solution with the boundary conditions; $T=T_b$ at $r=R$ and $T=T_a$ as $r \to \infty$ is

$$T^+(r^+) = \frac{T(r^+) - T_a}{T_b - T_a} = \frac{K_{1/2}(r^+)}{K_{1/2}(R^+)} \sqrt{\frac{R^+}{r^+}} = \frac{R^+}{r^+} e^{-(r^+-R^+)} \qquad (A.6)$$

where $T^+ = (T-T_a)/(T_b-T_a)$, $r^+ = r/R^*$, and $R^*=1/(\beta)^{1/2}$.

Or

$$T(r) = T_a + \frac{(T_b - T_a)}{K_{1/2}[R(\beta)^{1/2}]} K_{1/2}[r(\beta)^{1/2}] \sqrt{\frac{R}{r}} \qquad (A.7)$$

where $K_{1/2}$ is the modified spherical bessel function of the third kind and order zero.

Based on the above equation, the sensitivity term $(\partial T^+/\partial W)$, defined as the derivative of temperature with respect to the perfusion, is

$$\frac{\partial T^+}{\partial W} = \frac{-(r-R)}{2} \left[\frac{c_b}{kW} \right]^{1/2} \frac{R}{r} e^{-(\beta)^{1/2}(r-R)} \qquad (A.8)$$

It is these sensitivity terms that are one of the most important factors in determining the performance of the state and parameter estimation algorithm since they tell how sensitive the temperature at some location r (i.e., a distance r from the constant temperature interface) is to changes in the tissue perfusion. The larger the value

of this term, the more chance the unknown perfusion term can be accurately estimated in inverse problems.

To quantify this effect, four test cases were chosen in which the values of blood perfusion (W) were 0.5 and 8.0 kg/m^3-s and the values of R were 1.75 and 0.525 cm. These values of W and R were selected to be reasonable approximations to the sizes of the zones in Figure A.1. Figure A.4 plots the nondimensional temperature field as a function of r and Figure A.5 plots the sensitivity as a function of r.

Several trends regarding Figures A.2-5 can be seen. First, for a fixed perfusion value a sensor closer to the high temperature (at x=a or inner boundary at r = R) has a stronger signal than a sensor far away from that boundary. Second, for a given sensor location the signal for the low perfusion case is larger than that for the high perfusion case since the penetration depth of the high temperature signal is larger.

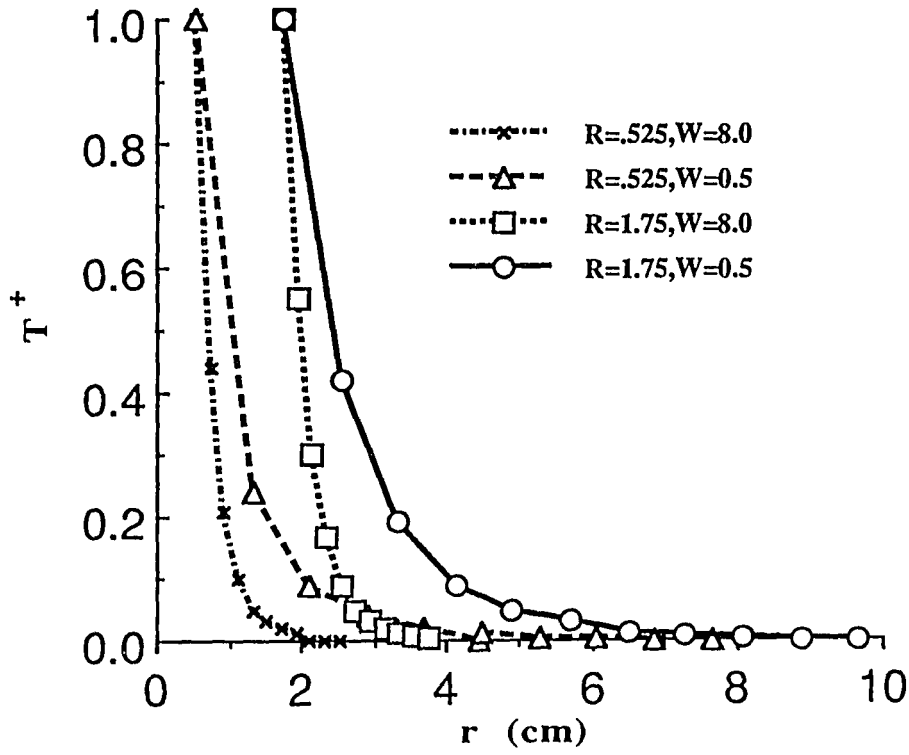

Figure A.4 Nondimensional steady-state temperature $T^+ = \frac{T(r) - Ta}{T_b - T_a}$ versus the distance (r) from the center of a constant temperature sphere of radius R, for two different values of the radius R and of the blood perfusion in the surrounding tissue (W).

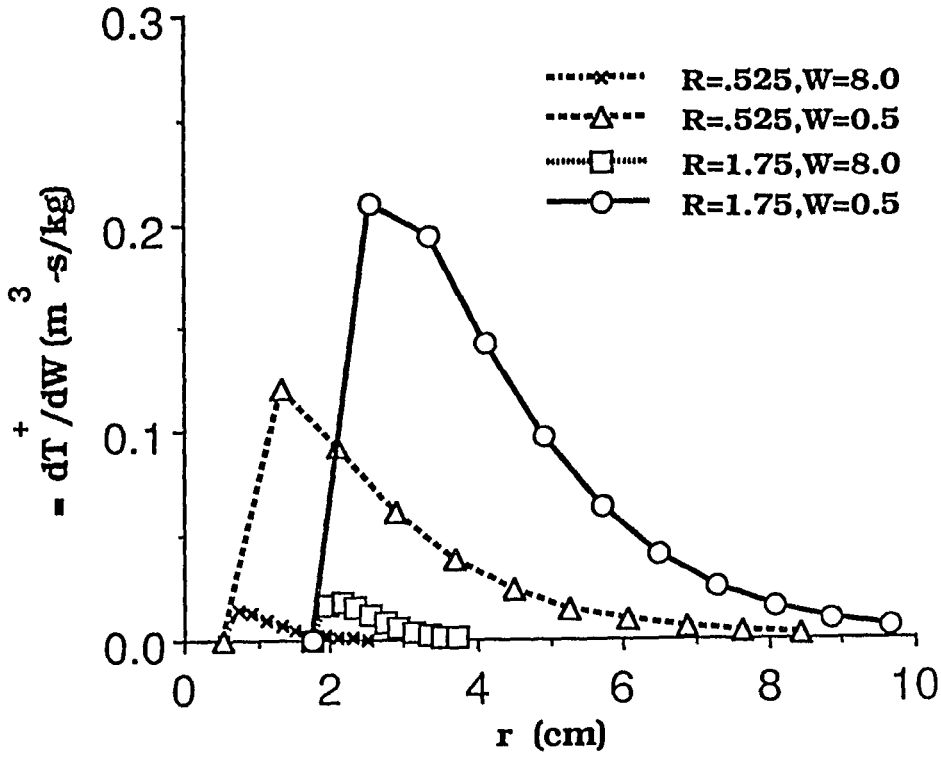

Figure A.5 Sensitivity Coefficient $\left[\frac{dT^+}{dW}\right]$ for the constant temperature sphere of Fig. 6 versus the radial distance (r) for two different values of the sphere radius R and of the blood perfusion (W).

APPENDIX B

EFFECTIVE PERFUSION USING POWER-ON DATA

During clinical situations, it is our attempt to use the transient power-on data to provide useful information to estimate the perfusion field, and thus obtain the complete temperature field inside the treatment region. A simple technique is developed to evaluate the magnitude of the perfusion around the temperature sensor. These perfusions can provide a good initial guess when using the state and parameter estimation algorithm. This technique essentially takes the bioheat transfer equation (1.1) and assumes that all conduction and blood perfusion effects can be lumped into a local tissue cooling coefficient term, U, which is defined as

$$- U(T-T_a) = k\nabla T^2 - c_b W(T-T_a). \qquad (B.1)$$

This assumption essentially neglects the conduction of the thermal energy and assumes that the heating is due to perfusion. Hence, it will give erroneous values of perfusion when the net rate of energy by conduction is significant. With this assumption, Pennes' bioheat transfer equation can be rewritten as

$$\rho c \frac{\partial T}{\partial t} = - U(T-T_a) + Q.$$

with an initial condition; $T(t=0) = T_a$.

Letting $T^* = T-T_a$, $\gamma = U/\rho c$, and $Q^* = Q/\rho c$

$$\frac{\partial T^*}{\partial t} = -\gamma T^* + Q^*. \qquad (B.2)$$

with an initial condition; $T^* = 0$.

Assuming that the thermophysical properties of the tissue (e.g., ρ, c, c_b, and U) are constant and the applied power (Q) is also constant, the general solution of equation (B.2) can be solved analytically. The solution can be written as

$$T^*(t) = \frac{Q^*}{\gamma} (1- e^{-\gamma t})$$

or

$$T(t) = T_a + \frac{Q}{U} [1-e^{-(U/\rho c)t}]. \qquad (B.3)$$

The relationship between the temperature (T(t)) and the local tissue cooling coefficient (U) is nonlinear from equation (B.3). Due to this nonlinearity, an iterative scheme is needed to optimize this local tissue cooling coefficient (U) by minimizing the difference between the measured and predicted temperatures. During the hyperthermia treatment, the transient power-on temperatures are recorded and used as the measured temperatures. A successive perfusion estimate can be derived by a Taylor series expansion for $T_{pr}(t;U^{k+1})$ at the k^{th} effective perfusion estimate (U^k) by neglecting the second and higher order terms. The resulting equation is expressed as

$$T_{pr}(t;U^{k+1}) = T_{pr}(t;U^{k}) + \frac{\partial T(t;U^{k})}{\partial U}\,(U^{k+1}-U^{k}), \qquad (B.4)$$

where $$\frac{\partial T}{\partial U} = -\frac{Q}{U^2}\,[1-e^{-(U/\rho c)t}] + \frac{Qt}{c\rho U}\,e^{-(U/\rho c)t}.$$

Assuming that the temperature term in the left hand side in equation (B.4) is close to the measured temperature (T_m), the new estimate of U is calculated as

$$U^{k+1} = U^{k} + \frac{\sum_{i=1}^{N_t} \frac{\partial T(t_i;U^{k})}{\partial U}\left\{T_m(t_i)-T_{pr}(t_i;U^{k})\right\}}{\sum_{i=1}^{N_t}\left\{\frac{\partial T(t_i;U^{k})}{\partial U}\right\}^2}.$$

A simple one-dimensional model with two equal-sized zones is used to create the transient power-on temperature measurements (T_m). The perfusion vector is [0.5,8.0] (kg/m^3-s) and the power is 36,800 W/m^3. Figure B.1 plots the resulting effective perfusion ($W_{eff} = U/c_b$) versus the number of time steps by using the transient power-on temperatures at 10 different sensor locations. The number of time steps is chosen from 10 to 100 by an increment of 10. Several traces can be seen from Figure B.1. First, the effective perfusion will be close to the true value if the sensor is located near the center of each zone, for example, 30 or 80 mm. This is because the temperature responses at the sensor is affected strongly by the local perfusion term. Second, when the sensor is close to the boundaries, the

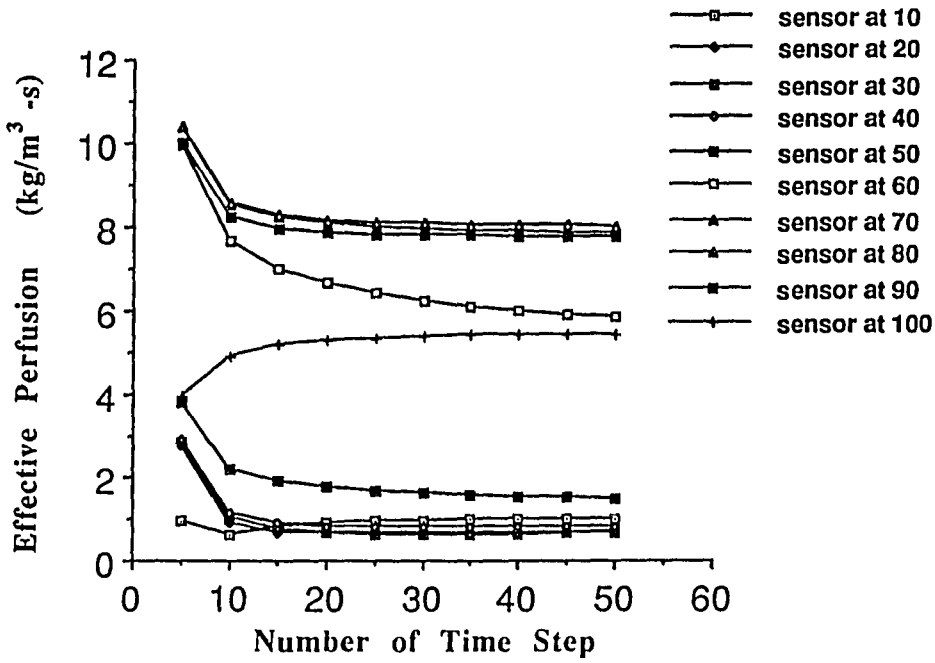

Figure B.1 Effective perfusion (W_{eff}) as a function of the number of time steps during the transient power-on heating for 10 sensor locations.

far from the true one because the temperature responses are affected by the boundary conditions. Third, when the sensor is located near the interface between two zones, say 60 mm, the effective perfusion will be away off the true value because both perfusions will affect the temperature responses. Fourth, the effective perfusion for the case with the sensor at 80 mm (in the high perfusion zone) is more accurate than that for the case with the sensor at 30 mm (in the low perfusion zone). This difference in perfusion accuracy is because at the high perfusion location the energy transmission mechanism is dominated by the blood perfusion, rather than the conduction. Therefore, equation B.1 gives a more accurate approximation. Finally, the optimal value for the number of time steps is about 15.

APPENDIX C

CPU TIMES FOR NUMERICAL SCHEMES

It is desirable to express the CPU time required to numerically solve the differential equations using different schemes in terms of the number of nodes in space, the number of sampling time steps, and the computational time for the addition, subtraction, multiplication, and division operations. For the present simulation, the solutions of the steady-state and transient power-off temperatures were solved numerically by a successive overrelaxation (SOR) scheme and an explicit forward difference scheme, respectively. Because the governing differential equation for the adjoint variable is similar to the bioheat transfer equation, the same explicit forward difference scheme was used to obtain the adjoint variable solution. For the adjoint formulation, the evaluation of the elements of the Jacobian matrix requires CPU intensive convolutions (see equation (2.17)).

STEADY-STATE TEMPERATURE FIELD

The steady-state temperature field was calculated numerically by an iterative scheme. In order to increase the rate of convergence of iterative methods, a successive overrelaxation (SOR) method (Smith

1978)) was used. In the SOR scheme, the discrete equation for equation (1.1) was expressed in the form of

$$T^{n}_{i,j,k} = \frac{\omega}{(6+DW_{i,j,k})} \left\{ T^{n-1}_{i+1,j,k} + T^{n-1}_{i-1,j,k} + T^{n-1}_{i,j+1,k} + T^{n-1}_{i,j-1,k} + T^{n-1}_{i,j,k+1} + T^{n-1}_{i,j,k-1} + D\,(T_a W_{i,j,k} + Q_{i,j,k}) \right\} + (1-\omega) T^{n-1}_{i,j,k}. \qquad (C.1)$$

where

$$D = \frac{(\Delta x)^2}{k} \quad (m^3 \cdot °C/W)$$

i,j,k	number of a node in x, y, and z, respectively; i=1,2,...,Nx, j=1,2,...,Ny, and k=1,2,...,Nz
n	iteration number in time; n=1,2,...,N_t
Δx	spatial resolution in meters of the grid system; $\Delta x=\Delta y=\Delta z$
Δt	time step in seconds
$T^{n}_{i,j,k}$	temperature at (i,j,k) node in space and $n\Delta t$ in time (°C)
$W_{i,j,k}$	perfusion value at (i,j,k) node in space ($kg/m^3/s$)
$Q_{i,j,k}$	power at (i,j,k) node in space (W/m^3)
T_a	arterial temperature (°C)
ω	overrelaxation factor, $1 < \omega < 2$

The total computational time for this SOR scheme can be expressed as

$$\tau_{SOR} = N_{iter}\, N_x\, N_y\, N_z (5\tau_{mul} + 9\tau_{add} + \tau_{sub} + \tau_{div}), \qquad (C.2)$$

where τ_{mul} is the CPU time for a multiplication operation; τ_{add} is the time for an addition operation; τ_{sub} is the time for a subtraction operation; τ_{div} is the time for a division operation. N_{iter} is the total number of iterations such that the temperature field will be within a prerequired accuracy. N_{iter} depends upon the required accuracy and the value of the overrelaxation factor w. In this study, the required accuracy is 10^{-6} °C and the value of w is 1.75.

TRANSIENT TEMPERATURE FIELD

To solve the transient power-off bioheat transfer equation numerically, a finite difference scheme (Smith 1978) was used in which the second spatial derivatives were approximated by a second order central difference formula on a uniform grid system and the first time derivative was approximated by an explicit forward difference formula. With these numerical approximations, the discrete equation for the bioheat transfer equation can be expressed in the form of

$$T^{n+1}_{i,j,k} = \frac{1}{(1+AW_{i,j,k})} \left\{ B(T^{n}_{i+1,j,k} + T^{n}_{i-1,j,k} + T^{n}_{i,j+1,k} + T^{n}_{i,j-1,k} + T^{n}_{i,j,k+1} + T^{n}_{i,j,k-1}) + AT_a W_{i,j,k} + CQ_{i,j,k} + (1-6B)T^{n}_{i,j,k} \right\}. \qquad (C.3)$$

where $Q_{i,j,k} = 0.0$ everywhere (no applied power),

$$A = \frac{c_b(\Delta t)}{\rho c} \qquad (m^3 s/kg)$$

$$B = \frac{k(\Delta t)}{(\Delta x)^2 \rho c} \qquad (\text{dimensionless})$$

$$C = \frac{\Delta t}{\rho c} \qquad (m^3 \cdot C/W)$$

To guarantee the accuracy of the finite difference scheme, a stability analysis is required to determine the maximum time interval (Liauh, 1988). If the required time interval is larger than the maximum time interval obtained from the stability analysis, there will be a need to divide this time interval into several smaller equal time intervals (2^{κ} intervals, κ a positive integer) such that the algorithm is stable. In the present work, the total number of steps to calculate the N_t transient power-off temperatures was always larger than N_t. The computational time needed can be expressed as

$$\tau_{EFD} = 2^{\kappa} N_t N_x N_y N_z (7\tau_{mul} + 9\tau_{add} + \tau_{sub} + \tau_{div}). \qquad (C.4)$$

Thus, the total computational time (τ_{FDT}) for solving the steady-state and transient power-off temperatures can be approximated by

$$\tau_{FDT} = \tau_{SOR} + \tau_{EFD}. \qquad (C.5)$$

Note that the computational time for obtaining the solution of the adjoint variable (τ_{FDA}) is close to the value of τ_{EFD}.

CONVOLUTION INTEGRAL

The convolution integral is evaluated by using a simple rectangular rule. The main reason for this choice is that the rectangular rule for an integral requires the minimum computational operations, thus giving the adjoint formulation its fastest possible implementation. Higher order approximations, for example, Simpson's rule, were tried but were found to be slower. The computational time (τ_{INT}) required to obtain the solutions of equation (2.17) for the algorithm used here can be expressed as

$$\tau_{INT}=\left\{(N_xN_yN_z+N_xN_y+N_x)\tau_{add}+2N_xN_yN_z(\tau_{add}+\tau_{mul})\right\}N_t(N_t+1)/2. \quad (C.6)$$

Then,

$$\frac{\tau_{INT}}{\tau_{FDT}} = \frac{N_xN_yN_zN_t\left\{1+\frac{1}{N_z}+\frac{1}{N_yN_z}+2(1+u)\right\}\tau_{add}(N_t+1)/2}{N_xN_yN_zN_t\left\{2^{\kappa}(9+7u+v+w)+\frac{N_{Iter}}{N_t}(9+5u+v+w)\right\}\tau_{add}},$$

$$= \frac{\left\{1+\frac{1}{N_z}+\frac{1}{N_yN_z}+2(1+u)\right\}(N_t+1)/2}{\left\{2^{\kappa}(9+7u+v+w)+\frac{N_{Iter}}{N_t}(9+5u+v+w)\right\}}, \quad (C.7)$$

where $u=\frac{\tau_{mul}}{\tau_{add}}$, $v=\frac{\tau_{sub}}{\tau_{add}}$, and $w=\frac{\tau_{div}}{\tau_{add}}$.

$$\frac{\tau_{FDA}}{\tau_{FDT}} = \frac{2^{\kappa}(9+7u+v+w)}{\left\{2^{\kappa}(9+7u+v+w)+\frac{N_{Iter}}{N_t}(9+5u+v+w)\right\}}. \quad (C.8)$$

Plugging equations (C.7) and (C.8) into equation (2.23), the value of χ can be expressed as

$$\chi = \frac{1}{1+N_p}\left\{1+N_s\frac{\left\{\left[1+\frac{1}{N_z}+\frac{1}{N_yN_z}+2(1+u)\right](N_t+1)/2+2^{\kappa}(9+7u+v+w)\right\}}{\left\{2^{\kappa}(9+7u+v+w)+\frac{N_{iter}}{N_t}(9+5u+v+w)\right\}}\right\}. \quad (C.9)$$

APPENDIX D

DETAILED DERIVATION OF THE ADJOINT FORMULATION

A detailed derviation of the adjoint integral is presented. Multiplying equation (2.9) by an adjoint variable $\psi(x,y,z,t)$ and integrating over the total domain Ω and integrating over time from zero to t_j gives

$$\int_0^{t_j}\int_\Omega \psi\left\{\frac{\partial(\delta T)}{\partial t} - \frac{1}{\rho c}\nabla\cdot[k\nabla(\delta T)] + \frac{Wc_h}{\rho c}\delta T\right\}dVdt = -\frac{c_h}{\rho c}\int_0^{t_j}\int_\Omega \psi\tilde{T}\delta W dVdt. \quad (D.1)$$

Applying integration by parts over time the first integral on the left hand side yields

$$\int_0^{t_j}\int_\Omega \psi\left\{\frac{\partial(\delta T)}{\partial t}\right\}dVdt = \int_\Omega \int_0^{t_j}\frac{\partial}{\partial t}(\psi\delta T)\, dtdV - \int_0^{t_j}\int_\Omega \delta T\frac{\partial\psi}{\partial t}\, dVdt$$

$$= \int_\Omega (\psi\delta T)\Big|_{t=0}^{t=t_j} dV - \int_0^{t_j}\int_\Omega \delta T\frac{\partial\psi}{\partial t}\, dVdt.$$

Plugging into the initial condition for δT, yielding

$$= \int_\Omega (\psi\delta T)\Big|_{t=t_j} dV - \int_0^{t_j}\int_\Omega \delta T\frac{\partial\psi}{\partial t}\, dVdt.$$

Applying Green's first identity, the second integral of the left hand side yields

$$\frac{1}{\rho c}\int_0^{t_j}\int_\Omega \psi\left\{\nabla\cdot k\nabla(\delta T)\right\}dVdt = \frac{1}{\rho c}\int_0^{t_j}\int_\Omega \psi(\nabla\cdot\bar{X})dVdt;\ \text{where } \bar{X} = k\nabla(\delta T).$$

$$\int_\Omega \psi(\nabla\cdot\bar{X})\ dV = \int_\Omega\left\{\nabla\cdot(\psi\bar{X}) - \bar{X}\cdot\nabla\psi\right\}\ dV$$

$$= \int_\Gamma \psi\bar{X}\cdot\bar{n}\ dA - \int_\Omega \bar{X}\cdot\nabla\psi\ dV$$

$$= \int_\Gamma \psi k\nabla(\delta T)\cdot\bar{n}\ dA - \int_\Omega k\nabla(\delta T)\cdot\nabla\psi\ dV$$

$$= \int_\Gamma \psi k\frac{\partial(\delta T)}{\partial n}\ dA - \int_\Omega \nabla(\delta T)\cdot(k\nabla\psi)\ dV$$

$$= \int_\Gamma \psi k\frac{\partial(\delta T)}{\partial n}\ dA - \int_\Omega \nabla\cdot\left\{(\delta T)k\nabla\psi\right\}\ dV - \int_\Omega \delta T(\nabla\cdot k\nabla\psi)\ dV$$

$$= \int_\Gamma \psi k\frac{\partial(\delta T)}{\partial n}\ dA - \int_\Gamma \delta T(k\frac{\partial\psi}{\partial n})\ dA - \int_\Omega \delta T(\nabla\cdot k\nabla\psi)\ dV.$$

Finally, equation (D.1) yields

$$\int_\Omega (\psi\delta T)\big|_{t=t_j}\ dV - \int_0^{t_j}\int_\Omega \delta T\left\{\frac{\partial\psi}{\partial t} + \frac{1}{\rho c}\nabla\cdot k\nabla\psi - \frac{Wc_h}{\rho c}\psi\right\}dVdt -$$

$$\int_0^{t_j}\int_S \frac{k}{\rho c}\left\{\psi\frac{\partial(\delta T)}{\partial n} - \delta T\frac{\partial\psi}{\partial n}\right\}dAdt = -\frac{c_h}{\rho c}\int_0^{t_j}\int_\Omega \psi\bar{T}\delta W\ dVdt. \quad (D.2)$$

APPENDIX E

REGULARIZATION METHOD

The regularization procedure has been studied by many researchers (Tikhonov 1963, Alliney and Sgallari 1984, Beck et. al, 1985) to modify the least square approach by adding factors that prevent or reduce the ill-posedness of inverse problems. For a linear algebraic system with N_p unknowns of x_i (i.e. $x=[x_1,x_2,\ldots,x_{Np})$,

$$Ax=b,$$

which is ill-posed, we try to compute a regularized solution x of the system, which minimizes the following quadratic functional

$$||Ax-b||^2 + \epsilon \left(\sum_{i=0}^{2} ||H_i x||^2\right).$$

Here $||\cdot||$ denotes the Euclidian norm; ϵ denotes the regularization parameter; H_0 denotes the identity matrix (I) of order N_p (i.e. $H_0 = c_0 I$); H_1 and H_2 are the matrices of dimensions, respectively, $(N_p-1)xN_p$ and $(N_p-2)xN_p$, given by

$$H_1 = c_1 \begin{bmatrix} -1 & 1 & 0 & 0 & \cdots & 0 \\ 0 & -1 & 1 & 0 & \cdots & 0 \\ 0 & 0 & -1 & 1 & \cdots & 0 \\ & & & \cdots & & \\ 0 & \cdots & & 0 & -1 & 1 \end{bmatrix},$$

$$H_2 = c_2 \begin{bmatrix} 1 & -2 & 1 & 0 & 0 & \cdots & 0 \\ 0 & 1 & -2 & 1 & 0 & \cdots & 0 \\ 0 & 0 & 1 & -2 & 1 & \cdots & 0 \\ & & & \cdots & & & \\ 0 & \cdots & & 0 & 1 & -2 & 1 \end{bmatrix},$$

where c_0, c_1, and c_2 are constant values. These matrices H_0, H_1, and H_2 are the matrices for the zeroth, first, and second order regularizers, respectively.

For the present inverse hyperthermia temperature estimation problems, a linear algebraic system is approximated by using the influence coefficient method. If there are N_s temperature measurement locations and W^k is the kth iteration estimate of the perfusion vector, a successive perfusion estimate can be derived by a Taylor series expansion for $T_{pr}(W^{k+1})$ at the k^{th} perfusion estimate (W^k), and can be expressed as

$$T_{pr}(W^{k+1}) = T_{pr}(W^k) + \left(\frac{\partial T_{pr}}{\partial W_\varsigma}\right) \bullet (W_\varsigma^{k+1} - W_\varsigma^k) + \text{H.O.T.} \quad \text{(E.1)}$$

where W_ς is the ς^{th} element in the perfusion vector W of size $N_p x 1$

$$W = [\, W_1 \; W_2 \; W_3 \; \cdots \; W_{N_p} \,]^T$$

and T_{pr} is the predicted temperature vector of size $(NtxN_s)x1$

$$T_{pr}=[T^1_{pr,1}\ T^2_{pr,1}\ \cdots\ T^{Nt}_{pr,1}\ T^1_{pr,2}\ \cdots\ T^{Nt}_{pr,2}\ \cdots\ T^1_{pr,N_s}\cdots\ T^{Nt}_{pr,N_s}]^T$$

Due to the nonlinearity of T_{pr} depending on W, the new perfusion vector W^{k+1} cannot be calculated directly. Assuming that $T_{pr}(W^{k+1})$ is close to the measured temperature vector T_m, the higher order terms (H.O.T.) can be neglected. Equation (G.1) yields

$$T_m - T_{pr} = \left[\frac{\partial T}{\partial W}\right](W^{k+1} - W^k)$$

or

$$E = J(\Delta W^k) \qquad (E.2)$$

Based on the linear system in equation (E.2), the quadratic functional can be expressed as

$$g(\Delta W^k) = (J\Delta W^k-E)^T(J\Delta W^k-E)+ \epsilon\{(\Delta W^k)^T H_0^T H_0 \Delta W^k+ (\Delta W^k)^T H_1^T H_1 \Delta W^k+ (\Delta W^k)^T H_2^T H_2 (\Delta W^k)\}. \qquad (E.3)$$

Minimization of this function with respect to ΔW^k yields

$$W^{k+1} = W^k + \left\{J^TJ + \epsilon(I+H_1^TH_1+H_2^TH_2)\right\}^{-1}J^TE, \qquad (E.4)$$

where I is the identity matrix. Note that when ϵ is equal to zero (i.e., without regularization), equation (E.4) is identical to

equation (2.3). If $c_1 = c_2 = 0$ and $c_0 \neq 0$, minimization of equation (E.3) is the so-called zeroth-order regularization procedure. Similarly, the procedure is called the first-order regularization method if $c_0 = c_2 = 0$ and $c_1 \neq 0$, and the second-order regularization method if $c_0 = c_1 = 0$ and $c_2 \neq 0$.

Two three-dimensional models with seven zones are used to determine which order of regularizer can help the estimation algorithm to obtain more successful temperature reconstructions. Two perfusion vectors are used; one is symmetric and the other is random listed as Cases A and D, respectively, in Table 3.5. As mentioned before, the problem becomes more ill-posed when the number of unknown parameters is greater than the number of temperature sensors. To overcome this ill-posedness, the regularization method is then implemented. The number of sensors is three for the present problem. These three sensor locations are either in the centers of the first, third, and fifth zones for the symmetric perfusion pattern or in the centers of the first, second, and third zones for the random perfusion pattern. The magnitudes of the regularization parameter (ϵ) are chosen as 1.0 and 0.01 for the symmetric and the random perfusion patterns, respectively (Liauh 1988). Table E.1 shows the maximum difference between the true and predicted temperature fields for these two perfusion patterns. Results illustrate that the performance of the zeroth-order regularizer is better than the performance of the first- and second-order regularizers.

Table E.1 Maximum difference between the true and predicted temperature fields for the three-dimensional seven zone model with four noise levels for (a) a symmetric or (b) a random perfusion pattern. SIN represents the case that the sensitivity (Jacobian) matrix is singular.

NOISE LEVEL (°C)	ORDER OF REGULARIZER NONE	ZEROTH	FIRST	SECOND
0.1	SIN	0.086	4.634	SIN
0.2	SIN	0.542	4.689	SIN
0.4	SIN	1.249	4.811	SIN
1.0	SIN	2.948	5.262	SIN

(a)

NOISE LEVEL (°C)	ORDER OF REGULARIZER NONE	ZEROTH	FIRST	SECOND
0.1	0.513	0.514	0.955	4.139
0.2	1.012	1.013	1.258	4.141
0.4	1.960	1.960	2.145	4.092
1.0	4.483	4.483	4.482	3.789

(b)

SELECTED BIBLIOGRAPHY

Abramowitz, M. and Stegan, I. A. (1972), Handbook of mathematical functions, Dover Publications, Inc., New York, 933.

Alliney, S. and Sgallari, F. (1984), "An ill-conditioned Volterra integral equation related to the reconstruction of images from projections", SIAM Journal of Applied Mathematics, 44, 627-645.

Arkin, H., Chen, M. M., and Holmes, K. R. (1986), "Adaptive thermal modeling: a concept for measurement of local blood perfusion in heated tissue", Transactions of the ASME, 108, 306-311.

Banks, H. T. and Lamm, P. D. (1985), "Estimation of variable coefficients in parabolic distributed systems", IEEE Tran. on Automatic Control, 30, 386-398.

Barlogie, B., Corry, P. M., Yip, E. et al. (1979), "Total body hyperthermia with and without chemotherapy for advanced human neoplasms", Cancer Research, 39, 1481-1489.

Baish, J. W., Ayyaswamy, P. S., and Foster, K. R. (1986a), "Heat transport mechanisms in vascular tissues: a model comparison", J. of Biomechanical Eng., 108, 324-331.

Baish, J. W., Ayyaswamy, P. S., and Foster, K. R. (1986b), "Small-scale temperature fluctuations in perfused tissue during local hyperthermia", J. of Biomechanical Eng., 108, 246-250.

Beck, J. V., Blackwell, B., and St. Clair, C. R. (1985), Inverse Heat Conduction Ill-posed Problems, John Wiley and Sons, New York.

Beck, J. V. (1968), "Surface heat flux determination using an integral method", Nucl. Eng. Des., 7, 170-178.

Beck, J. V. (1970), "Nonlinear estimation applied to the nonlinear inverse heat conduction problem", Int. J. Heat Mass Transfer, 13, 703-716.

Beck, J. V. and Arnold, K. J. (1977), Parameter Estimation in Engineering and Science, John Wiley and Sons, New York.

Becker, L. and Yeh, W. W-G. (1972), "Identification of parameters in unsteady open-channel flows", Water Resour. Res., 8, 956-965.

Ben Hur, E., Bronk, V. B., and Elkind, M. M. (1972), "Thermally enhanced radiosensitivity of cultured Chinese hamster cells", Nature, 238, 209-211.

Carter, R. D., Kemp, L. F., Pearce, A. C., and Williams, D. L. (1974), "Performance matching with constraints", Soc. Pet. Eng. J., 14, 187-196.

Charny, C.K. and Levin, R.L. (1989), "Bioheat transfer in a branching countercurrent network during hyperthermia", J. of Biomechanical Eng., 111, 263-270.

Chato, J. (1980), "Heat transfer to blood vessels", J. of Biomechanical Eng., 102, 110-118.

Chavent, G. (1974), "Identification of functional parameters in partial differential equations", in Identification of Parameters in Distributed Systems, edited by Goodson, R. E. and Polis, M., American Society of Mechanical Engineers, New York, 31-48.

Chen, M. M., and Holmes, K. R. (1980), "Microvascular contributions in tissue heat transfer", Annals New York Academy of Sciences, 355, 137-150.

Chen, M. M., Arkin, H., and Holmes, K. R. (1984), "On conduction boundary layers in steady state solutions of the bioheat transfer equation for perfused tissues", 1984 Advances in Bioengineering, ASME, New York, New York, 7-8.

Clegg, S. T., Roemer, R. B., and Cetas, T. C. (1985), "Estimation of complete temperature fields from measured transient temperatures", Int. J. Hyperthermia, 1, 265-286.

Clegg, S. T., and Roemer, R. B. (1985), "A comparative evaluation of unconstrained optimization methods applied to the thermal tomography problem", Transactions of the ASME, 107, 228-233.

Clegg, S. T., and Roemer, R. B. (1985), "A study of the effect of sensor placement and perfusion pattern variations on thermal tomography solutions in hyperthermia", IEEE Trans. on Biomed. Eng., 32, 677-682.

Clegg, S. T., Liauh, C. T., and Roemer, R. B. (1988), "Selecting the optimal amount of regularization to reconstruct three-dimensional temperature fields from limited noisy temperature measurements during hyperthermia", Computational Methods in Bioengineering, Ed. Spilker, R. L. and Simon, B. R., New York, 281-290.

Clegg, S. T., and Roemer, R. B. (1989), "Towards estimation of noisy three-dimensional temperature fields during hyperthermia", Int. J. Hyperthermia, 5, 467-484.

Clegg, S. T. (1988), Estimation of three-dimensional temperature fields from a limited number of transient temperature

measurements during hyperthermia, Ph.D. Dissertation, University of Arizona.

Coley, W. B. (1893), "The treatment of malignant tumors by repeated inoculations of erysipelas--with a report of ten original cases", Am. J. Med. Sci., 105, 487-511.

Crile, G., Jr. (1961), "Heat as an adjunct to the treatment of cancer; experimental studies", Cleve. Clin. Q., 28, 75-89.

Crile, G., Jr. (1962), "Selective destruction of cancers after exposure to heat", Ann. Surg., 156, 404-407.

Crile, G., Jr. (1963), "The effects of heat and radiation on cancers implanted into the feet of mice", Cancer Res., 23, 372-380.

Dewhirst, M. W., Sim, D. A., Sapareto, S., and Connor, W. G. (1984), "Importance of minimum tumor temperature in determining early and long-term responses of spontaneous canine and feline tumors to heat and radiation", Cancer Research, 44, 43-50.

Dewey, W. C., Westra, A., Miller, H. H., and Magasawa, H. (1971), "Heat-induced lethality and chromosomal damage in synchronized Chinese hamster cells treated with 5-bromodeoxyuridine", Int. J. Radiat. Biol., 20, 505-520.

Divrik, A. M., Roemer, R. B., Cetas, T. C. (1984), "Inference of complete tissue temperature fields from a few measured temperatures: an unconstrained optimization method", IEEE transactions of Biomedical Engineering, 31, 150-160.

Dogru, A. H. and Seinfeld, J. H. (1981), "Comparison of sensitivity coefficient calculation methods in automatic history matching", Soc. Pet. Eng. J., 21, 551-557.

Dixon, L. C. W., Spedicato, E. and Szego, E. P., Nonlinear Optimization: Theory and Algorithms, Birkhauser, Boston.

Emery, A. F. and Sekins, K. M. (1982), "The use of heat transfer principles in designing optimal diathermy and cancer treatment modalities", Int. J. of Heat Mass Transfer, 26, 823-834.

Field, S. B. and Franconi, K. M., ed. (1987), Physics and Technology of Hyperthermia, NATO ASI Series, series E:Applied Sciences, No. 127, Taylor and Francis, London.

Gavalas, G. R., Shah, P. C., and Seinfeld, J. H. (1976), "Reservoir history matching by Bayesian estimation", Soc. Pet. Eng. J., 16, 337-350.

Guthkelch, A. N., Hynynen, K., Shimm, D. S., Stea, B., Cassady, J. R., and Roemer, R. B. (1989), "Treatment of malignant brain tumors

with focussed ultrasound hyperthermia and radiation: experiences with a phase I trial", J. Neurosurgery (submitted).

Hahn, E. W., Feingold, S. M., and Kim, J. H. (1977), "Repair of normal tissue injury from local hyperthermia", Radiation Research, 70, 634.

Hand, J. W. and James, J. R., ed. (1986), Phsical Techniques in Clinical Hyperthermia, John Wiley and Sons, New York.

Hand, J. W., Ledda, J. L., and Evans, N. T. S. (1982), "Considerations of radiofrequency induction heating for localised hyperthermia", Phys. Med. Biol, 27, 1-16.

Harari, P. M., Hynynen, K., Roemer, R. B., Anhalt, D. P., Shimm, D. S., Stea, B., and Cassady, J. R. (1991), "The University of Arizona development of scanned focussed ultrasound hyperthermia: clinical response evaluation", Int. J. Radiat. Oncol. Biol. Phys., 21, 1-10.

Hensel, E. C. and Hills, R. (1989), "Steady-state two-dimensional inverse heat conduction", Numerical Heat Transfer, 15, 227-240.

Hills, R. and Hensel, E. C. (1986), "One-dimensional nonlinear inverse heat conduction technique", Numerical Heat Transfer, 10, 369-393.

Hume, S. P., and Margold, J. C. L. (1980), "Transient heat induced thermal resistance in the small intesting of mouse", Radiation Research, 82, 526-534.

Hynynen, K., DeYoung, D., Kundrat M., and Moros, E. (1989), "The effect of blood perfusion on the temperature distributions induced by multiple scanned and focussed beams in dog's kidneys in vivo", Int. J. of Hyperthermia, 5, 485-497.

Hynynen, K., Roemer, R. B., Anhalt, D., Johnson, C., and Moros, E. (1985), "Focussed scanned ultrasound for local hyperthermia", Proc. 7th Annu. Conf. IEEE/EMBS, 341-345.

Hynynen, K., Roemer, R. B., Anhalt, D., Johnson, C., Xu, Z. X., Swindell W., and Cetas, T. C. (1987a), "A scanned, focussed, multiple transducer ultrasounic system for localized hyperthermia treatments", Int. J. Hyperthermia, 3, 21-35.

Hynynen, K., Shimm, D., Roemer, R. B., Anhalt, D., and Cassady, J. R. (1987b), "Temperature distributions during clinical ultrasound hyperthermia", Proc. 9th Annu. Conf. IEEE/EMBS, 1644-1645.

Jacquard, P. and Jain, C. (1965), "Permeability distribution from field pressure data", Soc. Pet. Eng. J., 5, 281-294.

Jiji, L. M., Weinbaum, S., and Lemons, D. E. (1984a), "Theory and experiment for the effect of vascular microstructure on surface tissue heat transfer--part I: anatomical foundation and model conceptualization", J. of Biomechanical Eng., 106, 321-330.

Jiji, L. M., Weinbaum, S., and Lemons, D. E. (1984b), "Theory and experiment for the effect of vascular microstructure on surface tissue heat transfer--part II: model formulation and solution", J. of Biomechanical Eng., 106, 331-341.

Kamura, T., Nielsen, O. S., Overgaard, J., and Andersen, A. H. (1981), "Development of thermotolerance during fractionated hyperthermia in a solid tumor in vivo", Cancer Research, 42, 1744-1748.

Kitamura, S. and Nakagiri S. (1977), "Identifiability of spatially-varying and constant parameters in distributed systems of parabolic type", SIAM J. Contr. Optimiz., 15, 785-802.

Kravaris, C. and Seinfeld, J. H. (1986), "Identifiability of spatially varying conductivity from point observation as an inverse Sturm-Liouville problem", SIAM J. Control and Optimization, 24, 522-542.

Kravaris, C. and Seinfeld, J. H. (1985), "Identification of parameters in distributed parameter systems by regularization", SIAM J. Control and Optimization, 23, 217-241.

Lagendijk, J. J. W., Schellekens, M., Schipper, J., van der Linden, P. M. (1984), "A three-dimensional description of heating patterns in vascularized tissues during hyperthermic treatment", Phys. Med. Biol., 29, 495-507.

Lapidos, L. and Pinder, G. F. (1982), Numerical Solution of Partial Differential Equations in Science and Engineering, John Wiley and Sons, New York.

Larkin, J. M., Edwards, W. S., Smith, D. E., and Clark, P. J. (1977), "Systemic thermography: Description of a method and physiologic tolerance in clinical subjects", Cancer, 40, 3155-3159.

Lauster. G. K., Ray, W. H., and Martens, H. R. (1980), "Real time distributed parameter state estimation applied to a two-dimensional heated ingot", Automatica, 16, 335.

Law, M. P. (1979), "Induced thermal resistance in the mouse ear: relationship between heating and temperature", International Journal of Radiation Biology, 35, 481-485.

Law, M. P., Coultas, P. G., and Field, S. B. (1979), "Induced thermal resistance in the mouse ear", British Journal of Radiology, 52, 308-314.

Lax, P. D., and Richtmyer, R. D. (1956), "Survey of the stability of linear finite difference equations", Communications on Pure and Applied Mathematics, 9, 267-293.

Lele, P. P. (1983), "Physical aspects and clinical studies with ultrasonic hyperthermia", in Hyperthermia in Cancer Therapy, edited by Storm, F. K., Hall Medical Publishers, Boston, MA, 333-368.

Lele, P. P. (1986), "Rationale, technique and clinical results with scanned ultrasound (SIMFU) systems", Proc. 8th Annu. Conf. IEEE/EMBS, 1435-1440.

Lele, P. P. and Goddard, J. (1987), "Optimizing insonation parameters in therapy planning for deep heating by SIMFU", Proc. 9th Annu. Conf. IEEE/EMBS, 1650-1651.

Lele, P. P. and Parker, K. J. (1982), "Temperature distributions in tissues during local hyperthermia by stationary or steered beams of unfocussed or focussed ultrasound", Brit. J. Cancer, 45, 108-121.

Liauh, C-T. (1988), Estimating three-dimensional temperature fields during hyperthermia: studies of the optimal regularization parameter and time sampling period, MS Thesis, The University of Arizona.

Liauh, C-T., Clegg, S.T., and Roemer, R.B. (1991), "Estimating three-dimensional temperature fields during hyperthermia: studies of the optimal regularization parameter and time sampling period", J. of Biomechanical Engineering, 113, 230-238.

McElwee, C. D. (1982), "Sensitivity analysis and the groundwater inverse problem", Groundwater, 20, 723-735.

Moros, E. (1990), Experimental evaluation of scanned focussed ultrasound hyperthermia models in canine muscle in vivo, Ph.D. Dissertation, University of Arizona.

Neuman, S. P. (1973), "Calibration of distributed parameter groundwater flow models viewed as a multiple-objective decision process under uncertainty", Water Resources Research, 9, 1006-1021.

Oleson, J. R., Sim, D. A., and Manning, M. R. (1984), " Analysis of prognostic variables in hyperthermia treatment of 161 patients", Int. J. Radiat. Oncol. Biol. Phys., 10, 2231-2239.

Pennes, H. H. (1948), "Analysis of tissue and arterial blood temperatures in the resting human forearm", Journal of Applied Physiology, 1, 93-122.

Pettigrew, R. T., Galt, J. M., Ludgale, C. M., and Smith, A. N. (1974), "Clinical effects of whole body hyperthermia in advanced malignancy", Br. Med. J., 4, 679-682.

Plancot, M., Prevost, B., Chive, M., Fabre, J. J., Ledee, R., and Giaux, G. (1987), "A new method for thermal dosimetry in microwave hyperthermia using microwave radiometry for temperature control", Int. J. Hyperthermia, 3, 9-19.

Reynaud, M. and Beck, J. V. (1985), "Methodology for comparison of inverse heat conduction methods", ASME paper No. 85-WA/HT-40.

Roemer, R.B., Moros, E.G., and Hynynen, K. (1989), "A comparison of bioheat transfer and effective conductivity equation predictions to experimental hyperthermia data", Bioheat transfer-applications in hyperthermia, emerging horizons in instrumentation and modeling, 11-15.

Roemer, R. B., Swindell, W., Clegg, S. T., and Kress, R. L. (1984), "Simulation of focused, scanned ultrasonic heating of deep-seated tumors: the effect of blood perfusion", IEEE Trans. on Sonics and Ultrasonics, Su-31, 457-466.

Roemer, R. B., Fletcher, A. M., and Cetas, T. C. (1985), "Obtaining local SAR and blood perfusion data from temperature measurements: steady state and transient techniques compared", Int. J. Radiation Oncology Biol. Physics, 11, 1539-1550.

Roemer, R. B. (1988), "Heat transfer in hyperthermia treatment: basic principles and applications", in Biological, Physical and Clinical Aspects of Hyperthermia (Paliwal, B. R., Hetzel, F. W., and Dewhirst, M. W. ed.), American Institute of Physics, New York, 210-242.

Roemer, R. B. (1990), "The local tissue cooling coefficient: a unified approach to thermal washout and steady-state 'perfusion' calculations", Int. J. Hyperthermia, 6, 421-430.

Roemer, R. B. (1991), "Optimal Power Deposition in Hyperthermia I. The treatment goal: The ideal temperature distribution: The role of large blood vessels", Int. J. Hyperthermia, 7, 317-342.

Rohdenburg, G. L. (1918), "Fluctuations in the growth of malignant tumors in man, with special reference to spontaneous recession", J. Cancer Res., 3, 193-225.

Shah, P. C., Gavalas, G. R., and Seinfeld, J. H. (1978), "Error analysis in history matching: The optimum level of parameterization", Soc. Pet. Eng. J., 18, 219-228.

Sekins, K. M. (1989), "Microvascular bioheat transfer equations", in Hyperthermia Oncology 1988, edited by Tsutomu Sugahara and Masao Saito, Taylor and Francis, London, 2, 758-760.

Sekins, K. M., Emery, A. F., Lehmann, J. F., and MacDougall, J. A. (1982), "Determination of perfusion field during local hyperthermia with the aid of finite element thermal models", J. of Biomechanical Eng., 104, 272-279.

Sekins, K. M., Lehmann, J. F., Esselman, P., Dundore, D., Emery, A. F., deLateur, B. J., and Nelp, W. B. (1984), "Local muscle blood flow and temperature responses to 915 MHz diathermy as simultaneously measured and numerically predicted", Arch. Phys. Med. Rehabil., 65, 1-7.

Shimm, D. S., Hynynen, K., Anhalt, D. P., Roemer, R. B., and Cassady, J. R. (1988), "Scanned focussed ultrasound hyperthermia: initial clinical results", Int. J. Radiat. Oncol. Biol. Phys., 15, 1203-1208.

Smith, G. D. (1978), Numerical Solutions of Partial Differential Equations Finite Difference Methods, 2nd ed., Clarendon Press, Oxford.

Song, C. W., Lokshina, A., Rhee, J. G., Patten, M., and Levitt S. H. (1984), "Implication of blood flow in hyperthermic treatment of tumors", IEEE Trans. on Boimed. Eng., BME-31, 9-16.

Song, C. W. (1984), "Effect of local hyperthermia on blood flow and microenvironment: A review", Cancer Research, 44, 4721.

Sun, N. Z. and Yeh, W. W-G. (1985), "Identification of parameter structure in groundwater inverse problem", Water Resour. Res., 21, 869-883.

Sykes, J. F., Wilson, J. L., and Andrews, R. W. (1985), "Sensitivity analysis for steady-state groundwater flow using adjoint operators", Water Resour. Res., 21, 359-371.

Tikhonov, A. N. (1963), "Solution of incorrectly formulated problems and the regularization method", Soviet Mathematics Doklady, 4, 1035-1038.

Tikhonov, A. N. (1963), "Regularization of incorrectly posed problems", Soviet Mathematics Doklady, 4, 1624-1627.

Valvano, J. W., Allen, J. T., and Bowman, H. F. (1984), "The simultaneous measurement of thermal conductivity, thermal diffusivity, and perfusion in small volumes of tissue", Transactions of the ASME, 106, 192-197.

Van der Zee, J., Van Putten, W. L. J., Van den Berg, A. P., Van Rhoon, G. C., Wike Hooley, J. L.,Broekmeyer-Reurink, M. P., and Reihold, H. S. (1986), "Retrospective analysis of the response of tumors in patients treated with a combination of radiotherapy and hyperthermia", Int. J. Hyperthermia, 2, 337-349.

Waterman, F. M., Nerlinger, R. E., Moylan, D. J., and Leeper, D. B. (1986), "Reponse of human tumor blood flow to local hyperthermia", Int. J. Radiation Oncology Biol. Physics, 13, 75-82.

Weinbaum, S., and Jiji, L. M. (1989), "The matching of thermal fields surrounding countercurrent microvessels and the closure approximation in the Weinbaum-Jiji equation", J. of Biomechanical Engineering, 111, 271-275.

Weinbaum, S., and Jiji, L. M. (1987), "Discussion of papers by Wissler and Baish et al. concerning the Weinbaum-Jiji Bioheat equation", J. of Biomechanical Engineering, 109, 234-237.

Weinbaum, S., and Jiji, L. M. (1984), "Theory and Experiment for the effect of vascular microstructure on surface tissue heat transfer-part I: anatomical foundation and model conceptualization", J. of Biomechanical Engineering, 106, 321-330.

Weinbaum, S., and Jiji, L. M. (1984), "Theory and Experiment for the effect of vascular microstructure on surface tissue heat transfer-part II: model formulation and solution", J. of Biomechanical Engineering, 106, 321-330.

Weinbaum, S., and Jiji, L. M. (1985), "A new simplified bioheat equation for the effect of blood flow on local average tissue temperature", J. of Biomechanical Engineering, 107, 131-139.

Winget, J. M., Dewhirst, M. W., Engler, M. J., and Oleson, J. R. (1986), "The use of limited temperature observations to predict complete temperature fields", IEEE-Eighth Annual Conference of the Engineering in Medicine and Biology Society, 1507-1511.

Wissler E. H. (1987a), "Comments on the new bioheat equation proposed by Weinbaum and Jiji", J. of Biomechanical Engineering, 109, 226-233.

Wissler E. H. (1987b), "Comments on Weinbaum and Jiji's discussion of their proposed bioheat equation", J. of Biomechanical Engineering, 109, 355-356.

Wulff, W. (1974), "The energy conservation equation for tissue", IEEE Trans. Biomed. Eng., BME-21, 494-495.

Yeh, W., W-G. and Sun, N. Z. (1984), "An extended identifiability in aquifer parameter identification and optimal pumping test design", Water Resources Research, 20, 1837-1847.

Yeh, W., W-G. and Yoon, Y. S. (1976), "A systematic optimization procedure for the identification of inhomogeneous aquifer parameters", in Advances in Groundwater Hydrology, edited by Saleem, Z. A., American Water Resources Association, Minneapolis, 72-82.